Università degli studi di Pisa

Scuola di Dottorato in Ingegneria "Leonardo da Vinci"

Corso di Dottorato di Ricerca in

Ingegneria Chimica e dei Materiali

Tesi di Dottorato di Ricerca

Mixing and Phase Separation of Fluid Mixtures

Autore:
Dafne Molin

Relatore:
Prof. Ing. Roberto Mauri

Anno 2007

Summary

During the three years of the PhD project we extended the diffuse interface (DI) method and apply it to engineering related problems, particularly related to mixing and demixing of two fluids. To do that, first the DI model itself was validated, showing that, in agreement with its predictions, a single drop immersed in a continuum phase moves whenever its composition and that of the continuum phase are not at mutual equilibrium [D. Molin, R. Mauri, and V. Tricoli, "Experimental Evidence of the Motion of a Single Out-of-Equilibrium Drop," Langmuir 23, 7459-7461 (2007)]. Then, we developed a computer code and validated it, comparing its results on phase separation and mixing with those obtained previously. At this point, the DI model was extended to include heat transport effects in regular mixtures In fact, in the DI approach, convection and diffusion are coupled via a nonequilibrium, reversible body force that is associated with the Kortweg stresses. This, in turn, induces a material flux, which enhances both heat and mass transfer. Accordingly, the equation of energy conservation was developed in detail, showing that the influence of temperature is two-folded: on one hand, it determine phase transition directly, as the system is brought from the single-phase to the two-phase region of its phase diagram. On the other hand, temperature can also change surface tension, that is the excess free energy stored within the interface at equilibrium. These effects were described using the temperature dependence of the Margules parameter. In addition, the heat of mixing was also taken into account, being equal to the excess free energy. [D. Molin and R. Mauri, "Diffuse Interface Model of Multiphase Fluids," Int. J. Heat Mass Tranf., submitted]. The new model was applied to study the phase separation of a binary mixture due to the temperature quench of its two confining walls. The results of our simulations showed that, as heat is drawn from the bulk to the walls, the mixture phase tends to phase separate first in vicinity of the walls, and then, deeper and deeper within the bulk. During this process, convection may arise, due to the above mentioned non equilibrium reversible body force, thus enhancing heat transport and, in particular increasing the heat flux at the walls [D. Molin, and R. Mauri, "Enhanced Heat Transport during Phase Separation of Liquid Binary Mixtures," Phys. Fluids 19, 074102-1-10 (2007)]. The model has been extended then and applied to the case where the two phases have different heat con-

ductivities. We saw that heat transport depends on two parameters, the Lewis number and the heat conductivity ratio. In particular, varying these parameters can affect the orientation of the domains that form during phase separation. Domain orientation has been parameterized using an isotropy coefficient ξ, varying from -1 to 1, with $\xi = 0$ when the morphology is isotropic, $\xi = +1$ when it is composed of straight lines along the transversal (i.e. perpendicular to the walls) direction, and $\xi = -1$ when it is composed of straight lines along the longitudinal (i.e. parallel to the walls) direction [D. Molin, and R. Mauri, "Spinodal Decomposition of Binary Mixtures with Composition-Dependent Heat Conductivities," Int. J. Engng. Sci., in press (2007)]. In order to further extend the model, we removed the constraint of a constant viscosity, and simulated a well known problem of drops in shear flows. There we found that, predictably, below a certain threshold value of the capillary number, the drop will first stretch and then snap back. At lager capillary numbers, though, we predict that the drop will stretch and then, eventually, break in two or more satellite drops. On the other hand, applying traditional fluid mechanics (i.e. with infinitesimal interface thickness) such stretching would continue indefinitely [D. Molin and R. Mauri, " Drop Coalescence and Breakup under Shear using the Diffuse Interface Model," in preparation]. Finally, during a period of three months at the Eindhoven University, we extended the DI model to a three component fluid mixture, using a different form of the free energy, as derived by Lowengrub and Coworkers.. With this extension, we simulated two simple problems: first, the coalescence/repulsion of two-component drops immersed in a third component continuum phase; second, the effect of adding a third component to a separated two phase system. Both simulations seem to capture physical behaviors that were observed experimentally [D. Molin, R. Mauri and P. Anderson, " Phase Separation and Mixing of Three Component Mixtures," in preparation].

Contents

Introduction

The theory of multiphase systems was developed at the beginning of the 19th century by Young, Laplace and Gauss, assuming that different phases are separated by an interface, that is a surface of zero thickness. In this approach, physical properties such as density and concentration, may change discontinuously across the interface and the magnitude of these jumps can be determined by imposing equilibrium conditions at the interface. For example, imposing that the sum of all forces applied to an infinitesimal curved interface must vanish leads to the Young-Laplace equation, stating that the difference in pressure between the two sides of the interface (where each phase is assumed to be at equilibrium) equals the product of surface tension and curvature. Later, this approach m was generalized by defining surface thermodynamical properties, such as surface energy and entropy, and surface transport quantities, such as surface viscosity and heat conductivity, thus formulating the thermodynamics and transport phenomena of multiphase systems. At the end of the 19th century, though, another approach was proposed by Rayleigh (1892) and Van der Waals (1893), who assumed that interfaces have a non-zero thickness, i.e. they are "diffuse". Actually, the basic idea was not new, as it dated back to Maxwell (1876) and Gibbs (1876), Poisson (1831) and Leibnitz (1765) or even Lucretius (50 B.C.E.), who wrote that "a body is never wholly full nor void." Concretely, in a seminal article published in 1893, Van der Waals used his equation of state to predict the thickness of the interface, showing that it becomes infinite as the critical point is approached. Later, in 1901, Korteweg continued this work and proposed an expression for the capillary stresses, which are generally referred to as Korteweg stresses, showing that they reduce to surface tension when the region where density changes from one to the other equilibrium value collapses into a sharp interface (see Rowlinson and Widom, 1982, for a review of the molecular basis of capillarity). In the first half of the 20th century, the diffuse interface (D.I.) approach was basically ignored because assuming that interfaces are sharp allows one to obtain a few analytical results and seemed to better fit the needs of the multiphase scientific community. However, at mid 1900, Cahn and Hillard (again the Dutch school!) first applied Van der Waals' D.I. approach to binary mixtures (Cahn and Hillard, 1958) and then used it to describe nucleation (Cahn and Hillard, 1959) and

spinodal decomposition (Cahn, 1961). This approach was later extended to model spinodal decomposition of polymer blends and alloys (de Gennes, 1980; Pincus, 1981). Then, in the mid 1980's, the D.I. approach was coupled to hydrodynamics, developing a set of conservation equations, thanks to the work by Kawasaki (1970), Siggia (1979), Hohenberg and Halperin (1977) and others. These latter authors referred to this approach as "model H" and only later the name "diffuse interface method" was introduced. Finally, recent development in computing technology has stimulated a resurgence of the D.I. approach, above all in the study of systems with complex morphologies and topological changes. Detailed discussion about D.I. theory coupled with hydrodynamics can be found in Antanovskii (1996), Lowengrub and Truskinovsky (1997) and Anderson, McFadden and Wheeler (1998). In order to better understand the basic idea underlying the D.I. theory, let us remind briefly the classical approach to multiphase flow that is used in fluid mechanics. There, the equation of conservation of mass, momentum, energy and chemical species are written separately for each phase, assuming that temperature, pressure, density and composition of each phase are equal to their equilibrium values. Accordingly, these equations are supplemented by boundary conditions at the interface, namely (see for example Davis and Scriven, 1982),

$$|\Delta\tau|_{+}^{-} \cdot \mathbf{n} = \kappa\sigma\mathbf{n}; \tag{1}$$

$$|\Delta\mathbf{v}|_{+}^{-} = 0, \tag{2}$$

with $\mathbf{n}$ denoting the normal at the interface, stating that the jump of the stress tensor at the interface is related to the product of the curvature and the surface tension , while velocity $\mathbf{v}$ and temperature T are continuous (unless we introduce concepts such as surface viscosity and surface heat conductivity, so that they become discontinuous as well). Naturally, this results in a free boundary problem, which means that one of the main problems of this approach is to determine the position of the interface. To that extend, many interface tracking methods have been developed, which have proved very successful in a wide range of situations. However, there are few instances where the interface tracking breaks down. That happens when the interface thickness is comparable to the lengthscale of the phenomenon that is being studied, such as a) in near-critical fluids or partially miscible mixtures, as the interface thickness diverges at the critical point; b) near the contact line along a solid surface or in the breakup/coalescence of liquid droplets, as the related physical processes act on lengthscales that are comparable to the interface thickness. In addition, interface tracking becomes very problematic for self intersecting free boundaries. In front of these difficulties, the D.I. method offers an alternative approach. Quantities that in the free boundary approach are localized in the interfacial surface, here

are assumed to be distributed within the interfacial volume. For example, surface tension is the result of distributed stresses within the interfacial region, which are often called capillary, or Korteweg, stresses. In general, the interphase boundaries are considered as mesoscopic structures, so that any material property varies smoothly at macroscopic distances along the interface, while the gradients in the normal direction are steep. Accordingly, the main characteristic of the D.I. method is the use of an "order parameter" which undergoes a rapid but continuous variation across the interphase boundary, while it varies smoothly in each bulk phase, where it can even assume constant equilibrium values. For a single-component system, the order parameter is the fluid density ρ, for a liquid binary mixture it is the molar (or mass) fraction ϕ, while in other cases it can be any other parameter, not necessarily with any physical meaning, that allows to reformulate free boundary problems. In all these cases, the D.I. model must include a characteristic interface thickness, over which the order parameter changes. In fact, in the asymptotic limit of vanishing interfacial width, the diffuse interface model reduces to the classical free boundary problem. In Chapter 1 we formulate the diffuse interface model for single-component fluids and liquid binary mixtures at equilibrium, respectively. Then, in the next sections, the equations of motion are developed for non-dissipative systems, while at the end these results are generalized to the model dissipative systems. In Chapter 2, we presents some theory about the implementation of the model in and in Chapter 3 some results of numerical simulations are presented for the case of regular liquid binary mixtures, in particular in the first section is described an experimental result that it is used to validate the theoretical finding, in section two a validation of the code is presented based on reproducing the numerical results already published by Valdimirova et al. previously.

Chapter 1

Diffuse Interface Model

Reproduced in part from

"Diffuse Interface Model of Multiphase Fluids" D. Molin and R. Mauri, *Int. J. Heat Mass Tranf.*, submitted.

1.1 The free energy and Van der Waals' equation

All thermodynamical properties can be determined from the Helmholtz free energy. This, in turn, depends on the intermolecular forces which, in a dense fluid, are a combination of weak and strong forces. Fortunately, strong interactions nearly balance each other, so that the net forces acting on each molecule are weak and long-range. In addition, mean field approximation is assumed to be applicable, meaning that molecular interactions are smeared out and can be replaced by the action of a continuous effective medium (see discussion in Pismen, 2001). Based on these assumptions, the case of dense fluids can be treated as that of nearly ideal gases, so that, allowing for variable density, the molar Helmholtz free energy at constant temperature T can be written as (Landau & Lifshitz, 1980, Ch. 74):

$$f[\rho(\mathbf{x})] = f_{id} + \frac{1}{2} RTN_A \int \left(1 - e^{U(r)/kT}\right) \rho(\mathbf{x}+\mathbf{r}) d^3\mathbf{r}, \tag{1.1}$$

where k is Boltzmann's constant, $R = N_A k$ is the gas constant, with N_A the Avogadro number, U is the pair interaction potential, which depends on the distance $r = |\mathbf{r}|$, ρ is the molar density, while the factor $1/2$ compensates counting twice the interacting molecules. The first term on the RHS,

$$f_{id} = RT \ln \rho, \tag{1.2}$$

is the molar free energy of an ideal gas (where molecules do not interact). Now, we assume that the interaction potential consists of a long-range term,

decaying as r^{-6} (like in the Lennard-Jones potential), while the short-range term is replaced by a hard-core repulsion, i.e. (see Israelachvili, 1992)

$$U(r) = \begin{cases} -U_0(r/l)^6 & (r > d) \\ \infty & (r < d) \end{cases} \tag{1.3}$$

where d is the nominal hard-core molecular diameter, l is a typical intermolecular interaction distance, and the non-dimensional constant U_0 represents the strength of the intermolecular potential. When the density is constant, Eq. (1.1) gives the thermodynamic free energy, f_{Th},

$$f_{Th}(T, \rho) = f_{id}(T, \rho) + f_{ex}(T, \rho), \tag{1.4}$$

where

$$f_{ex}(T, \rho) = RT\rho B(T), \tag{1.5}$$

is the excess (i.e. the non ideal part) of the free energy, with

$$B(T) = \frac{1}{2} N_A \int_0^\infty (1 - e^{-U(r)/kT}) 4\pi r^2 dr \tag{1.6}$$

denoting the first virial coefficient. This integral can be solved as:

$$B(T) = 2\pi N_A \int_0^d r^2 dr + 2\pi N_A \int_d^\infty (1 - e^{\frac{U_0}{kT}(l/r)^6}) r^2 dr = b - \frac{a}{RT} \tag{1.7}$$

where

$$b = \frac{2}{3}\pi d^3 N_A \tag{1.8}$$

is the excluded molar volume and

$$a = \frac{2}{3}\pi U_0 N_A^2 l^6 / d^3 \tag{1.9}$$

is a pressure adding term. Finally we obtain:

$$f_{Th}(\rho, T) = f_{id} + RTb\rho - a\rho \approx RT \ln\left(\frac{\rho}{1 - b\rho}\right) - a\rho, \tag{1.10}$$

that is

$$f_{Th}(\rho, T) = RT \ln(v - b) - \frac{a}{v}, \tag{1.11}$$

where $v = \rho^{-1}$ is the molar volume. At this point, applying the thermodynamic equality (Landau & Lifshitz, 1980, Ch. 76) $P = -(\partial f/\partial v)_{N,T}$, we obtain van der Waals'equation,

$$\left(P + \frac{a}{v^2}\right)(v - b) = RT. \tag{1.12}$$

1.1.1 The critical point

In the $P-T$ diagram, the vapor-liquid equilibrium curve stops at the critical point, characterized by a critical temperature T_C and a critical pressure P_C. At higher temperatures, $T > T_C$ and pressures, $P < P_C$, the differences between liquid and vapor phases vanish altogether and we cannot even speak of two different phases In addition, as the critical point is approached, the difference between the specific volume of the vapor phase and that of the liquid phase decreases, until it vanishes at the critical point. Accordingly, near the critical point, since the specific volumes of the two phases, v and $v + \delta v$, are near to each other, we obtain:

$$P(T, v) = P(T, v + \delta v) = P(T, v) + \left(\frac{\partial P}{\partial v}\right)_T \delta v + \frac{1}{2}\left(\frac{\partial^2 P}{\partial v^2}\right)_T (\delta v)^2 + ..., \tag{1.13}$$

where we have considered that the two phases at equilibrium have the same pressure, in addition of having the same temperature. At this point, dividing by v and letting $\delta v \to 0$, we see that at the critical point we have:

$$\left(\frac{\partial P}{\partial v}\right)_T = 0, \text{ that is } \kappa_T \to \infty \text{ as } T \to T_C, \tag{1.14}$$

where κ_T is the isothermal compressibility. Note that this condition is the limit case of the inequality $(\partial P/\partial v)_T \leq 0$, which manifests the internal stability of any single-phase system. In addition, since near an equilibrium point, $\delta f + P\delta v > 0$, expanding δf in a power series of δv, with constant T, we obtain:

$$\begin{aligned} \delta f_{Th} &= \left(\frac{\partial f_{Th}}{\partial v}\right)_T (\delta v) + \frac{1}{2!}\left(\frac{\partial^2 f_{Th}}{\partial v^2}\right)_T (\delta v)^2 + \frac{1}{3!}\left(\frac{\partial^3 f_{Th}}{\partial v^3}\right)_T (\delta v)^3 \\ &+ \frac{1}{4!}\left(\frac{\partial^4 f_{Th}}{\partial v^4}\right)_T (\delta v)^4 + ... \end{aligned}$$

Finally, considering that $(\partial f_{Th}/\partial v)_T = -P$ and that at the critical point $(\partial^2 f_{Th}/\partial v^2)_T = 0$, we obtain:

$$\frac{1}{3!}\left(\frac{\partial^2 P}{\partial v^2}\right)_{T_C} (\delta v)^3 + \frac{1}{4!}\left(\frac{\partial^3 P}{\partial v^3}\right)_{T_C} (\delta v)^4 + ... < 0. \tag{1.15}$$

Since this equality must be valid for any value (albeit small) of δv (both positive and negative), we obtain:

$$\left(\frac{\partial^2 P}{\partial v^2}\right)_{T_C} = 0; \qquad \left(\frac{\partial^3 P}{\partial v^3}\right)_{T_C} < 0. \tag{1.16}$$

Therefore, the critical point corresponds to a horizontal inflection point in the $P - v$ diagram, which means that, since $P = -(\partial f_{Th}/\partial v)_T$,

$$\left(\frac{\partial^2 f_{Th}}{\partial v^2}\right)_{T_C} = 0; \qquad \left(\frac{\partial^3 f_{Th}}{\partial v^3}\right)_{T_C} = 0. \tag{1.17}$$

Imposing that at the critical point the $P-v$ curve has a horizontal inflection point, we can determine the constant a e b in the Van der Waals equation (the same is true for any 2 parameter cubic equation of state) in terms of the critical constant T_C and P_C, finding (Landau & Lifshitz, 1980, Ch. 84):

$$a = \frac{9}{8}RT_C v_C = \frac{27}{64}\frac{(RT_C)^2}{P_C} \quad \text{and} \quad b = \frac{1}{3}v_C = \frac{1}{8}\frac{RT_C}{P_C}. \tag{1.18}$$

Viceversa, the critical pressure, temperature and volume can be determined as functions of a and b as follows:

$$P_C = \frac{1}{27}\frac{a}{b^2}; \quad T_C = \frac{8}{27}\frac{a}{Rb}; \quad v_C = 3b; \quad Z_C = \frac{P_C v_C}{RT_C} = \frac{3}{8} = 0.375. \tag{1.19}$$

Note that, imposing that $P_C v_C = (3/8)RT_C$ and substituting the expressions for a and b in terms of the intermolecular potential, we obtain the following relation:

$$\left(\frac{l}{d}\right)^2 = \frac{3}{2}\left(\frac{kT_C}{U_0}\right)^{1/3} \tag{1.20}$$

Using these expressions, the Van der Waals equation can be written in terms of the reduced coordinates as:

$$\left(P_r + \frac{3}{v_r^2}\right)(3v_r - 1) = 8T_r; \quad P_r = \frac{P}{P_C}; \quad v_r = \frac{v}{v_C}; \quad T_r = \frac{T}{T_C}. \tag{1.21}$$

This equation represents a family of isotherms in the $P_r - v_r$ plane describing the state of any substance, which is the basis of the law of corresponding states. As expected, when $T_r > 1$, the isotherms are monotonically decreasing, in agreement with the stability condition $(\partial P/\partial v)_T < 0$, while when $T_r < 1$, each isotherm has a maximum and a minimum point and between them we have an instability interval, with $(\partial P/\partial v)_T > 0$, corresponding to the two-phase region (see Figure 1.3).

1.1.2 Coexistence and spinodal curves

Let us consider a one-component system at equilibrium, whose pressure and temperature are below their critical values, so that it is separated into two coexisting phases, say α and β. According to the Gibbs phase rule, these two phases have the same pressure and temperature and therefore, defining the Gibbs molar free energy $g_{Th} = f_{Th} + Pv$, with $dg_{Th} = -sdT + vdP$,

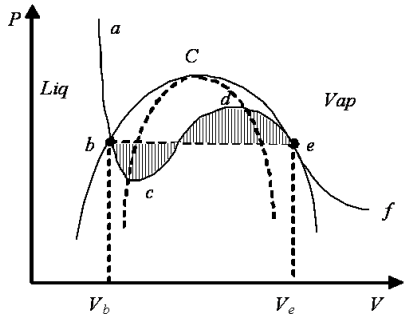

Fig. 1.1: Phase diagram $(P - v)$ of a single component fluid and $(\mu - \phi)$ of a binary mixture.

the corresponding equilibrium, or saturation, pressure P_{sat} at a given temperature can be easily determined from the equilibrium condition, stating that at equilibrium the Gibbs molar free energies of the two phases must be equal to each other. So we obtain:

$$g_{Th}^{\beta} - g_{Th}^{\alpha} = \int_b^e dg_{Th} = 0 \Longrightarrow \int_b^e v dP = \int_b^e v \left(\frac{\delta P}{\delta v}\right)_T dv = 0, \qquad (1.22)$$

where $P = P(v)$ represents an isotherm transformation. From a geometrical point of view, this relation manifests the equality between the shaded area of Figure 1.1 (Maxwell's rule), where the point b and e correspond to the equilibrium, or saturation, point of the liquid and vapor phases at that temperature at equilibrium, respectively, with specific volumes v_e^{α} and v_e^{β}. Conversely, the specific volumes of the two phases at equilibrium could also be determined from the molar free energy f_{Th}, rewriting Eq. (1.20) in terms of reduced coordinates as

$$\frac{f_{Th}}{RT_C} = T_r \ln(v_C) - T_r \ln\left(v_r - \frac{1}{3}\right) - \frac{9}{8v_r}. \qquad (1.23)$$

When $T_r < 1$, a typical curve of the free energy is represented in Figure 1.2. Now, keeping T_r fixed and considering that the two phases at equilibrium have the same pressure, using the relation $P = -(\partial f_{Th}/\partial v)_T$, we obtain:

$$P^{\alpha} = P^{\beta} \Longrightarrow \left(\frac{\partial f_{th}}{\partial v}\right)_T^{\alpha} = \left(\frac{\partial f_{Th}}{\partial v}\right)_T^{\beta}, \qquad (1.24)$$

which, in Figure 1.2, represents the fact that the two equilibrium points have the same tangent. From this relation we can determine the specific

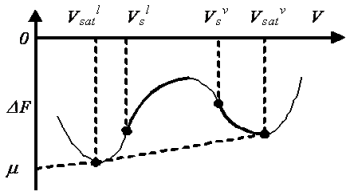

Fig. 1.2: Typical double-well curve of the free energy of a single component fluid.

volumes of the two phases at equilibrium, v_e^α and v_e^β. This relation can also be obtained considering that the specific volumes of the two phases at equilibrium minimizes the total free energy, i.e.

$$F_{Th} = \int \hat{f}_{Th}(\rho) d^3\mathbf{x} = min., \tag{1.25}$$

where $\hat{f} = \rho f$ is the free energy per unit volume,

$$\hat{f}_{Th} = \rho f_{Th} = \hat{f}_{id} + \hat{f}_{ex} = RT[\rho \ln \rho + \rho^2 B(T)]. \tag{1.26}$$

This minimization is carried over in Section 1.1.5. In Figure 1.1, besides the equilibrium curve, we have represented the, so called, spinodal curve, defined as the locus of all points (like c and d) satisfying $(\partial P/\partial v)_T = 0$. When the equilibrium and spinodal points are plotted in a $T - v$ diagram, we obtain the curves of Figure 1.3.

All points lying outside the region encompassing the equilibrium curve are stable and represent homogeneous, single-phase systems; all points lying inside the region within the bell-shaped spinodal curve are unstable and represent systems that will separate into two phases (one liquid and another vapor, in this case); the region sandwiched between the equilibrium and the spinodal curves represents metastable systems, that is overheated liquid and undercooled vapor. The spinodal points can be also determined using the relation $(\partial P/\partial v)_T = 0$, obtaining:

$$\left(\frac{\partial^2 f_{Th}}{\partial v^2}\right)_T = 0, \tag{1.27}$$

determining the spinodal specific volumes $\tilde{v}_s^\alpha$ and $\tilde{v}_s^\beta$.

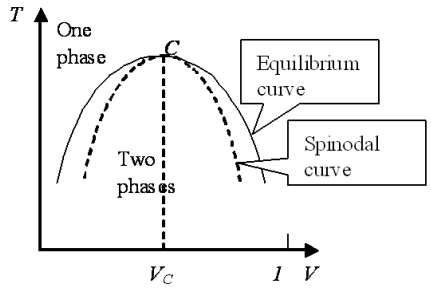

Fig. 1.3: Phase diagram $(T - v)$ of a single component fluid and $(T - \phi)$ of a binary mixture.

1.1.3 The critical exponents

Let us turn now to study the equation of state of a single component system close to its critical point. Then, instead of T, P and v, it is convenient to use the following variables:

$$\tilde{t} \equiv T_r - 1 = \frac{T - T_C}{T_C};\ \ \tilde{p} \equiv P_r - 1 = \frac{P - P_C}{P_C};\ \ \tilde{v} \equiv v_r - 1 = \frac{v - v_C}{v_C}, \quad (1.28)$$

where $T_r = T/T_C$, $P_r = P/P_C$ and $v_r = v/v_C$ are the reduced variables. At the end of a tedious, but elementary power expansion in terms of these variables, we see that the Van der Waals equation reads, neglecting higher order terms,

$$\tilde{p} = 4\tilde{t} - 5\tilde{t}\tilde{v} - \frac{3}{2}\tilde{v}^3. \quad (1.29)$$

Note that we cannot have any term proportional to $\tilde{v}$ or $\tilde{v}^2$, in agreement with the conditions $(\partial P/\partial\tilde{v})_{T_C} = (\partial^2 P/\partial\tilde{v}^2)_{T_C} = 0$, while the coefficient of the $\tilde{v}^3$-term must be negative, as $(\partial^3 P/\partial\tilde{v}^3)_{T_C} < 0$. When $\tilde{t} > 0$, all states of the system are stable, that is there is no phase separation and the system remains homogeneous. That means that, when $\tilde{t} > 0$, it must be $(\partial P/\partial\tilde{v})_{T_C} < 0$, and therefore the coefficient of the $\tilde{t}\tilde{v}$-term must be negative. Finally, note that the $\tilde{t}\tilde{v}^2$ and $\tilde{t}^2\tilde{v}$-terms have been neglected because they are much smaller than $\tilde{t}\tilde{v}$, while the $\tilde{t}\tilde{v}$-term must be kept, despite being much smaller than $\tilde{t}$, for reasons that will be made clear below. In general, in the vicinity of the critical point the isotherms of a homogeneous system can be written as

$$\tilde{p} = b_c\tilde{t} - 2a_c\tilde{t}\tilde{v} - 4B_c\tilde{v}^3. \quad (1.30)$$

This expression for the free energy is the basis of Landau's mean field theory (Landau & Lifshitz, 1980, Ch. 146, 148); it corresponds to Van der Waals' Eq. (1.29) with $a_c = 3, b_c = 4$ and $B_c = 3/8$. At the critical point, where $\tilde{t} = 0$, from (1.30) we obtain: $\tilde{p} \propto \tilde{v}^{\delta}$, where $\delta = 3$ is a critical exponent, that we find unaltered in all critical phenomena. Following an isotherms $\tilde{t} = costant$, in the unstable region between the spinodal points, where $(\partial P/\partial v)_T > 0$, the system separates into two coexisting phases. At equilibrium, the two specific volumes satisfy Eq. (1.24), and considering that

$$\left(\frac{\partial \tilde{p}}{\partial \tilde{v}}\right)_{\tilde{t}} = -2a_c\tilde{t} - 12B_c\tilde{v}^2, \tag{1.31}$$

we can determine the specific volumes of the two phases at equilibrium:

$$\tilde{v}_e^{\alpha} = -\tilde{v}_e^{\beta} = \sqrt{\frac{-a_C\tilde{t}}{2B}} \quad \Rightarrow \quad \Delta\tilde{v}_e^{\alpha\beta} = \tilde{v}_e^{\alpha} - \tilde{v}_e^{\beta} \propto (-\tilde{t})^{\beta}, \tag{1.32}$$

where $\beta = 1/2$ is another critical exponent. Now we see why we could not neglect the $\tilde{v}\tilde{t}$ term: if we did it, the two specific volumes would result equal to each other. Note that the difference between the specific volumes of points that lye on the spinodal curve can be determined as well, applying the condition $(\partial\tilde{p}/\partial\tilde{v})_{\tilde{T}} = 0$, obtaining:

$$\tilde{v}_s^{\alpha} = -\tilde{v}_s^{\beta} = \sqrt{\frac{-a_c\tilde{t}}{6B_c}}. \tag{1.33}$$

The critical properties can also be determined from the free energy f_{Th}. In fact, integrating $(df_{Th})_T = -Pdv$ and substituting (1.30), we see that in the vicinity of the critical point the free energy has the following expression:

$$f_{Th}(\tilde{v}, \tilde{T}) = P_C v_C[h(\tilde{T}) + (1 + b_c\tilde{T})\tilde{v} + a_c\tilde{T}\tilde{v}^2 + B_c\tilde{v}^4], \tag{1.34}$$

where $h(\tilde{t})$ is an undetermined function of the temperature. For a Van der Waals system, we obtain the same result expanding (1.21); in that case, $h(\tilde{t}) = (1 + \tilde{t})\ln[3/(2v_C)] - 9/8$. Finally, applying (1.24) and (1.27), we obtain again (1.32) and (1.33). Another critical exponent, γ , is defined as $\kappa_T^{-1} \propto \tilde{t}^{\gamma}$, where κ_T is the isothermal compressibility coefficient. From its definition, we obtain:

$$\kappa_T^{-1} = -v\left(\frac{\partial P}{\partial v}\right)_T = -P_C(1 + \tilde{v})\left(\frac{\partial \tilde{p}}{\partial \tilde{v}}\right)_{\tilde{T}} \cong 2a_c P_C\tilde{t}, \tag{1.35}$$

showing that $\gamma = 1$. On the equilibrium curve, with $\tilde{t} < 0$ and $\tilde{v} = 0$, we have $\tilde{p} = b_c\tilde{t}$ [see Eq. (1.30)]. Therefore, applying the Clausius-Clapeyron equation,

$$\left(\frac{dP}{dT}\right)^{sat} = \frac{\Delta h^{\alpha\beta}}{T(v^{\beta} - v^{\alpha})} \Longrightarrow \frac{d\tilde{P}}{d\tilde{t}} = b \cong \frac{\Delta h^{\alpha\beta}}{P_C v_C(\tilde{v}^{\beta} - \tilde{v}^{\alpha})}, \tag{1.36}$$

where $\Delta h^{\alpha\beta}$ is the latent heat of vaporization, we obtain an expression for $\Delta h^{\alpha\beta}$ near the critical point,

$$\Delta h^{\alpha\beta} \cong b_c R T^C (\tilde{v}^\beta - \tilde{v}^\alpha) = \sqrt{\frac{a_c b_c^2}{B_c}} R T^C \sqrt{-\tilde{t}}, \tag{1.37}$$

where we have substituted Eq. (1.32), considering that $P_C V_C \cong R T_C$. From this equation we see that on approaching the critical point the latent heat of evaporation vanishes like $\sqrt{-\tilde{t}}$.

Finally, the last thermodynamical quantity to be determined is the specific heat. From the definition, $c_v = (\partial u_{Th}/\partial T)_V$, where u_{Th} is the molar internal energy, and considering that $u_{Th} = f_{Th} + Ts = f_{Th} - T(\partial f_{Th}/\partial T)_v$, we obtain from Eq. (1.34)

$$c_v^{sat} = \frac{P_C v_C}{T_C} \left[1 + b_c + f_{Th}(0) - \frac{df_{Th}}{d\tilde{t}}(0) \right]. \tag{1.38}$$

Therefore, we see that c_v^{sat} remains finite at the critical point and it does not depend on $\tilde{t}$, that is $c_v \propto \tilde{t}^\alpha$, where $\alpha = 0$ is another critical exponent. Consequently, using the well known relation

$$c_p - c_v \propto \left[\left(\frac{\partial \tilde{p}}{\partial \tilde{t}} \right)_{\tilde{v}} \right]^2 \Big/ \left(\frac{\partial \tilde{p}}{\partial \tilde{v}} \right), \tag{1.39}$$

we see that, since $(\partial \tilde{p}/\partial \tilde{t})_{\tilde{t}=0,\tilde{v}=0} = b_c$ and $(\partial \tilde{p}/\partial \tilde{v})_{\tilde{t}=0,\tilde{v}=0} = 0$, the specific heat c_p diverges. In fact, we find:

$$c_p \propto \frac{1}{(\partial \tilde{p}/\partial \tilde{t})_{\tilde{t}}} = \frac{1}{-2a_c\tilde{t} - 12B_c\tilde{v}^2} \propto \frac{1}{\tilde{t}}, \tag{1.40}$$

where we have considered that on the equilibrium curve, $\tilde{v} \propto \sqrt{\tilde{t}}$. It has been shown (see Le Bellac, Ch. 1.3) that the mean field theory provides results that compare favorably with those that have been obtained by molecular dynamics simulations.

1.1.4 The diffuse interface

Suppose now that the molar density of the system is not constant. Accordingly, when $U \ll kT$, Eq. (1.1) can be rewritten as

$$f(\mathbf{x}) = f_{Th}(\mathbf{x}) + \Delta f_{NL}(\mathbf{x}), \tag{1.41}$$

where f_{Th} is the molar free energy (1.4) corresponding to a system with constant density, while

$$\Delta f_{NL}(\mathbf{x}) = \frac{1}{2} N_A^2 \int_{r>d} U(r)[\rho(\mathbf{x}+\mathbf{r}) - \rho(\mathbf{x})] d^3\mathbf{r}, \tag{1.42}$$

is a non local molar free energy, due to density changes, typical of the diffuse interface model. In fact, when there is an interface separating two phases at equilibrium, this term corresponds to the interfacial energy. This result is a direct consequence of the "exact" expression (1.1), showing that the free energy is non-local, that is its value at any given point does not depend only on the density at that point, but it depends also on the density at neighboring points. As stated by Van der Waals (1893), "the error that we commit in assuming a dependence on the density only at the point considered vanishes completely when the state of equilibrium is that of a homogeneous distribution of the substance. If, however, the state of equilibrium is one where there is a change of density throughout the vessel, as in a substance under the action of gravity, then the error becomes general, however feeble it may be." Now, in (1.42) the density can be expanded as

$$\rho(\mathbf{x}+\mathbf{r}) = \rho(\mathbf{x}) + \mathbf{r}\cdot\nabla\rho + \frac{1}{2}\mathbf{rr} : \nabla\nabla\rho + .. \tag{1.43}$$

As we have tacitly assumed that the system is isotropic, we see that the contribution of the linear term vanishes, so that, at leading order, we obtain (Pismen, 2001):

$$\Delta f_{NL}(\mathbf{x}) = -\frac{1}{2}RTK\nabla^2\rho(\mathbf{x}), \tag{1.44}$$

with

$$K = \frac{2\pi}{3}\frac{N_A U_0}{kT}\frac{l^6}{d} = \frac{9\pi}{4}\frac{T_C}{T}N_A d^5, \tag{1.45}$$

where we have substituted (1.20). Note that, defining a non-dimensional molar, $\tilde{\rho} = N_A d^3\rho$, the non local free energy can be rewritten as

$$\Delta f_{NL}(\mathbf{x}) = -\frac{1}{2}RTa^2\nabla^2\tilde{\rho}(\mathbf{x}), \tag{1.46}$$

where

$$a = \sqrt{\frac{K}{N_A d^3}} = \sqrt{\frac{9\pi T_C}{4T}}d \tag{1.47}$$

is the characteristic length. The total free energy is therefore:

$$F = \int_V \hat{f} dV d^3\mathbf{x}, \tag{1.48}$$

where $\hat{f} = \rho f$ is the free energy per unit volume. Now, observing that, integrating by part,

$$\int \rho(\mathbf{x})\nabla^2\rho(\mathbf{x})d^3\mathbf{x} = -\int |\nabla\rho(\mathbf{x})|^2 d^3\mathbf{x}, \tag{1.49}$$

we see that the free energy per unit volume is:

$$\begin{aligned}\hat{f}(\rho,\nabla\rho,T) &= RT\left[\rho\tilde{f}_{Th}(\rho,T) + \frac{1}{2}K(T)(\nabla\rho)^2\right] \\ &= RT\left[\rho\ln\rho + B(T)\rho^2 + \frac{1}{2}K(T)(\nabla\rho)^2\right],\end{aligned}$$

where $\tilde{f}_{Th} = f_{Th}/RT$. Now, at equilibrium, the total free energy F will be minimized, subjected to the constraint of having a constant number of moles, $\int \rho d^3\mathbf{x} = const$. Accordingly, introducing a Lagrange multiplier, $RT\tilde{\mu}$, the minimization condition is:

$$\delta \int (\rho f - RT\tilde{\mu}\rho) d^3\mathbf{x} = 0, \tag{1.50}$$

that is,

$$\delta \int \rho(\mathbf{x})[\tilde{f}_{Th}[\rho(\mathbf{x})] - \tilde{\mu}] + \frac{1}{2}K|\nabla\rho(\mathbf{x}|^2) d^3\mathbf{x} = 0. \tag{1.51}$$

1.1.5 The generalized chemical potential

The Euler-Lagrange equation corresponding to the minimization condition (1.51) is (see derivation in Section 1.2.5):

$$\tilde{\mu} = \frac{1}{RT}\frac{\delta(\rho\hat{f})}{\delta\rho} = \frac{d(\rho\tilde{f}_{Th})}{d\rho} - K\nabla^2\rho. \tag{1.52}$$

Now, by definition, $RT\tilde{\mu} = f_{Th} - v(\partial f_{Th}/\partial v)_T$ is Gibbs free energy, which, in a one-component system, coincides with the chemical potential, i.e.,

$$\tilde{\mu}_{Th} = \frac{d(\rho\tilde{f}_{Th})}{d\rho} = \tilde{f}_{Th} - v\frac{d\tilde{f}_{Th}}{dv}. \tag{1.53}$$

This (apart from the dimensional constant RT) is the equation of the straight line represented in Figure 1.2, stating that two phases at mutual equilibrium have the same chemical potential. Therefore, Eq. (1.52) can be rewritten as

$$\tilde{\mu}(\rho, \nabla\rho) = \tilde{\mu}_{Th}(\rho) - K\nabla^2\rho, \tag{1.54}$$

showing that at equilibrium, when ρ is non-uniform, it is $\tilde{\mu}$, and not $\tilde{\mu}_{Th}$, that remains uniform. Note that the thermodynamic chemical potential, $\tilde{\mu}_{Th}$, can be determined from the solvability condition of Eq. (1.53), that is:

$$\tilde{\mu}_{Th} = \frac{\rho^\alpha\tilde{f}^\alpha_{Th} - \rho^\beta\tilde{f}^\beta_{Th}}{\rho^\alpha - \rho^\beta} = \frac{v^\alpha\tilde{f}^\alpha_{Th} - v^\beta\tilde{f}^\beta_{Th}}{v^\alpha - v^\beta}, \tag{1.55}$$

as it can also be seen geometrically from Figure 1.2, stating that the chemical potential equals the intercept of the tangent line on the $v = 0$ vertical axis. Accordingly, as at the critical point this tangent line becomes horizontal, there the chemical potential must vanish [this result can also be obtained from Eq. (1.32) and (1.34)]. When two phases are coexisting at equilibrium, separated by a planar interfacial region centered on $z = 0$, Eq. (1.52) can be solved once the equilibrium molar free energy f is known, imposing that, far from the interface region, the density is constant and equal to its

equilibrium value, so that the generalized chemical potential is equal to its thermodynamic value (1.53). In particular, in the vicinity of the critical point, the chemical potential vanishes, the free energy is given by Eq. (1.34) and we obtain at leading orders the following equation:

$$\frac{d^2\tilde{v}}{d\tilde{z}^2} - 2a\tilde{t}\tilde{v} - 4B\tilde{v}^3 = 0, \qquad \tilde{z} = z/\lambda; \qquad \lambda = \sqrt{\frac{K}{v_C(-a\tilde{t})}}, \tag{1.56}$$

to be solved imposing that

$$\tilde{v}(\tilde{z} \longrightarrow \pm\infty) = \pm\tilde{v}_e = \pm\sqrt{\frac{-a\tilde{t}}{2B}}.$$

The solution, due (again!) to Van der Waals (1893), is:

$$\tilde{v}(\tilde{z}) = \tilde{v}_e \tanh \tilde{z}, \tag{1.57}$$

showing that λ is a typical interfacial thickness. For a Van der Waals system, considering that K is given by Eq. (1.45), $v_C = 3b = 6\pi d^3 N_A$ and $a = 3$, we obtain:

$$\lambda = \sqrt{\frac{A}{27(-\tilde{t})}}\frac{l^3}{d^2} = \sqrt{\frac{1}{8(-\tilde{t})}}d, \tag{1.58}$$

where we have substituted Eq. (1.20). As expected, the interfacial thickness diverges like $(-\tilde{t})^{-1/2}$ as we approach the critical point, while far from the critical point it is of $O(d)$. Recently, Pismen (2001) pointed out that Eq. (1.56) is flawed, as some of the neglected terms diverge at the critical point. In fact, Pismen showed that in the correct solution the specific volume tends to its equilibrium value as $|z|^{-4}$, instead of exponentially, as in the Van der Waals solution.

1.1.6 The surface tension

In the previous section we have seen that the total free energy is the sum of a thermodynamical, constant density, part, and a non local contribution (1.42). When the system is composed of two phases at equilibrium, separated by a plane interfacial region, we may define the surface tension as the energy per unit area stored in this region. This quantity can be calculated through the following integral:

$$\sigma = -\frac{1}{2}RTK\int_{-\infty}^{\infty}\rho\frac{d^2\rho}{dz^2}dz = \frac{1}{2}RTK\int_{-\infty}^{\infty}\left(\frac{d\rho}{dz}\right)^2 dz, \tag{1.59}$$

where we have integrated by parts and considered that, outside the interfacial region, the integrand is identically zero as density is constant. We see that, near the critical point,

$$\sigma \approx RT_C K(\Delta\rho_e)^2/\lambda \approx \frac{kT_C}{d^2}(-\tilde{t})^{3/2}, \tag{1.60}$$

where we have considered Eqs. (1.32), (1.45) and (1.58). In fact, using the density profile (1.57), Eq. (1.59) yields, for a Van der Waals system:

$$\sigma = \frac{2}{3} RT_C(-a\tilde{t})^{3/2} \left(\frac{K}{v_c^3}\right) = C\frac{kT_C}{d^2}(-\tilde{t})^{3/2}, \tag{1.61}$$

with $C = 3^{3/2}/(2^{3/2}\pi)$, where we have used Eq. (1.20). These results show that the surface tension decreases as we approach criticality, until it vanishes at the critical point. A more detailed numerical solution based on the solution of the Van der Waals equation can be found in Pismen and Pomeau (2000). Applying this approach, Van der Waals (1893) showed that in a curved interface region there arises a net force [see Section 1.3.1], which is compensated by a pressure term, thus obtaining the Young-Laplace equation. To see that, let us denote the position of the interface by $z = h(\xi)$, where ξ is the 2D vector in the support plane, and assume that $|\nabla_\xi h| \ll 1$, where $|\nabla_\xi h|$ is the 2D gradient (see Pismen, 2001). Now, the free energy increment due to the interface curvature can be written as

$$\Delta F = \sigma \int \left(\sqrt{1 + |\nabla_\xi h|^2} - 1\right) d^2\xi \approx \frac{1}{2}\sigma \int |\nabla_\xi h|^2 d^2\xi. \tag{1.62}$$

This increment is the free energy induces an increment in the pressure,

$$\Delta P = \delta F/\delta h = -\sigma\nabla^2 h = -\kappa\sigma, \tag{1.63}$$

where $\kappa = \nabla^2 h$ is the curvature of a weekly curved interface. Applying a rigorous regular perturbation approach to Eq. (1.52), Pismen (2000) derived both the Young-Laplace equation (1.63) and the Gibbs-Thomson law, relating the equilibrium temperature or pressure to the interfacial curvature.

1.2 Binary mixtures

In this Section we will show that Van der Waals' approach can be applied to study binary solutions. To simplify matters, at first let us confine ourselves to the case of regular binary solutions, that are mixtures in which the volume and the entropy of mixing are both equal to zero. That means that when we mix the two species, say 1 and 2, a) the volume remains unchanged, so that the mixture can be considered to be incompressible, and b) the entropy change is equal to that of ideal mixtures (see Sandler, 1999, Section 7.6). Generalization to non regular, even compressible, binary mixtures can be found in Lowengrub and Truskinovsky (1997).

1.2.1 The Gibbs free energy

The molar free energy can be determined using the same procedure as for single component systems. Consider a mixture composed of species 1 and

species 2, with molar fraction $x_1 = \phi$ and $x_2 = (1 - \phi)$ and let us first determine the molar free energy when the composition of the mixture is uniform. Considering the definition of Gibbs free energy, $g = f + P/\rho$, from Eq. (1.1) we obtain:

$$g_{Th}(\phi) = g_{id}(\phi) + g_{ex}(\phi). \tag{1.64}$$

Here g_{id} is the Gibbs free energy of an ideal mixture, that is a mixture where the intermolecular potentials U_{ij} between molecule i and molecule j are all the same, i.e. $U_{11} = U_{22} = U_{12}$. Generalizing the expression of the free energy for a single component fluid, $RT \ln \rho$, we obtain:

$$g_{id} = RT[x_1 \ln(x_1\rho) + x_2 \ln(x_2\rho)],$$

that is:

$$g_{id} = RT \ln \rho + RT[\phi \log \phi + (1 - \phi) \log(1 - \phi)]. \tag{1.65}$$

Note that for a pure fluid the molar density ρ is a variable, while for a regular binary mixture the total molar density ρ can even be constant, since the variables are the molar densities of the two components, $x_1\rho$ and $x_2\rho$.

The second term in the RHS of Eq. (3.44), g_{ex}, is the so called excess, that is non ideal, part of the free energy. This term has a particularly convenient form for regular mixtures, as it is explained below. The theory of regular mixtures was developed by Van Laar (a student of van der Waals), who assumed that (a) the two species composing the mixture are of similar size and energies of interaction, and (b) the Van der Waals equation of state applies to both the pure fluids and the mixture. Consequently, regular mixtures have negligible excess volume and excess entropy of mixing, i.e. their volume and entropy coincide with those of an ideal gas mixture, with $s_{ex} = 0$ and $v_{ex} = 0$. Therefore, we see that for a regular mixture, since $s_{ex} = -(\partial g_{ex}/\partial T)_{P,x} = 0$, then g_{ex} must be independent of T. In addition, as the excess Gibbs free energy results to be equal to the excess internal energy, i.e. $g_{ex} = u_{ex}$, it can be shown (see Sandler, 1999, Section 7.6) that the Gibbs free energy of a regular mixture with molar fractions x_1 and $x_2 = 1 - x_1$ is:

$$g_{ex} = x_1 \frac{a_1}{b_1} + x_2 \frac{a_2}{b_2} - \frac{a_{mix}}{b_{mix}}, \tag{1.66}$$

where we have used obvious notations to indicate the Van der Waals constants (a and b) for the pure fluids, 1 and 2, and for the mixture, and we have considered that $u_{ex} = a/b$. From here, assuming that

$$b_{mix} = b_1 = b_2; \quad a_{mix} = x_1^2 a_1 + x_2^2 a_2 + 2x_1 x_2 a_{12}, \tag{1.67}$$

with $a_{12} = \sqrt{a_1 a_2}$, we obtain,

$$g_{ex} = \frac{1}{b} x_1 x_2 (a_1 + a_2 - 2\sqrt{a_1 a_2}). \tag{1.68}$$

Thus, we see again that the excess free energy does not depend on T, so that $s_{ex} = 0$. Similar considerations can be applied to the dependence of the free energy on the pressure, confirming that $v_{ex} = 0$ for regular mixtures.

The same conclusions can be reached starting from the fundamental expression (1.1) for the Helmholtz free energy and considering that:

$$g_{ex} = f_{ex} + Pv_{ex}. \tag{1.69}$$

Applying Eq. (1.20) to a system with constant molar density ρ, i.e. with $v_{ex} = 0$, we obtain: $g_{ex} = f_{ex} = RT\rho B$, where B is the virial coefficient,

$$B = x_1^2 B_{11} + 2x_1 x_2 B_{12} + x_2 B_{22}. \tag{1.70}$$

Here B_{ij} characterizes the repulsive interaction between molecule i and molecule j [see Eq. (1.6)],

$$B_{ij} = \frac{1}{2} N_A \int \left[1 - \exp\left(-\frac{U_{ij}(r)}{kT} \right) \right] d^3\mathbf{r}. \tag{1.71}$$

In particular, for symmetric solutions, $U_{11} = U_{22} \neq U_{12}$, so that $B_{11} = B_{22} \neq B_{12}$. Accordingly, denoting $x_1 = \phi$, we obtain:

$$g_{ex} = \rho RTB = 2\rho RT(B_{12} - B_{11})\phi(1 - \phi),$$

that is,

$$g_{ex}(T, P, \phi) = RT\Psi(T, P)\phi(1 - \phi), \tag{1.72}$$

where

$$\Psi(T, P) = 2\rho(B_{12} - B_{11}), \tag{1.73}$$

is the so called Margules coefficient (Sandler, 1999). In particular, for an ideal mixture, $B_{11} = B_{12}$ and therefore $\Psi = 0$. For a mixture composed of Van der Waals fluids at constant pressure, substituting the expression (1.6) for B and assuming that the characteristic lengths d and l are the same for the two species, we obtain:

$$\Psi = \frac{2\rho}{RT}(a_{11} - a_{12}) = \frac{4\pi}{3} \frac{\rho N_A^2 l^6}{RTd^3}(U_{0,11} - U_{0,12}), \tag{1.74}$$

where $U_{0,11}$ and $U_{0,12}$ characterize the strength of the potential between molecules of the same species and that of different species, respectively. From this expression we see that $\Psi \propto T^{-1}$, confirming that g_{ex} is independent of T. Note that when $\Psi > 0$ the repulsive forces $\cong U_{0,12}/d$ between unlike molecules are weaker than those between like molecules, $\cong U_{0,11}/d$. As shown in Mauri, Shinnar and Triantafyllou (1996), when the solution is not symmetric, this approach is easily generalized by defining two Margules coefficients.

1.2.2 Coexistence and spinodal curve

In the previous Section, we saw that the free energy of a homogenous symmetric binary mixture can be written as:

$$g_{Th} = g_1 + RT[\phi \log \phi + (1-\phi)\log(1-\phi) + \Psi\phi(1-\phi)]. \tag{1.75}$$

Now, the thermodynamic state of a one-component system is determined by fixing two quantities, e.g. P and T. In binary mixtures, we have an additional degree of freedom, i.e. the molar fraction of the two species, x_1. Associated with x_1 and x_2 we can define the respective chemical potentials, $RT\mu_i = \partial(Ng_{Th}/N_i)_{j\neq i}$. Generalizing the relation obtained in the previous Section, at equilibrium the chemical potentials μ_1 and μ_2 are uniform everywhere and, in particular, they must be the same in each phase, i.e. $\mu_1^\alpha = \mu_1^\beta$ and $\mu_2^\alpha = \mu_2^\beta$. Considering that x_1 and x_2 depend on each other, there is a relation between μ_1 and μ_2, namely the Gibbs-Duhem relation (see Sandler, 1999), $x_1\nabla\mu_1 = -x_2\nabla\mu_2$. This relation can be easily obtained by imposing that the specific Gibbs free energy, g_{th}, defined as,

$$Ng_{Th} = Nu_{Th} - NTs + NPv + RTN_1\mu_1 + RTN_2\mu_2, \tag{1.76}$$

where u_{Th} is the molar internal energy, must satisfy the following equality,

$$dg_{Th} = -sdT + vdP + RT\mu d\phi, \tag{1.77}$$

where $\mu = \mu_1 - \mu_2$ is the chemical potential difference. This last relation reveals that the chemical potential difference is the quantity that is thermodynamically conjugated with the composition ϕ. This same result can be obtained from the identities (Sandler, 1999),

$$RT\mu_1(T,P,\phi) = g_{Th}(T,P,\phi) + \left(\frac{dg_{Th}}{d\phi}\right)(1-\phi), \tag{1.78}$$

$$RT\mu_2(T,P,\phi) = g_{Th}(T,P,\phi) + \left(\frac{dg_{Th}}{d\phi}\right)\phi, \tag{1.79}$$

obtaining,

$$\mu = \mu_1 - \mu_2 = \frac{d(g_{Th/RT})}{d\phi} = \log\left(\frac{\phi}{1-\phi}\right) + \Psi(1-2\phi), \tag{1.80}$$

where we have substituted Eq. (1.75). At constant temperature T and pressure P, since Ψ is a known function of T and P, this equation gives the dependence of the chemical potential difference on the composition, just like the equation of state, e.g. Van der Waals' equation, gives the dependence of the pressure on the specific volume. Clearly, μ represents the tangent to the free energy curve and it is the same for the two phases at equilibrium.

Accordingly, this equation leads to the determination of the equilibrium composition of the two coexisting phases, ϕ_e^α and ϕ_e^β. In particular, in our case, where we have considered symmetric mixtures, the tangent is horizontal and therefore $\mu = 0$. Note that, as expected, in this case $\phi_e^\alpha = 1 - \phi_e^\beta$. Now we can apply to binary mixtures the same considerations about the critical point that we made in the previous Section on one-component systems, observing that chemical potential difference μ and composition ϕ play the same role as pressure and density (or specific volume). In fact, in the $\mu - T$ diagram, the liquid-liquid equilibrium curve stops at the critical point, characterized by a critical temperature T_C and a critical chemical potential difference, $\mu_C = 0$ (note that for symmetric mixtures $\mu = 0$ at any equilibrium state, while in general that is true only at the critical point). At higher temperatures, $T > T_C$, the differences between the two liquid phases vanish altogether and the system is always in a single phase. In addition, as the critical point is approached from below (i.e. with two coexisting phases), the difference between the composition of the two phases decreases, until it vanishes altogether at the critical point. Accordingly, near the critical point, since the composition of the two phases, ϕ and $\phi + \delta\phi$, are near to each other, we obtain (Landau and Lifshitz, 1980, Ch. 97):

$$\begin{aligned} 0 = \mu_C(T,\phi) &= \mu_C(T,\phi+\delta\phi) \Longrightarrow 0 = \left(\frac{\partial\mu}{\partial\phi}\right)_{T_C,P_C} \delta\phi \\ &+ \frac{1}{2}\left(\frac{\partial^2\mu}{\partial\phi^2}\right)_{T_C,P_C} (\delta\phi)^2 + ..., \end{aligned}$$

where we have considered that, since the two phases are at equilibrium, they have the same chemical potential (in addition to having the same pressure and temperature). At this point, dividing by $\delta\phi$ and letting $\partial\phi \longrightarrow 0$, we see that at the critical point we have:

$$\left(\frac{\partial\mu}{\partial\phi}\right)_{T_C,P_C} = 0. \tag{1.81}$$

Note that this condition is the limit case of the inequality $(\partial\mu/\partial\phi)_{T,P} \leq 0$, which manifests the internal stability of any two-phase system. In addition, expanding δg_{Th} in a power series of $\delta\phi$, with constant T and P, we obtain:

$$\begin{aligned} \delta g_{Th} &= \left(\frac{\partial g_{Th}}{\partial\phi}\right)_{T,P} (\delta\phi) + \frac{1}{2!}\left(\frac{\partial^2 g_{Th}}{\partial\phi^2}\right)_{T,P} (\delta\phi)^2 + \frac{1}{3!}\left(\frac{\partial^3 g_{Th}}{\partial\phi^3}\right)_{T,P} (\delta\phi)^3 \\ &+ \frac{1}{4!}\left(\frac{\partial^4 g_{Th}}{\partial\phi^4}\right)_{T,P} (\delta\phi)^4 + .. \end{aligned}$$

Therefore, since near an equilibrium point, we have:

$$\delta u_{Th} - T\delta s + P\delta v - RT\mu\delta\phi = \delta g_{Th} - RT\mu\delta\phi > 0,$$

considering that $(\partial g_{Th}/\partial\phi)_{T,P} = RT\mu$ and that at the critical point $(\frac{\partial^2 g_{Th}}{\partial\phi^2})_{T,P} = 0$, we obtain:

$$\frac{1}{3!}\left(\frac{\partial^2\mu}{\partial\phi^2}\right)_{T_C,P_C}(\delta\phi)^3 + \frac{1}{4!}\left(\frac{\partial^3\mu}{\partial\phi^3}\right)_{T_C,P_C}(\delta\phi)^4 + .. > 0. \tag{1.82}$$

Since this equality must be valid for any value (albeit small) of $\partial\phi$ (both positive and negative), we obtain:

$$\left(\frac{\partial^2\mu}{\partial\phi^2}\right)_{T_C,P_C} = 0; \qquad \left(\frac{\partial^3\mu}{\partial\phi^3}\right)_{T_C,P_C} > 0. \tag{1.83}$$

Therefore, the critical point corresponds to a horizontal inflection point in the $\mu - \phi$ diagram (see Figure 1.1), which means that,

$$\left(\frac{\partial^2 g_{Th}}{\partial\phi^2}\right)_{T_C,P_C} = 0; \qquad \left(\frac{\partial^3 g_{Th}}{\partial\phi^3}\right)_{T_C,P_C} = 0. \tag{1.84}$$

Imposing that at the critical point the $\mu-\phi$ curve has a horizontal inflection point, from Eq. (1.80) we see that $\phi_C^\alpha = \phi_C^\beta = 1/2$, confirming that $\Psi_C = 2$. Therefore, considering that $\Psi \propto T^{-1}$, we obtain:

$$\Psi = \frac{2T_C}{T} \tag{1.85}$$

In particular, near the critical point, defining $\tilde{\psi} = (\Psi - 2)/2$ and $\tilde{t} = (T_C - T)/T_C$, we obtain at leading order:

$$\tilde{\psi} = -\tilde{t}. \tag{1.86}$$

Now, let us consider a binary liquid mixture at equilibrium, whose chemical potential difference and temperature are below their critical values, so that the mixture is separated into two coexisting phases. At equilibrium, the phase transition takes place at constant temperature, pressure and chemical potential difference and therefore it can be represented as a horizontal isotherm isobaric segment in a $\mu - \phi$ diagram. Now, define a generalized potential (see Landau and Lifshitz, 1980, Ch. 85) as $\Phi_{Th} = g_{Th} - \mu\phi$, with $d\Phi_{Th} = -sdT + vdP - RT\phi d\mu$ and $(\partial\Phi/\partial\mu)_{T,P} = RT\phi$. The chemical potential difference μ at a given temperature and pressure can be easily determined, considering that at equilibrium the generalized potentials of the two phases must be equal to each other, that is

$$\Phi_{Th}^\beta - \Phi_{Th}^\alpha = \int_b^e d\Phi_{Th} = 0 \Rightarrow \int_b^e \phi d\mu = \int_b^e \phi\left(\frac{\partial\mu}{\partial\phi}\right)_{T,P} d\phi = 0, \tag{1.87}$$

where we have considered that the phase transition is isothermal and isobaric. From a geometrical point of view, this relation manifests the equality

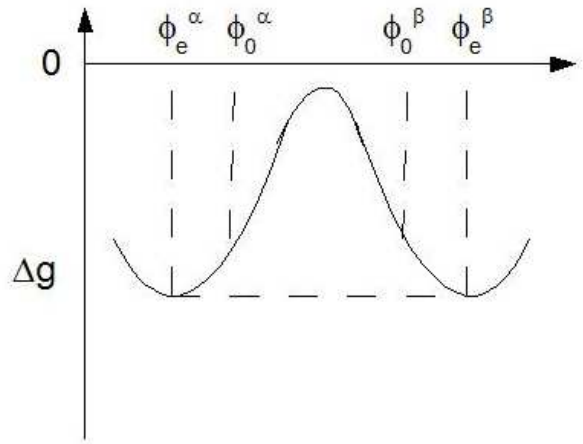

Fig. 1.4: Typical double-well curve of the free energy of a symmetric binary mixture.

between the shaded area of Figure 1.1 (Maxwell's rule), where the point b and e correspond to the saturation points of the two phases at that temperature and pressure, with compositions ϕ^{α} and ϕ^{β}. Conversely, the composition of the two phases at equilibrium can be determined from the molar free energy g of Eq. (1.75) as follows. A typical curve of the free energy g for a symmetric binary mixture is represented in Figure 1.4, when $T < T_C$ (i.e. when $\Psi > 2$). The condition (1.87) expresses the fact that at equilibrium the two phases have the same temperature, pressure and chemical potential (so that the chemical potential difference μ is identically zero). Being on an isotherm-isobar, the first two conditions are automatically satisfied while, using the relation $\mu = (\partial g/\partial\phi)_{T,P}$, the last condition gives:

$$\mu^{\alpha} = \mu^{\beta} = 0 \Longrightarrow \left(\frac{\partial g_{Th}}{\partial \phi}\right)_{T,P}^{\alpha} = \left(\frac{\partial g_{Th}}{\partial \phi}\right)_{T,P}^{\beta} \Longrightarrow (\phi_e^{\alpha}, \phi_e^{\beta}), \qquad (1.88)$$

which, in Figure 1.4, represents the fact that the two equilibrium point have the same tangent and this tangent is a horizontal line. When the mixture is not symmetric, the $g_{Th} - \phi$ curve is similar to the $f_{Th} - v$ curve of Figure 1.2. Consequently, it is still true that $\mu^{\alpha} = \mu^{\beta}$, but, in general, they are not equal to zero, i.e. the tangent to the Gibbs free energy curve is not horizontal.

In Figure 1.1, besides the equilibrium curve, we have represented the, so called, spinodal curve, defined as the locus of all points (like c and d)

satisfying $(\partial\mu/\partial\phi)_{T,P} = 0$. When the equilibrium and spinodal points are plotted in a $T - \phi$ diagram (at constant pressure), we obtain the curves of Figure 1.3. All points lying outside the region encompassing the equilibrium curve represent homogeneous, single-phase mixtures in a state of stable equilibrium, while all points lying inside that region represent systems in a state of non equilibrium, which tend to separate into two phases. However, all points lying in the region inside the spinodal curve are unstable, that is any infinitesimal perturbation can trigger the phase transition process, while all points sandwiched between the equilibrium and the spinodal curves represent metastable systems, i.e. mixtures that need an activation energy to phase separate. The spinodal points can be also determined using the relation $(\partial\mu/\partial\phi)_{T,P} = -(\partial^2 g_{Th}/\partial\phi^2)_{T,P} = 0$, obtaining:

$$\left(\frac{\partial^2 g_{Th}}{\partial\phi^2}\right)_{T,P} = 0 \Longrightarrow (\phi_s^\alpha, \phi_s^\beta). \tag{1.89}$$

1.2.3 The critical exponents

Let us turn now to study the behavior of a binary mixture close to its critical point. Then, instead of Ψ and ϕ, it is convenient to use the following variables,

$$\tilde{\psi} = \frac{1}{2}(\Psi - 2); \quad \tilde{u} = 2\phi - 1. \tag{1.90}$$

Consequently, neglecting higher order terms, we obtain from the equation of state (1.80),

$$\mu = -2\tilde{\psi}\tilde{u} + \frac{2}{3}\tilde{u}^3. \tag{1.91}$$

Note that we cannot have any term proportional to $\tilde{u}$ or $\tilde{u}^2$, in agreement with the conditions $(\partial\mu/\partial\phi)_{T_c,P_c}$ and $(\partial^2\mu/\partial\phi^2)_{T_c,P_c} = 0$, while the coefficient of the $\tilde{u}^3$-term must be positive, as $(\partial^3\mu/\partial\phi^3)_{T_c,P_c} > 0$. When $\tilde{\psi} < 0$, all states are stable, that is there is no phase separation and the mixture remains homogeneous. That means that, when $\tilde{\psi} < 0$, it must be $(\partial\mu/\partial\phi)_{T,P} < 0$, and therefore the coefficient of the term $\tilde{\psi}\tilde{u}$ must be negative. Equation (1.91) is a particular case of the general expression (1.30), with $a_c = 1, b_c = 0$ and $B_c = -1/6$. Accordingly, all considerations that we made in the Section 1.1.3 relative to this expression can be repeated now. In particular, the critical exponent are the same. Based on the expression (1.91) it is easy to evaluate the composition of the two coexisting phases at equilibrium and those on the spinodal curve near the critical point. In fact, at constant temperature and pressure (and therefore at constant Ψ) we saw that $(\partial g/\partial\phi)_\Psi = 0$, so that $\mu = \mu_1 - \mu_2 = 0$. Therefore, substituting the expansion (1.91) valid near the critical point, we obtain:

$$\tilde{u}_e = \pm\sqrt{3\tilde{\psi}}. \tag{1.92}$$

The spinodal point, instead, can be determined via Eq. (1.89), obtaining, near the critical point:

$$\tilde{u}_s = \pm\sqrt{\tilde{\psi}}. \tag{1.93}$$

Note that, as expected, $|\tilde{u}_s| < |\tilde{u}_e|$.

1.2.4 The diffuse interface

Suppose now that the composition of the system is not constant. Accordingly, Eq. (1.1) can be rewritten as

$$g(\mathbf{x}) = g_{Th}(\mathbf{x}) + \Delta g_{NL}(\mathbf{x}), \tag{1.94}$$

where g_{Th} is the molar free energy (1.75) corresponding to a system with constant density,

$$g_{Th} = [g_1\phi + g_2(1-\phi)] + RT[\phi\log\phi + (1-\phi)\log(1-\phi) + \Psi\phi(1-\phi)], \tag{1.95}$$

while Δg_{NL} is a non local molar free energy, due to changes in composition, typical of the diffuse interface model. In fact, when there is an interface separating two phases at equilibrium, this term corresponds to the interfacial energy. Using a procedure similar to that seen in the previous Section, we can derive an expression, originally due to Cahn and Hilliard (1958),

$$\Delta g_{NL} = \Delta g_{CH} = \frac{1}{2}RTa^2(\nabla\phi)^2, \tag{1.96}$$

stating that whenever there is an interface, or even a change in composition, there must be an increase of energy (see van der Waals, 1893, for an extended discussion about this term). Therefore, we may conclude that the expression for the free energy in this case is basically identical to that or a single-phase fluid [cf. Eq. (1.50)], i.e.,

$$g(\phi, \nabla\phi) = g_{Th}(\phi) + \frac{1}{2}RTa^2(\nabla\phi)^2. \tag{1.97}$$

Here a is a characteristic length, roughly equal to the interface thickness at equilibrium which, for a regular mixture, has the same value as that seen in Eq. (1.47), i.e.,

$$a = \sqrt{\frac{9\pi T_C}{4T}}d, \tag{1.98}$$

where d is the excluded volume length defined in (1.3). Now, following the same procedure as in Section 1.1.6, observe that at the end of the phase segregation process, a surface tension σ can be measured at the interface and from that, as shown by van der Waals (1893), a can be determined as

$$a \approx \frac{1}{\sqrt{\tilde{\psi}}(\Delta\phi)^2_{eq}}\frac{\sigma M_w}{\rho RT}, \tag{1.99}$$

where $\tilde{\psi} = (\Psi - 2)/2$, while $(\Delta\phi)_{eq}$ is the composition difference between the two phases at equilibrium. This relation can be easily derived considering that at equilibrium the surface tension σ is equal to the integral of the Cahn-Hilliard free energy across the interface, i.e. $\sigma \approx (\rho l/M_w)\Delta g_{eq}$, where $\Delta g_{eq} \approx RT(\Delta\phi_{eq})^2 a^2/l^2$ is a typical value of the change in the Cahn-Hilliard molar free energy within the interface at equilibrium, while $l \approx a/\sqrt{\tilde{\psi}}$ is the characteristic interface thickness (Van der Waals, 1979; see below).

1.2.5 The generalized chemical potential

At equilibrium, the total free energy is minimized, i.e.

$$\int_V g(\phi, \nabla\phi) d^3\mathbf{x} = min., \tag{1.100}$$

with the constraint

$$\int_V \phi(\mathbf{x}) d^3\mathbf{x} = const., \tag{1.101}$$

Therefore, applying to the system a virtual change in composition, $\delta\phi(\mathbf{x})$, we obtain:

$$\delta \int_V [g(\phi, \nabla\phi) - (RT\tilde{\mu})\phi] d\mathbf{x} = 0, \tag{1.102}$$

where $RT\tilde{\mu}$ is a Lagrange multiplier, to be determined using the constraint (3.31) of mass conservation. Now consider that

$$\partial g = \frac{\partial g}{\partial \phi}\delta\phi + \frac{\partial g}{\partial(\nabla_i\phi)}\delta(\nabla_i\phi), \text{ with } \delta(\nabla_i\phi) = \nabla_i(\delta\phi) \tag{1.103}$$

where the last equality is easily derived considering that $\delta\phi$ is arbitrary. In addition,

$$\int_V \frac{\partial g}{\partial \nabla_i\phi}\nabla_i(\delta\phi) d^3\mathbf{x}dt = \oint_S n_i \frac{\partial g}{\partial \nabla_i\phi}\delta\phi dS - \int_V \nabla_i\left(\frac{\partial g}{\partial \nabla_i\phi}\right)\delta\phi d^3\mathbf{x}, \tag{1.104}$$

where the surface integral on the RHS is identically zero because the virtual change in concentration, $\delta\phi$, is identically zero at the boundary. Finally, we obtain:

$$\int \left[\frac{\partial g}{\partial \phi} - \nabla_i\left(\frac{\partial g}{\partial \nabla_i\phi}\right) - (RT\tilde{\mu})\right]\delta\phi d^3\mathbf{x} = 0. \tag{1.105}$$

From here, since $\delta\phi$ is arbitrary, we obtain, as expected, the Euler-Lagrange equation,

$$\tilde{\mu} = \frac{1}{RT}\frac{\delta g}{\delta\phi} = \frac{1}{RT}\left(\frac{\partial g}{\partial\phi} - \nabla_i\frac{\partial g}{\partial(\nabla_i\phi)}\right) = \mu(\phi) - \frac{1}{RT}\nabla_i\frac{\partial g}{\partial(\nabla_i\phi)}, \tag{1.106}$$

showing that $\tilde{\mu}$ is the generalized chemical potential difference, which must be uniform at equilibrium. Substituting Eq. (1.97) and reminding that $\mu =$

$\mu_1 - \mu_2$ is the difference between the thermodynamical chemical potentials of the two species (1.86), we obtain:

$$\tilde{\mu}(\phi, \nabla\phi) = \mu(\phi) - a^2\nabla^2\phi. \tag{1.107}$$

Near the critical point, the generalized chemical potential difference is zero and therefore, in 1D, along z, substituting Eq. (1.107) into (1.91), we obtain:

$$\partial_{zz}\tilde{u} + 4\tilde{\psi}\tilde{u} - (4/3)\tilde{u}^3 = 0, \tag{1.108}$$

with $\partial_z = \partial/\partial\tilde{z}$, where $O(u^5)$ terms have been neglected, while $\tilde{u}$ and $\tilde{\psi}$ have been defined in (1.90). Solving this equation imposing that $\tilde{u}(\pm\infty) = \pm\tilde{u}_e = \pm\sqrt{3\tilde{\psi}}$ (this is the composition at equilibrium, when $\tilde{\psi} \ll 1$) we obtain Van der Waal's solution,

$$\tilde{u}(z) = \tilde{u}_e \tanh(\sqrt{2\tilde{\psi}}z/a). \tag{1.109}$$

As shown in Mauri, Shinnar and Triantfyllou (1996), this solution can be generalized to finite systems, obtaining a family of Jacobi's elliptic functions. This solution shows that the typical interface thickness l is of $O(a/\sqrt{\tilde{\psi}})$. As we have remarked in the previous Section, Pismen (2001) solved the full problem, showing that u tends to its equilibrium value as $|\tilde{z}|^{-4}$, instead of exponentially, as in the Van der Waals solution.

1.3 Equations of motion for non-dissipative mixtures

1.3.1 The Korteweg stresses

In this Section, we confine ourselves to study a binary mixture with constant density, composed of two species with the same molecular weight, M_w. However, the case of a single-component system and that of non-symmetric and even compressible binary mixtures can be handled in the same way, obtaining very similar results. These generalizations can be found in Lowengrub and Truskinovsky (1997) and Anderson, McFadden and Wheeler (1998). First, let us consider the reversible, dissipation-free case. Then, there is no diffusion and therefore the concentration field can be derived from the initial conditions, knowing the velocity field. In fact, if $\mathbf{x}(t, \mathbf{x}_0)$ denotes the trajectory of a material particle which is located at $\mathbf{x}_0$ at time $t = 0$, i.e. with $\mathbf{x}_0 = \mathbf{x}(0, \mathbf{x}_0)$, then the fluid velocity field is $\mathbf{v}(\mathbf{x}, t) = \dot{\mathbf{x}}(t, \mathbf{x}_0)$, where the dot denotes time derivative at constant $\mathbf{x}_0$, while the concentration field $\phi(\mathbf{x}, t) = \phi(\mathbf{x}_0)$ does not depend explicitly on time, and therefore $\dot{\phi} = 0$. According to the Hamilton, minimum action, principle, the motion of any

conservative system minimizes the following functional:

$$S = \int_0^t \int_V L(\mathbf{v}, \phi, \nabla\phi) d^3\mathbf{x} dt, \tag{1.110}$$

where

$$L = L(\mathbf{v}, \phi, \nabla\phi) = \rho(\frac{1}{2}v^2 - \frac{1}{M_w}g) \tag{1.111}$$

is the Lagrangian of the system, subjected to the constraint of incompressibility,

$$\nabla \cdot \mathbf{v} = 0. \tag{1.112}$$

Accordingly, starting from the minimum condition, let us give a virtual displacement δx_i, corresponding to an infinitesimal change of the fluid flow. Among all the possible virtual displacements, let us choose those such that $\delta\phi = \nabla_i\phi \cdot \delta x_i = 0$. Since the action S in (1.110) is minimized, we have:

$$\delta S = \int_0^t \int_V \rho v_i \delta v_i d^3\mathbf{x} dt - \int_0^t \int_V \frac{\rho}{M_w} \delta g d^3\mathbf{x} dt - \int_0^t \int_V q(\nabla_i v_i) d^3\mathbf{x} dt = 0, \tag{1.113}$$

where $q(x,t)$ is a function to be determined through the constraint (1.112). Note that the constraint (3.31) does not apply here because the concentration field remains unchanged, following the evolution equation $\dot{\phi} = 0$. Considering that $\delta(dx_i) = d(\delta x_i)$, the first integral gives, after integrating by parts:

$$\int_0^t \int_V \rho v_i \delta v_i d^3\mathbf{x} dt = \int_0^t \int_V \rho v_i \delta \frac{dx_i}{dt} d^3\mathbf{x} dt = \tag{1.114}$$

$$\int_0^t \int_V \rho v_i \frac{d}{dt}(\delta x_i) d^3\mathbf{x} = \int_V [\rho v_i \delta x_i]_{t_1}^{t_2} d^3\mathbf{x} - \int_0^t \int_V \rho \frac{dv_i}{dt} \delta x_i d^3\mathbf{x} dt,$$

i.e.

$$\int_0^t \int_V \rho v_i \delta v_i d^3\mathbf{x} dt = -\int_0^t \int_V \rho \frac{dv_i}{dt} \delta x_i d^3\mathbf{x} dt, \tag{1.115}$$

where the first integral after integrating by parts is identically zero because we assume that the virtual displacement is equal to zero at the beginning and at the end, i.e. when $t = t_1$ and $t = t_2$, and also on the boundary, S, of the volume V of integration. The second integral in the RHS of Eq. (1.113) gives, considering that $g = g(\phi, \nabla\phi)$:

$$\int_0^t \int_V \delta g d^3\mathbf{x} dt = \int_0^t \int_V \frac{\partial g}{\partial \phi} \delta\phi d^3\mathbf{x} dt + \tag{1.116}$$

$$\int_0^t \int_V \frac{\partial g}{\partial \nabla_i \phi} \delta(\nabla_i \phi) d^3\mathbf{x} dt$$

Now, considering that $\delta\phi = 0$, the first term on the RHS is identically zero. In addition, applying the following equality,

$$\delta(\nabla_j\phi) = \frac{\partial(\nabla_j\phi)}{\partial x_i}\delta x_i = (\nabla_i\nabla_j\phi)\delta x_i = \nabla_j(\delta\phi) - (\nabla_i\phi)\nabla_j(\delta x_i) = -(\nabla_i\phi)\nabla_j(\delta x_i), \tag{1.117}$$

we obtain:

$$\int_0^t \int_V \delta g d^3\mathbf{x}dt = -\int_0^t \int_V \frac{\partial g}{\partial\nabla_j\phi}(\nabla_i\phi)(\nabla_j\delta x_i)d^3\mathbf{x}dt = \tag{1.118}$$

$$-\int_0^t \oint_S n_j \frac{\partial g}{\partial\nabla_j\phi}\nabla_i\phi\delta x_i dSdt + \int_0^t \int_V \nabla_j\left(\frac{\partial g}{\partial(\nabla_h\phi)}\nabla_i\phi\right)\delta x_i d^3\mathbf{x}dt,$$

where we have integrated by parts. Here, too, the surface integral is identically zero, because $\delta x_i = 0$ at the boundary, so that

$$\int_0^t \int_V \delta g d^3\mathbf{x}dt = \int_0^t \int_V \nabla_j\left(\frac{\partial g}{\partial(\nabla_h\phi)}\nabla_i\phi\right)\delta x_i d^3\mathbf{x}dt. \tag{1.119}$$

Finally, the last integral on the RHS of (1.113) gives:

$$\int_0^t \int_V q\delta(\nabla_i v_i)d^3\mathbf{x}dt = \int_0^t \oint_S n_i q\delta v_i dSdt - \int_0^t \int_V \delta v_i(\nabla_i q)d^3\mathbf{x}dt = \tag{1.120}$$

$$-\int_V [(\nabla_i q)\delta x_i]_0^t d^3\mathbf{x} + \int_0^t \int_V \left(\nabla_i\frac{\partial q}{\partial t}\right)\delta x_i d^3\mathbf{x}dt = \int_0^t \int_V (\nabla_i p)\delta x_i d^3\mathbf{x}dt,$$

where $p = \partial q/\partial t$ and we considered that δx_i (and δv_i as well) vanishes at the boundary S and for $t = t_1$ and $t = t_2$. Concluding, substituting (1.115), (1.119) and (1.120) into Eq. (1.114) gives:

$$\int_0^t \int_V \left(\rho\frac{dv_i}{dt} + \nabla_i p - \nabla_j P_{ji}\right)\delta x_i d^3\mathbf{x}dt = 0, \tag{1.121}$$

where

$$P_{ij} = -\frac{\rho}{M_w}\frac{\partial g}{\partial(\nabla_i\phi)}\nabla_j\phi \tag{1.122}$$

is the Cauchy stress tensor. Now, considering the arbitrariness of the virtual displacement δx_i and applying Reynolds theorem, we finally obtain the linear momentum equation:

$$\rho\frac{dv_i}{dt} + \nabla_i p = F_{\phi,i} = \nabla_j P_{ji}, \tag{1.123}$$

where d/dt is the material derivate, to be solved with the incompressibility constraint:

$$\nabla_i v_i = 0. \tag{1.124}$$

In addition, for non-dissipative systems, the heat equation and the equation of conservation of chemical species have trivially only the convective term, that is,

$$\frac{dT}{dt} = \frac{\partial T}{\partial t} + \mathbf{v} \cdot \nabla T = 0, \tag{1.125}$$

$$\frac{d\phi}{dt} = \frac{\partial \phi}{\partial t} + \mathbf{v} \cdot \nabla \phi = 0, \tag{1.126}$$

with diffusive fluxes that are identically zero. The body force $\mathbf{F}_\phi$ in Eq. (1.123) can be rewritten as:

$$\begin{aligned} F_{\phi,i} &= \nabla_j P_{ji} = -\frac{\rho}{M_w}\left[\nabla_j\left(\frac{\partial g}{\partial \nabla_i \phi}\right)\nabla_i\phi - \frac{\partial g}{\partial \nabla_j \phi}\nabla_i\nabla_j\phi \pm \frac{\partial g}{\partial \phi}\nabla_i\phi\right] \\ &= \frac{\rho RT}{M_w}\tilde{\mu}\nabla_i\phi - \frac{\rho}{M_w}\nabla_i g, \end{aligned}$$

and therefore the momentum equation becomes

$$\rho\frac{dv_i}{dt} + \nabla_i p' = \frac{\rho RT}{M_w}\tilde{\mu}\nabla_i\phi, \tag{1.127}$$

where the pressure term has been redefined as $p' = p + (\rho/M_w)g$. Alternatively, this equation can also be written as

$$\rho\frac{dv_i}{dt} + \nabla_i p'' = -\frac{\rho RT}{M_w}\phi\nabla_i\tilde{\mu}, \tag{1.128}$$

with a pressure term $p'' = p' - (\rho RT/M_w)\tilde{\mu}\phi$. Similar results were also obtained by Jasnow and Vinals (1996) and Antanovskii (1996). It should be stressed that the body force $\mathbf{F}_\phi$ is non dissipative, as it arises from the minimum action principle. Its expression in (1.128) is quite intuitive: the momentum flux is directed towards regions with smaller chemical potential differences. Finally, note that, using the expression (1.94)-(1.96) for the free energy, the Cauchy stress tensor $\mathbf{P}$ becomes:

$$P_{ij} = -\left(\frac{\rho RT}{M_w}\right)a^2(\nabla_i\phi)(\nabla_j\phi), \tag{1.129}$$

which coincides with the Korteweg stresses (1901), provided that composition ϕ is replaced by density ρ.

1.3.2 Noether's theorem

The result (1.129) could be more easily determined by applying Noether's theorem. Let us illustrate this theorem for a somewhat simplified problem, where we omit the dependence of the Lagrangian L on $\mathbf{v}$, so that

$$L = L(\phi, \nabla\phi) = -\frac{\rho}{M_w}g(\phi, \nabla\phi). \tag{1.130}$$

Accordingly, the system will follow a path that is described through the Euler-Lagrange equation,

$$\frac{\partial g}{\partial \phi} - \nabla_k \frac{\partial g}{\partial(\nabla_k \phi)} = 0. \tag{1.131}$$

Now, consider the following equality,

$$\frac{\partial g}{\partial x_i} = \frac{\partial g}{\partial \phi}\frac{\partial \phi}{\partial x_i} + \frac{\partial g}{\partial(\nabla_k \phi)}\frac{\partial(\nabla_k \phi)}{\partial x_i}. \tag{1.132}$$

Substituting the Euler-Lagrange equation we obtain:

$$\frac{\partial g}{\partial x_i} - \left[\nabla_k \frac{\partial g}{\partial(\nabla_k)}\right](\nabla_i \phi) - \left[\frac{\partial g}{\partial(\nabla_k \phi)}\right](\nabla_k \nabla_i \phi) = 0, \tag{1.133}$$

that is:

$$\nabla_k \left\{ g\delta_{ik} - \left(\frac{\partial g}{\partial(\nabla_k \phi)}\right)(\nabla_i \phi)\right\} = 0 \tag{1.134}$$

In our case, since g is not an explicit function of position, $\nabla_i g = 0$ and therefore we obtain the equation

$$\nabla \cdot \mathbf{P} = 0, \tag{1.135}$$

where $\mathbf{P}$ represents the Korteweg stresses (1.122) and (1.129). Naturally, including the kinetic term in the Lagrangian, we would obtain also the acceleration and the pressure gradient term.

1.4 Dissipative terms

1.4.1 The stress tensor

When dissipation is taken into account, the equation of motion remains basically Eq. (1.123), where the stress tensor can be considered as the sum of a Korteweg term and a viscous term, S_{ij}, i.e.

$$\rho \frac{dv_i}{dt} = \nabla_j (P_{ji} + S_{ji}), \tag{1.136}$$

with

$$S_{ij} = -p\delta_{ij} + \eta(\nabla_i v_j + \nabla_j v_i), \tag{1.137}$$

where η is an effective viscosity, that, assuming Newtonian behavior, is independent of the shear rate, so that $\eta = \eta(\phi)$.

1.4.2 The diffusive molar flux

The equation of conservation of chemical species now will contain a dissipative term as well, that is

$$\frac{d\phi}{dt} + \nabla \cdot \mathbf{J}_\phi = r_\phi, \tag{1.138}$$

where J_ϕ is a diffusive molar flux, while r_ϕ is the chemical reaction term, that is the number of moles of component 1 that are generated per unit volume and time. In the following, we will assume that $r_\phi = 0$, that is chemical species do not react. As for the diffusive fluxes, when the Cahn-Hilliard part of the free energy is neglected, the mass flux of component 1 is proportional to the gradient of the chemical potential of component 1 as (Cussler, 1984, page 180),

$$\mathbf{J}_1 = -Dx_1 \nabla \mu_1, \tag{1.139}$$

where D is the molecular diffusivity (i.e. D is a function of temperature and pressure, but not of composition), while the proportionality term (Dx_1) has been chosen so that in the ideal case we obtain Fick's constitutive law (see below). For symmetric binary mixtures, substituting (1.75) into (1.78), we obtain the chemical potential as:

$$RT\mu_1 = g_1 + RT[\ln x_1 + \Psi x_2^2], \tag{1.140}$$

so that (1.139) yields:

$$\mathbf{J}_1 = -Dx_1 \frac{d\mu_1}{dx_1} \nabla x_1 \Rightarrow \mathbf{J}_1 = -D^* \nabla x_1, \tag{1.141}$$

where

$$D^* = D(1 - 2\Psi x_1 x_2) \tag{1.142}$$

is the diffusion coefficient. Inverting the suffices 1 and 2 in (1.141) and (1.142) we see that a) the diffusivity of component 1 into 2 equals the diffusivity of component 2 into 1, as it should, and b) the flux of species 2 is opposite to the flux of species 1, that is $\mathbf{J}_2 = -\mathbf{J}_1$, showing that these are really diffusive fluxes, with no convective components. In general, from (1.139) and applying the Gibbs-Duhem relation, $x_1 \nabla \mu_1 = -x_2 \nabla \mu_2$, we see that it is always true that $\mathbf{J}_2 = -\mathbf{J}_1$. Therefore, for ideal or dilute mixtures, i.e. when either $\Psi = 0$ or $x_1 << 1$ (or $x_2 << 1$) we obtain that $D^* = D$ and therefore Eq. (1.141) reduces to Fick's law. When we plot D^* as a function of x_1 we see that for $\Psi > 2$ there is a region of negative diffusion, as it corresponds to the region where $d^2g/dx_1^2 < 0$. Going back to our notation, i.e. $x_1 = \phi$, observe that, denoting $\mathbf{J}_\phi \equiv \mathbf{J}_1$, the constitutive relation (1.139) can also be written as

$$\mathbf{J}_\phi = -D\phi(1 - \phi)\nabla \mu, \tag{1.143}$$

where $\mu = \mu_1 - \mu_2$. This can be proven considering that

$$\begin{aligned} -D\phi(1-\phi)\nabla\mu_{Th} &= -D\phi(1-\phi)\nabla\mu_1 + D\phi(1-\phi)\nabla\mu_2 \\ &= (1-\phi)\mathbf{J}_1 - \phi\mathbf{J}_2 = \mathbf{J}_1 - \phi(\mathbf{J}_1 + \mathbf{J}_2) = \mathbf{J}_1. \end{aligned}$$

At this point, a natural extension of the constitutive relation (1.143) is the following one:

$$\mathbf{J}_\phi = -D\phi(1-\phi)\nabla\tilde{\mu}. \tag{1.144}$$

This is the constitutive equation that has been used in Mauri, Shinnar & Triantafyllou (1996) and in all subsequent works by Mauri and coworkers.

1.4.3 The diffusive heat flux and the energy dissipation term

The equation of energy conservation (1.125) in general can be written as

$$\rho c\frac{dT}{dt} + \nabla\cdot\mathbf{J}_q = \dot{q}, \tag{1.145}$$

where $\mathbf{J}_q$ is the diffusive heat flux, while $\dot{q}$ is the energy dissipation term. Assuming a simple Fourier constitutive relation, we have:

$$\mathbf{J}_q = -k\nabla T, \tag{1.146}$$

where k is the heat conductivity, that, in general, depends on the composition, i.e. $k = k(\phi)$. The energy dissipation term is the sum of three contributions: the dissipative work of non-conservative external forces, $\mathbf{F}_{nc}^{(e)}$, viscous dissipation and the enthalpy of mixing term:

$$\dot{q} = \mathbf{F}_{nc}^{(e)}\cdot\mathbf{v} + \eta|\nabla\mathbf{v}|^2 + \dot{h}_{mix}, \tag{1.147}$$

where $\dot{h}_{mix} = (\rho/M_w)h_{ex}\dot{\phi}$. In most practical cases, viscous dissipation is negligible. Therefore, in the absence of any external force, dissipation is due exclusively to the enthalpy of mixing, h_{ex}, which is the energy that is either generated or consumed when the two components of the mixture are isothermally mixed together. As is well known from classical thermodynamics (see Sandler, 1999),

$$\frac{h_{ex}}{RT} = -T\left[\frac{\partial(g_{ex}/RT)}{\partial T}\right]_{P,\phi}, \tag{1.148}$$

showing that $h_{ex} = 0$ when $g_{ex} \propto RT$, i.e. when Ψ in the expression (1.72) is independent of T. In that case, the processes of mixing and demixing can occur isothermally, with $\dot{q} = 0$. In our case, though, i.e. for regular mixtures where g_{ex} does not depend on T, we obtain:

$$h_{ex} = g_{ex}. \tag{1.149}$$

1.4.4 Summary of the equations (binary mixtures)

In the case of incompressible regular binary mixtures, assuming that density ρ , viscosity η, specific heat c and thermal conductivity k of the two components are equal to each other, we have:

$$\frac{d\phi}{dt} = -\nabla \cdot \mathbf{J}_\phi; \tag{1.150}$$

$$\rho \frac{d\mathbf{v}}{dt} = \nabla \cdot (\mathbf{P} + \mathbf{S}) + \mathbf{F}^{(e)}; \quad \nabla \cdot \mathbf{v} = 0, \tag{1.151}$$

$$\rho c \frac{dT}{dt} = k\nabla^2 T + \dot{q}, \tag{1.152}$$

where ϕ is the molar fraction of component 1, $\mathbf{J}_\phi$ is the diffusion flux (1.143), $\mathbf{v}$ the average local velocity of the fluid mixture, $\mathbf{P}$ are Korteweg stresses (1.129), $\mathbf{S}$ the viscous stresses, $\mathbf{F}^{(e)}$ is the external force, T the temperature and $\dot{q}$ the heat generated (3.28). As shown above [see Eq. (1.144)], $\mathbf{J}_\phi$ is proportional to the gradient of the chemical potential through the relation,

$$\mathbf{J}_\phi = -\phi(1-\phi)D\nabla\tilde{\mu}, \tag{1.153}$$

where D is the molecular diffusivity, and $\tilde{\mu}$ is the generalized chemical potential difference between the two species defined in (1.107),

$$\tilde{\mu} = \delta(\Delta g/RT)/\delta\phi. \tag{1.154}$$

Here Δg denotes the molar Gibbs free energy, defined as:

$$\Delta g/RT = \phi\log\phi + (1-\phi)\log(1-\phi) + \Psi\phi(1-\phi) + \frac{1}{2}a^2(\nabla\phi)^2, \tag{1.155}$$

where R is the gas constant, a is a characteristic microscopic length and Ψ is the Margules parameter, which describes the relative weight of enthalpic versus entropic forces. Since $\Psi_c = 2$ is the critical value of Ψ, we find that the single-phase region of the phase diagram corresponds to values $\Psi < 2$, while, conversely, $\Psi > 2$ in the two-phase region. For an incompressible fluid, considering that $S_{ij} = -p\delta_{ij} + \eta(\nabla_i v_j + \nabla_j v_i)$, with η denoting the (here constant) fluid viscosity, Eq. (1.151) reduces to the simpler following equation:

$$\rho\frac{d\mathbf{v}}{dt} + \nabla p = \eta\nabla^2\mathbf{v} + \mathbf{F}_\phi \qquad \nabla\cdot\mathbf{v} = 0. \tag{1.156}$$

Here $\mathbf{F}_\phi = \nabla\cdot\mathbf{P}$ is a non equilibrium body force, which equals the generalized gradient of the free energy and therefore it is driven by chemical potential gradients within the mixture [see Eq. (1.128)],

$$\mathbf{F}_\phi = -\left(\frac{\rho RT}{M_w}\right)\phi\nabla\tilde{\mu}. \tag{1.157}$$

In particular, when the system presents well-defined phase interfaces, such as at the late stages of phase separation, this body force reduces to the more conventional surface tension, as shown by Jasnow and Viñals (1996) and by Jacqmin (2000). Therefore, being proportional to $\nabla\tilde{\mu}$ which is identically zero at local equilibrium, $\mathbf{F}_\phi$ can be thought of as a non-equilibrium capillary force. Since $\mathbf{F}_\phi$ is driven by surface energy, it tends to minimize the energy stored at the interface resulting in a non-equilibrium attractive force between drops of the same phase, therefore driving, say, drops of the α phase towards regions of the same phase. The ratio between convective and diffusive mass fluxes defines the Peclet number, $N_{Pe} = Va/D$, where V is a characteristic velocity, which can be estimated through (1.150) and (1.156), obtaining (see Vladimirova, Malagoli and Mauri, 1999a,b),

$$N_{Pe} = \frac{Va}{D} \approx \frac{a^2}{D}\frac{\rho}{\eta}\frac{RT}{M_w} \approx \frac{\sigma a}{\eta D}. \tag{1.158}$$

For systems with very large viscosity (e.g. polymer solutions) or very large diffusivity (e.g. mixtures very close to the critical point), N_{Pe} is small and the model describes a diffusion-driven separation process. For low-viscosity liquid mixtures, far from criticality, N_{Pe} is very large, showing that diffusion is important only in the vicinity of local equilibrium, when the body force $\mathbf{F}_\phi$ is negligibly small. In general, therefore, for fluid mixtures that are in conditions of non-equilibrium, either phase-separating or mixing, convection dominates diffusion. Although this approach has been developed for very idealized systems, it seems to capture the main features of real mixtures, at least during the phase separation process. This is why we did not add further terms to generalize our model, although they can be derived rather easily.

1.4.5 Energy dissipation

Now we show that the time derivative of the energy of the system equals its energy dissipation, i.e.

$$\frac{d}{dt}\int_V (\rho cT + \frac{1}{2}\rho v^2 + \frac{\rho}{M_w}g)d^3\mathbf{x} = \int_V \dot{e}d^3\mathbf{x}, \tag{1.159}$$

where $\dot{e}$ is the energy dissipation per unit volume,

$$\dot{e} = \dot{q} + \mathbf{J}_q \cdot \nabla T - \mathbf{S} : (\nabla\mathbf{v}) + \mathbf{J}_\phi \cdot \nabla\tilde{\mu} = \dot{q} - k|\nabla T|^2 - \eta||\nabla\mathbf{v}||^2 - D(\phi)|\nabla\tilde{\mu}|^2, \tag{1.160}$$

and the integrals are taken over a material volume $V = V(t)$. First, considering Eq. (1.153), we obtain:

$$\frac{d}{dt}\int_V (\rho cT)d^3\mathbf{x} = \int_V (\dot{q} - \nabla\cdot\mathbf{J}_q)d^3\mathbf{x}. \tag{1.161}$$

Multiplying Eq. (1.156) by v_i and volume integrating we obtain:

$$\frac{d}{dt}\int_V \left(\frac{1}{2}\rho v^2\right) d^3\mathbf{x} = \int_V \left[-v_i(\nabla_i p) + \eta v_i(\nabla^2 v_i) + \left(\frac{\rho RT}{M_w}\right)\tilde{\mu} v_i(\nabla_i \phi)\right] d^3\mathbf{x}. \tag{1.162}$$

Now, using the incompressibility condition, the RHS becomes:

$$\oint_S n_i[-v_i p + \eta(\nabla_i v_j)v_j]dS - \int_V \left[\eta(\nabla_i v_j)(\nabla_i v_j) + \left(\frac{\rho RT}{M_w}\right)\tilde{\mu} v_i(\nabla_i \phi)\right] d^3\mathbf{x}, \tag{1.163}$$

where the first term is identically zero because of the no-slip (or periodic) boundary conditions. The last term in (1.163) can be simplified considering:

$$\tilde{\mu} v_i(\nabla_i \phi) = -\tilde{\mu}\frac{\partial \phi}{\partial t} - \frac{1}{\rho}[\nabla_i(\tilde{\mu} J_1) - J_1 \nabla_i \tilde{\mu}]. \tag{1.164}$$

Integrating by parts and applying the no-flux boundary condition, the second term of the RHS in (1.164) is identically zero. In addition, considering that

$$\frac{g}{RT} = \mu_2 + \phi\tilde{\mu}, \tag{1.165}$$

we have:

$$\frac{\partial g}{\partial t} = RT\tilde{\mu}\frac{\partial \phi}{\partial t}, \tag{1.166}$$

where we have applied the Gibbs-Duhem relation,

$$\phi\frac{d\mu_1}{d\phi} + (1-\phi)\frac{d\mu_2}{d\phi} = 0 \Longrightarrow \frac{\partial \mu_2}{\partial t} + \phi\frac{\partial \tilde{\mu}}{\partial t} = 0. \tag{1.167}$$

Finally, substituting (1.161) and (1.163)-(1.165) into (1.162), we obtain Eq. (1.159)-(1.160). The same result was obtained by Antanovskii (1995,1996), by maximizing the entropy production of the system.

1.4.6 Summary of the equation (one-component systems)

Very similar results can be obtained for the equations of motion of one-component systems subjected to conservative forces. As we saw in Section 2, in this case the order parameter is the density ρ , which is different in the two phases. Therefore, the mixture is not incompressible, even when each phase can be assumed to be incompressible (think, for example, to a solid-liquid phase transition). Accordingly, mass conservation equation is the usual continuity equation for compressible fluids. Similarly, the momentum conservation equation is the usual Navier-Stokes equation, with an additional body force which is identical to $\mathbf{F}_\phi$, with composition ϕ replaced by density ρ (in fact, Korteweg stresses were originally derived for this case). Therefore, the equations of motion are the following:

$$\frac{d\rho}{dt} = -\rho(\nabla \cdot \mathbf{v}), \tag{1.168}$$

$$\rho \frac{d\mathbf{v}}{dt} = \nabla \cdot (\mathbf{P} + \mathbf{S}) + \mathbf{F}_e, \tag{1.169}$$

$$\frac{dT}{dt} = \alpha \nabla^2 T + \frac{\dot{q}}{\rho c}, \tag{1.170}$$

where $\alpha = k/\rho c$ is the heat diffusivity, $\mathbf{P}$ are Kortweg stresses,

$$\mathbf{P} = -K(\nabla\rho)(\nabla\rho) \tag{1.171}$$

while $\mathbf{S}$ is the stress tensor, which for compressible fluids reads:

$$S_{ij} = [-p + (\zeta - \frac{2}{3}\eta)(\nabla \cdot \mathbf{v})]\delta_{ij} + \eta(\nabla_i v_j + \nabla_j v_i), \tag{1.172}$$

with ζ denoting the second viscosity. These equations are supplemented with Van der Waals equation of state that fixes the pressure p as a function of density ρ and temperature T.

Chapter 2

Numerical Methods

2.1 Finite difference scheme

The numerical treatment of partial differential equations is, by itself, a vast subject. Partial differential equations are at the heart of many, if not most, computer analysis or simulations of continuous physical systems, such as fluids, electromagnetic fields, the human body, etc.

In general partial differential equations (PDEs) are classified into the three categories, hyperbolic, parabolic, and elliptic, on the basis of their characteristics, or curves of information propagation. The prototypical examples of a hyperbolic equation is the one-dimensional wave equation

$$\frac{\partial^2 u}{\partial t^2} = v^2 \frac{\partial^2 u}{\partial x^2} \tag{2.1}$$

where $v = constant$ is the velocity of wave propagation. The prototypical parabolic equation is the diffusion equation

$$\frac{\partial u}{\partial t} = \frac{\partial}{\partial x}(D\frac{\partial u}{\partial x}) \tag{2.2}$$

where D is the diffusion coefficient. The prototypical elliptic equation is the *Poisson* equation

$$\frac{\partial^2 u}{\partial x^2} + \frac{\partial^2 u}{\partial y^2} = \rho(x, y) \tag{2.3}$$

where the source term ρ is given. If the source term is equal to zero, the equation is *Laplace's equation*. From a computational point of view, the classification into these three canonical types is not very meaningful - or at least not as important as some other essential distinctions. Equations (2.1) and (2.2) both define *initial value* or *Cauchy* problems: If information on u is given at some initial time t_0 for all x, then the equations describe how $u(x, t)$ propagates itself forward in time. In other words, eq (2.1) and (2.2) describe time evolution. The goal of a numerical code should be track

that time evolution with some desired accuracy. By contrast, equation (2.3) directs us to find a single "static" function $u(x, y)$ which satisfies the equation within some (x, y) region of interest, and which - one must also specify - has some desired behavior on the boundary of the region of interest. These problems are called *boundary value problems*. In general it is not possible stably to just "integrate in from the boundary" in the same sense that an initial value problem can be "integrated forward in time". Therefore, the goal of a numerical code is somehow to converge on the correct solution everywhere at once.

2.1.1 Boundary value problems

The questions that define a boundary value problem are

- What are the variables?
- What equations are satisfied in the interior of the region of interest?
- What equations are satisfied by points on the boundary of the region of interest.

In contrast to initial value problems, stability is relatively easy to achieve for boundary for boundary value problems. Thus, the *efficiency* of the algorithms, both in computational load and storage requirements, becomes the principal concern. Because all the conditions on a boundary value problem must be satisfied "simultaneosly", these problems usually boil down, at least conceptually, to the solution of large numbers of simultaneous algebraic equations. When such equations are nonlinear, they are usually solved by linearization and iteration; so without much loss of generality we can view the problem as being the solution of special, large linear sets of equations. Let's represent the function $u(x, y)$ by its values at the discrete set of points

$$x_j = x_0 + k\Delta, \qquad j = 0, 1, ..., J, \tag{2.4}$$

$$y_l = y_0 + l\Delta, \qquad l = 0, 1, ..., L, \tag{2.5}$$

$$\tag{2.6}$$

where Δ is the *grid spacing*. From now on, we will write $u_{j,l}$ for $u(x_i, y_l)$, and ρ_j, l for $\rho(x_j, y_l)$. We can then substitute a finite-difference representation:

$$\frac{u_{j+1,l} - 2u_{j,l} + u_{j-1,l}}{\Delta^2} + \frac{u_{j,l+1} - 2u_{j,l} + u_{j,l-1}}{\Delta^2} = \rho_{j,l} \tag{2.7}$$

or equivalently

$$u_{j+1,l} + u_{j-1,l} + u_{j,l+1} + u_{j,l-1} - 4u_{j,l} = \Delta^2 \rho_{j,l} \tag{2.8}$$

To write this system of linear equations in matrix form we need to make a vector out of u. Let us number the two dimensions of grid points in a single one-dimensional sequence by defining

$$i \equiv j(L+1) + l \text{ for } j = 0, 1, .., J, l = 0, 1, ..., L \tag{2.9}$$

In other words, i increases most rapidly along the columns representing y values. Equation (2.8) now becomes

$$u_{i+L+1} + u_{i-(L+1)} + u_{i+1} + u_{i-1} - 4u_i = \Delta^2 \rho_i \tag{2.10}$$

This equation only holds at the interior points $j = 1, 2...J-1$; $l = 1, 2, ...L-1$. The points where

$$j = 0 \qquad [i.e., i = 0, ..., L] \tag{2.11}$$
$$j = J \qquad [i.e., i = J(L+1), .., J(L+1) + L] \tag{2.12}$$
$$l = 0 \qquad [i.e., i = 0, L+1, .., J(L+1)] \tag{2.13}$$
$$l = L \qquad [i.e., i = L, L+1+L, .., J(L+1) + l] \tag{2.14}$$
$$\tag{2.15}$$

are boundary points where either u or its derivative has been specified. If we pull all this "known" information over to the right-hand side of equation, then the equation takes the form

$$\mathbf{A} \cdot \mathbf{u} = \mathbf{b} \tag{2.16}$$

where $\mathbf{A}$ has the form of a matrix with diagonal blocks that are themselves tridiagonal, and sub- and super-diagonal blocks that are diagonal. This form of matrix is called "tridiagonal with fringes". A general linear second-order elliptic equation

$$\begin{aligned} a(x,y)\frac{\partial^2 u}{\partial x^2} &+ b(x,y)\frac{\partial u}{\partial x} \\ &+ c(x,y)\frac{\partial^2 u}{\partial y^2} + d(x,y)\frac{\partial u}{\partial y} \\ &+ e(x,y)\frac{\partial^2 u}{\partial x \partial y} + f(x,y)u = g(x,y) \end{aligned}$$

will lead to a matrix of similar structure except that the nonzero entries will not be constants. As a rough classification, there are three different approaches to the solution of equation, not all applicable in all cases: relaxation methods, "rapid" methods, and direct matrix methods. Relaxation methods make immediate use of the structure of the sparse matrix $\mathbf{A}$. The matrix is split into two parts

$$\mathbf{A} = \mathbf{E} - \mathbf{F} \tag{2.17}$$

where $\mathbf{E}$ is easily invertible and $\mathbf{F}$ is the remainder. Then becomes

$$\mathbf{E} \cdot \mathbf{u} = \mathbf{F} \cdot \mathbf{u} + \mathbf{b} \tag{2.18}$$

The relaxation method involves choosing an initial guess $\mathbf{u}^{(0)}$ and then solving successively for iterates $\mathbf{u}^{(r)}$ from

$$\mathbf{E} \cdot \mathbf{u}^{(r)} = \mathbf{F} \cdot \mathbf{u}^{(r-1)} + \mathbf{b} \tag{2.19}$$

Since $\mathbf{E}$ is chosen to be easily invertible, each iteration is fast. Rapid methods apply for only a rather special class of equations: those with constant coefficients, or, more generally, those that are separable in the chosen coordinates. In addition, the boundaries must coincide with coordinate lines.

2.1.2 Flux-conservative initial value problems

A large class of initial value PDEs in one space dimension can be cast into the form of a *flux-conservative equation*,

$$\frac{\partial \mathbf{u}}{\partial t} = -\frac{\partial \mathbf{F}(\mathbf{u})}{\partial x} \tag{2.20}$$

where $\mathbf{u}$ and $\mathbf{F}$ are vectors, and where $\mathbf{F}$ may depend not only on $\mathbf{u}$ but also on spatial derivatives of $\mathbf{u}$. The vector $\mathbf{F}$ is called the *conserved flux*. For example, the prototypical hyperbolic equation, the one-dimensional wave equation with constant velocity of propagation v

$$\frac{\partial^2 u}{\partial t^2} = v^2 \frac{\partial^2 u}{\partial x^2} \tag{2.21}$$

can be rewritten as a set of two first-order equations

$$\frac{\partial r}{\partial t} = v \frac{\partial s}{\partial x} \tag{2.22}$$

$$\frac{\partial s}{\partial t} = v \frac{\partial r}{\partial x} \tag{2.23}$$

$$\tag{2.24}$$

where

$$r \equiv v \frac{\partial u}{\partial x} \tag{2.25}$$

$$s \equiv \frac{\partial u}{\partial t} \tag{2.26}$$

$$\tag{2.27}$$

In this case r and s become the two components of $\mathbf{u}$, and the flux is given by the linear matrix relation

$$\mathbf{F}(\mathbf{u}) = \begin{pmatrix} 0 & -v \\ -v & o \end{pmatrix} \cdot \mathbf{u} \tag{2.28}$$

Let's consider a prototypical example of the general flux-conservative equation (2.20), namely the equation for a scalar u

$$\frac{\partial u}{\partial t} = -v\frac{\partial u}{\partial x} \tag{2.29}$$

with v a constant. As it happens, we already know analytically that the general solution of this equation is a wave propagating in the positive x-direction,

$$u = f(x - vt) \tag{2.30}$$

where f is an arbitrary function. However, the numerical strategies that we develop will be equally applicable to the more general equations represented by (2.20). In some contexts, equation (2.29) is called an advective equation, because the quantity u is trasported by a "fluid flow" with a velocity v. To finite differencing equation (2.29) the straightforward approach is to choose equally spaced points along both the $t-$ and $x-$ axes. Thus denote

$$x_j = x_0 + j\Delta x, j = 0, 1, ..., J, \tag{2.31}$$

$$t_n = t_0 + n\Delta t, n = 0, 1, ..., N. \tag{2.32}$$

$$\tag{2.33}$$

Let u_j^n denote $u(t_n, x_j)$. We have several choices for representing the time derivative term. The obvious way is to set

$$\frac{\partial u}{\partial t}|_{j,n} = \frac{u_j^{n+1} - u_j^n}{\Delta t} + O(\Delta t) \tag{2.34}$$

This is called *forward Euler* differencing. While forward Euler is only first-order accurate in Δt, it has the advantage that one is able to calculate quantities at timestep $n + 1$ in terms of only quantities known at timestep n. For the space derivative, we can use a second-order representation still using only quantities known at timestep n:

$$\frac{\partial u}{\partial x}|_{j,n} = \frac{u_{j+1}^n - u_{j-1}^n}{2\Delta x} + O(\Delta x^2) \tag{2.35}$$

The resulting finite-difference approximation to equation is called the FTCS representation

$$\frac{u_j^{n+1} - u_j^n}{\Delta t} = -v(\frac{u_{j+1}^n - u_{j-1}^n}{2\Delta x}) \tag{2.36}$$

which can easily be rearranged to be a formula for u_j^{n+1} in terms of the other quantities. The FTCS is a nice examples of an algorithm that is easy to derive, takes little storage, and execute quickly. It is a explicit scheme, that means that u_j^{n+1} for each j can be calculated explicitly from the quantities that are already known. This algorithm is also an example of a *single-level* scheme, since only values at time level n have to be stored to find values at time level *n+1*.

2.1.3 Von Neumann stability analysis

Unfortunately, equation (2.36) is of very limited usefulness. It is an *unstable* method, which can only be used to study waves for a short fraction of one oscillation period. To find an alternative methods with more general applicability, we must introduce the *von Neumann stability analysis*. The von Neumann analysis is local: we imagine that the coefficients of the difference equations are so slowly varying as to be considered constant in space and time. In that case, the independent solutions, or *eigenmodes*, of the difference equation are all of the form

$$u_j^n = \sigma^n e^{ikj\Delta x} \tag{2.37}$$

where k is a real spatial wave number and $\xi = \xi(k)$ is a complex number that depends on k. The key fact is that the time dependence of a single eigenmode is nothing more than successive integer powers of the complex number ξ. Therefore, the difference equations are unstable if $|\xi(k)| > 1$ for some k. The number ξ is called the *amplification factor* at a given wave number k. The factor is given by:

$$\xi(k) = 1 - i\frac{v\Delta t}{\Delta x} sink\Delta x \tag{2.38}$$

whose modulus is > 1 for all k; so the FTCS scheme is unconditionally unstable. If the velocity v were a function of t and x, then we would write v_j^n in eq. In the von Neumann stability analysis we would still treat v as a constant, the idea being that for v slowly varying the analysis is local. In fact, even in the case of strictly constant v, the von Neumann analysis does not rigorously treat the end effects at $j = 0$ and $j = N$. More generally, if the equation's right-hand side were nonlinear in u, then a von Neumann analysis would linearize by writing $u = u_0 + \delta u$, expanding to linear order in δu. Assuming that the u_0 quantities already satisfy the difference equation exactly, the analysis would look for an unstable eigenmode of δu.

2.2 Finite element scheme

The finite-element method is an approximation procedure for solving differential equations of boundary and/or initial-value type in engineering and mathematical physics. The procedure employs subdivision of the solution domain into many smaller regions of convenient shapes, such as triangles and quadrangles, and uses approximation theory to quantize behavior on each finite element. Suitably disposed coordinates are specified for each element, and the action of the differential equation is approximately replaced using values of the dependent variables at these nodes. Using a variational principle, or a weighted.residual method, the governing differential equations are then transformed into finite-element equations governing the isolated element. These local equations are collected together to form a global system of ordinary differential or algebraic equations including a proper accounting of the boundary conditions. The nodal vales of the dependent variables are determined from solution of this matrix equation system.

The finite-element method was originally developed bu engineers in the 1950s to analyze large structural system for aircraft. Turnet et al. (1956) presented the first paper on the subject; these authors were followed by Clough (1960) and Argyris (1963), among others. Application of the finite-element method to nonstructural problems, such as elementary flow and electromagnetism, was first reported by Zienkiewicz and Cheung (1965). Applications to a wide class of problems in nonlinear mechanics were contributed by Oden (1972). As the finite-element method matured in application, the concept of "force balance" was replaced by a robust theoretical analysis founded in the classical variational calculus and Rayleigh-Ritz methods (Rayleigh, 1877; Ritz, 1909). There have been many contributions to the development of the mathematical theory of finite elements, including those of Babuska and Aziz (1972), Ciarlet and Raviart (1972), Aubin (1972), strang and Fix (1973), Oden and Reddy (1976), and the pioneering works of Lions and Magenes (1972). The direct extension of these classical theoretical concepts to algorithm construction for most problem classes in fluid mechanics is not possible. The principal difficulty is that the typical eulerian reference frame renders the expression for conservation of momentum explicitly nonlinear. Therefore, a variational principle is not assured even to exist, let alone be found. For this reason, at least, the most widely practiced construction for approximation procedures for fluid mechanics has been direct replacement of derivatives by divided difference quotients, that is, finite differences. A variation of this concept has been the integration of conservation equations over a discretization, using the divergence theorem and replacing cell fluxes with difference quotients, yielding finite volumes (Patankar, 1980). The particle in cell method (Evans and Harlow, 1957), employs the cell flux concept, but uses pseudolagrangian particle distributions to approximately enforce the basic conservation laws. Most of the difference quotient-based

algorithm constructions in fluid mechanics can be viewed in a unified manner as specific criteria within a weighted-residuals framework. Here, the error in the approximate satisfaction of the conservation equations is not set to zero itself, but instead its integral with respect to selected "weights" is required to vanish (Finlayson, 1972). Within weighted residuals, the *collocation method* reproduced the classical finite difference quotients. Conversely, the family of finite volume algorithms is retrieved by using constant weights. Generalizing the weights to be function and defining them as identical to the the approximation functions for the conservation variables yields the *Galerkin criteria*, named after the original procedure of Galerkin (1915). For a linear elliptic differential equation, this definition reproduces exactly the classical variational principle extremization, the successor formulation of the original finite-element concept. Finally, defining the weights to be the differential approximation error itself yields the *least-squares method*. Pioneering research on finite element applications to fluid mechanics problems has employed several of these weighted-residuals criteria. Oden (1972) was among the first to derive the basic theoretical analog for the Navier-Stokes equations. Baker (1971, 1973, 1974) published results for an elementary incompressible flow with recirculation, obtained using the Galerkin criteria. Olson (1972) published a pseudo-variational finite-element algorithm for the biharmonic equation streamfunction analog for two-dimensional incompressible flow. Lynn (1974) utilized the least-squares criteria to develop a finite-element algorithm for laminar boundary-layer flow that preserved a symmetric matrix structure. Popinski and Baker (1976) developed a Galerkin criteria algorithm for laminar boundary-layer flow and published direct comparisons with results of a Crank-Nicolson finite-difference algorithm. Chung and Chiou (1976) published a similar algorithm construction for laminar boundary-layer flow behind a shock. From the current perspective, it appears that the Galerkin criteria weighted-residuals formulation is most representative of a direct extension from the classical concepts. Therefore, in this text, the finite-element algorithm is synonymous with Galerkin weighted residual when addressed to a nonlinear problem definition. Thereby, for the introductory linear problem classes, we always retrieve the classical variational principle extremization. Let us now review some basic analytical solution procedures for linear differential equations, as a means of reviewing terminology and concepts appropriate to the important developments.

2.2.1 Galerkin criteria

While it is possible to develop simple finite-element algorithm for linear field problems, linearity is a to big constraint for the vast majority of the problem classes in fluid mechanics and heat transfer. For finite-element algorithm to exhibit wide-ranging applicability, it is imperative that an alternative residuals (MWR) is the theoretical vehicle required. This method has been

introduced by Garlekin (1915) in its first formulation for a problem class in elasticity.

The fundamental concept in MWR is to deal directly with the governing differential equation L(q) and the boundary condition l(q). Any approximate solution, say q^h, is hypothesized to exist; upon direct substitution, $L(q^h)$ and $l(q^h)$ are statements of the error in the solution approximation. Defining any set of weighting functions say $W(\mathbf{x})$, the generated error is required to be orthogonal on R^n and on ∂R in the sense that:

$$\int_{R^n} W(x)L(q^h)d\tau - \lambda \int_{\partial R} W(x)l(q^h)d\sigma \equiv 0 \tag{2.39}$$

In the equation, λ is an arbitrary multiplier that can take on a convenient value, and there are as many (scalar) equations as members w_k of the weight set $W(x), 1 \leq k \leq K$. The essential step is restatement of the main equation onto the assembly of operations performed on a finite-element domain basis. The required matrix operator is S_e hence equation 2.39 takes the form :

$$S_e \left[\int_{Re^n} W(x)L(q_e)d\tau - \lambda \int_{\partial R_e \cap \partial R} W(x)l(q_e)d\sigma \right] \equiv 0 \tag{2.40}$$

where $q_e(x)$ is the elemental contribution to the approximate solution q^h:

$$q^x \equiv \sum_{e=1}^{M} q_e(x) = \sum_{e=1}^{M} N_k(x)^T Q_e \tag{2.41}$$

Equation 2.40 is sufficiently general to encompass the theoretical statement of practically all discrete approximation algorithms in the Eulerian description of fluid dynamics, including finite differences, finite volume, control volume, and discrete element procedures. The basic distinction between these methods and a finite-element algorithm is selection of the weight function basis $W(x)$. The psychology of the finite-element definition is simply to faithfully reproduce the energy functional extremization

$$S_e \left[\frac{\partial I^h}{\partial Q_e} \right] \equiv 0 \tag{2.42}$$

for the linear, steady-state heat-conduction problem statement, since in this instance the theoretical structure guarantees an optimally accurate approximation. The differential equation statement for the steady-state conduction problem is

$$L(T) = \nabla \cdot k\nabla T + p\dot{q} = 0 \tag{2.43}$$

$$l(T) = k\nabla T \cdot \hat{n} + h(T - T_r) = 0 \tag{2.44}$$

$$\tag{2.45}$$

Direct substitution yields to

$$S_e \left[\int_{Re^n} W(\nabla \cdot k\nabla T_e + p\dot{q}_e)d\tau - \lambda \int_{\partial R_e \bigcap \partial R} W[k\nabla T_e]d\sigma \right] \equiv 0 \qquad (2.46)$$

Correspondingly the extremization of elemental contribution to the energy functional, for the variational statement equivalent to 2.43 is

$$S_e \left[\int_{Re^n} [k\nabla N_k \cdot \nabla {N_k}^T Q_e - N_k \rho \dot{q}]d\tau + \int_{\partial R_e \bigcap \partial R} N_k h[{N_k}^T Q^e - T_r]d\sigma \right] = 0 \qquad (2.47)$$

2.2.2 An example using Galerkin FEM

Lets consider the Poisson equation in a region Ω:

$$-\nabla^2 u = f \text{ on } \Omega \qquad (2.48)$$

with boundary conditions

$$u = u_D \text{ on } \Gamma_D \qquad (2.49)$$

$$-\frac{\partial u}{\partial n} = -\mathbf{n} \cdot \nabla u = h_N \text{ on } \Gamma_N \qquad (2.50)$$

$$(2.51)$$

where the boundary $\Gamma = \Gamma_D \bigcup \Gamma_N$ has been split into a Dirichlet and a Neumann part. The weak part can be obtained by multiplying Eq. (2.48) with a testfunction v:

$$(v, -\nabla^2 u - f) = 0 \text{ for all } v \qquad (2.52)$$

where the standard inner product on $L^2(\Omega)$ is

$$(a, b) = \int_\Omega abdx \qquad (2.53)$$

With

$$\nabla \cdot (\nabla u)v = \nabla \cdot ((\nabla u)v) - \nabla u \cdot \nabla v \qquad (2.54)$$

and the divergence theorem (Gauss):

$$\int_\Omega \nabla \cdot \mathbf{a}dx = \int_\Gamma \mathbf{n} \cdot \mathbf{a}d\Gamma \qquad (2.55)$$

we get the weak form, that means we have to find $u \in SS$ such that

$$(\nabla v, \nabla u) + (v, h_N)_{\Gamma_N} = (v, f) \qquad (2.56)$$

for all $v \in V$. where S and V are suitable functional spaces for u and v, respectively. Notes

- $v = 0$ on Γ_D, $u = u_D$ on Γ_D
- we have silently introduced that:

$$\begin{aligned}(\mathbf{a}, \mathbf{b}) &= \int_\Omega \mathbf{a} \cdot \mathbf{b} d\Omega \\ (a, b)_\Gamma &= \int_\Gamma abd\Gamma\end{aligned}$$

The weak form can be used to obtain an approximate solution using the Galerkin FEM technique. For this we define approximating spaces S_h and V_h, that means that we have to divide the region into elements:

$$\Omega = \bigcup_e \Omega_e, \Omega_e \bigcap \Omega_f = \emptyset fore \neq f \tag{2.57}$$

and interpolate u and v by polynomials on each element (approximation denoted by u_h and v_h)

$$\begin{aligned}u_h(x,t) &= \sum_i u_i(t)\phi_i(x) = \phi^T(x)u(t) \\ v_h(x,t) &= \sum_i v_i(t)\phi_i(x) = \phi^T(x)v(t)\end{aligned}$$

where $\phi(x)$ are global shape functions. Substituting into the weak form leads to

$$v^T K u = v^T f \text{ for all } v \tag{2.58}$$

or

$$Ku = f \tag{2.59}$$

where the 'stiffness matrix' K and the right-hand side f are given by

$$\begin{aligned}K = (\nabla\phi, \nabla\phi^T) \quad &\text{or} \quad K_{ij} = (\nabla\phi_i, \nabla\phi_j) \\ f = (\phi, f) - (\phi, h_N)_{\Gamma_N} \quad &\quad f_i = (\phi_i, f) - (\phi_i, h_N)_{\Gamma_N}\end{aligned}$$

where the left column is in matrix notation and the right column in index notation.

Chapter 3

Results

In this chapter we are going to presents some of the results obtained applying the Diffuse Interface Model to engineering problems. In the first section we present the experimental evidence of the motion of a single non-equilibrium drop due to a non-equilibrium force that arise whenever its composition and that of the continuum phase are not at mutual equilibrium. This effect was shown in a previous work by Vladimirova et al. applying the diffuse interface model to a non-equilibrium drop. The experiment allowed us to check the theoretical assumption that are present in the model. The second section that we present in this chapter includes some results on the mixing/demixing problem that have been solved and modeled by Vladimirova et al. This simulations were done to check the validity of our own written code. The successive four sections we present contain some new results coming from the application of the diffuse interface model to engineering problems, like the behavior of a drop or of a group of drops in a shear flow, the enhancement to the separation process due to a temperature effect and how the presence of a two different phase with different conductivities can determine with the orientation of the spinodal domains during the phase separation. Finally, we presents some results from a collaborative project with the Eindhoven University, done over a three component system.

3.1 Motion of a single non-equilibrium drop

Reproduced in part from

"Experimental Evidence of the Motion of a Single Out-of-Equilibrium Drop" D. Molin and R. Mauri, *Langmuir* , **23**, 7459-7461 (2007)

3.1.1 Introduction

In this work, we intend to document with a "clean" experiment that a single, neutrally buoyant drop at conditions of chemical nonequilibrium experiences

a force that induces its movement, whereas, at equilibrium, such drop remains still.

The movement of out-of-equilibrium drops has been extensively observed in the study of the process of phase separation of liquid binary mixtures. In fact, it was observed that, even in the viscous regime, i.e. in the absence of any buoyancy forces, liquid-liquid phase transition is driven by convection. This conclusion was reached in the early works by Chou & Goldburg (1979) and Wong & Knobler (1981) using light scattering techniques, or, more recently, by Guenoun *et al.* (1987), Tanaka (1995), Tanaka & Araki (1998) and Poesio *et al.* (2006) by direct observation. In particular, 10 μm droplets during phase separation are observed to move with $10 \div 100 \mu m/s$ typical speeds. (Gupta *et al.*, 1999) As a result, phase separation of partially miscible solvent mixtures occurs very rapidly, irrespective of the presence of emulsifying compounds within the solution. (Ullmann *et al.*, 1995) However, no clean experiment has even been conducted to document the movement of a single drop.

Theoretically, phase transition of fluid mixtures has been successfully described through the diffuse interface model, Anderson *et al.* (1998), Lowengrub and Triskinovsky (1998) and Vladimirova *et al.* (1999) also known as H model under the taxonomy of Hohenberg and Halperin (1977). Here, transports of mass and momentum are coupled *via* a Korteweg body force. This force, which arises from minimizing the free energy of the system, is proportional to chemical potential gradients, and therefore it is identically zero at thermodynamic equilibrium. As shown in many simulations, the Korteweg body force is responsible for diffusiophoresis, that is the strong motion of the single-phase domains that is observed experimentally during liquid-liquid phase transition (Lamorgese and Mauri, 2005; Lamorgese and Mauri, 2006). As expected, when the system is composed of single-phase domains separated by sharp interfaces, the Korteweg force reduces to the more conventional Marangoni capillary force (Jasnow and Vinals, 1996; Jacqmin, 2000). Imposing that such non equilibrium capillary force balances viscous forces (assuming that inertial forces are negligible), Siggia (1979) showed that the enhanced coalescence caused by such effects can explain the experimentally observed linear growth of the nucleating droplet size during phase separation.

In related works, Karpov (1995) and Karpov and Oxtoby (1997) noticed that capillary forces drive the motion of nucleating droplets along a composition gradient, leading to particle clustering and direct coalescence. Similar phenomenon was also observed by Santonicola *et al.* (2001), who also noticed that convection starts to occur as soon as the temperature of the mixture reaches its critical value, well before the appearance of nucleating droplets.

Here we are interested in the motion of a single drop in conditions of nonequilibrium. Such phenomenon has been studied in other contexts as

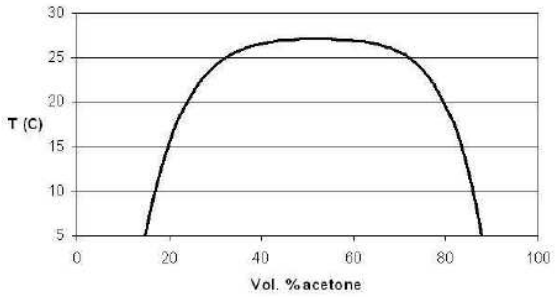

Fig. 3.1: Phase diagram of the acetone-hexadecane liquid mixture (data taken from Macedo and Rasmussen [70]).

well. In particular, Kogi *et al.* (2001) studied the behavior of a single micrometer-size oil droplet that forms at the end of a capillary tube and is immersed in an aqueous surfactant solution. The drop appears to vibrate, with oscillation frequencies and amplitudes that depend on the droplet size and the surfactant concentration. Also, Magome and Yoshikawa (1996) studied the self-movement in an oil/water system generated by chemically driven Marangoni instability. This effect was also studied theoretically by Tsemakh *et al.* (2004).

In all these works, the movement of the isolated drop arises as a result of uneven surfactant concentration at the interphase during adsorption. As noted above, though, a similar phenomenon can also arise in generic nonequilibrium conditions, even when the initial configuration is isotropic. In fact, numerical simulations by Vladimirova, Malagoli and Mauri (2003) have shown that a single drop in nonequilibrium conditions is unstable and starts to move, due to the effects of the Korteweg body force. In this letter, we intend to document experimentally this movement.

3.1.2 Experimental setup and results

We employed the acetone-hexadecane mixture that was used in previous works (Mauri *et al.*, 2003; Califano *et al*, 2005) It consists of an isopycnic, partially miscible binary liquid mixtures, with the two coexisting phases having the same density, so that buoyancy forces can be neglected. The phase diagram of this binary system is shown in Figure 3.1.

At 20^oC, acetone and hexadecane have a $\Delta\rho = 4 \times 10^{-4} g/cm^3$ (i.e. less than 0.1%) density difference and the mixture separates into two phases having 0.25 and 0.80 acetone volume fractions.

The following procedure was utilized in a standard experiment. After a

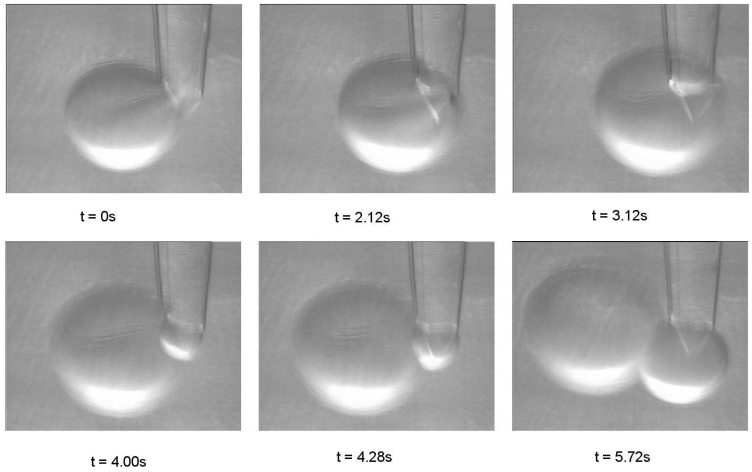

Fig. 3.2: Dynamic of the injection of a hexadecane-rich phase drop in the acetone-rich phase mixture. Pictures were taken from above, showing the movement of the drops in a horizontal plane.

50% acetone - 50% hexadecane mixture was prepared at ambient temperature, we waited for the two phases to separate and then filled a glass tube with the acetone-rich phase. Then, we injected a drop, which was composed either of the hexadecane-rich phase at equilibrium, or of pure hexadecane. In the first case, the drop was at thermodynamic equilibrium with the surrounding phase, while in the second case it was not. The drop was generated and injected using an Eppendorf (CellTram Vario) microinjector, with a capillary tip ranging from 1 μm to 100 μm in diameter, so that the drop size was in the $10\mu m$ to $500\mu m$ range, with a Bond number not exceeding 10^{-5}. After the injection, the movement of the droplet was monitored from above, i.e. on a horizontal plane, using a CCD camera-video system attached to a Nikon (Eclipse 80i) optical microscope. The experimental setup was designed to avoid vibration of the capillary tip as well as solvent evaporation. All experiments were carried out at room temperature.

Figure 3.2 shows the typical behavior of a drop at equilibrium with the surrounding phase, using a capillary tip with $10\mu m$ diameter. As the drop exits the capillary end, it does not move, until it is pushed away by a new drop. Clearly, although this behavior was largely expected, since drops and continuum phase are at equilibrium with each other, it shows that there were no spurious effects, such as buoyancy and thermocapillarity, affecting the results of our experiments. The experiment was repeated with drops ranging from $50\mu m$ to $500\mu m$ in diameter, with identical results.

Figure 3.3 shows the typical behavior of a $20\mu m$ pure hexadecane drop immersed in the surrounding acetone-rich phase. Here, as soon as it is in-

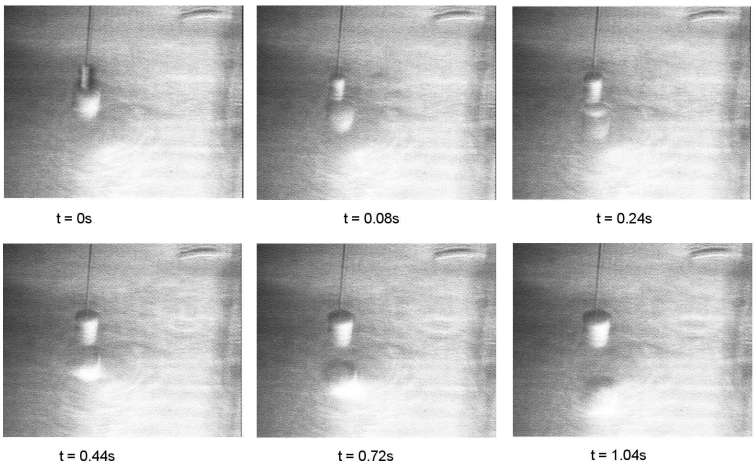

Fig. 3.3: Dynamic of the injection of a pure hexadecane phase drop in the acetone-rich phase mixture. Pictures were taken from above, showing the movement of the drops in a horizontal plane.

jected, the drop moves in the horizontal plane, away from the capillary tip. Since gravity is perpendicular to the observation plane, this movement cannot be due to buoyancy. As the droplet moves, its composition changes, tending to reach equilibrium with the surrounding. Eventually, when equilibrium is attained, the drop stops moving. The experiment was repeated with drops ranging from $10\mu m$ to $100\mu m$ in diameter and different out-of-equilibrium compositions, with identical results. A few experiments were also conducted using a water-acetonitrile-toluene mixture, obtaining similar results.

A rough estimate shows that $10 \div 100\,\mu m$, out-of-equilibrium drops move at speeds exceeding $10\,\mu m/s$. Such velocities do not appear to depend strongly on the drop size, although further experiments are needed to support such statement. Since no linear increase of the drop velocity with its size was observed, we conclude that the motion of the drop cannot be due to thermocapillary effects induced by non uniform temperature distributions. (Lavrenteva and Nir, 2001) Accordingly, the observed movement of the isolated, out-of-equilibrium drop must result from diffusiophoresis, thus confirming the instability predicted by Vladimirova *et al.*. (1999) Also, following the dimensional analysis of Gupta *et al.*, (1999) we see that the Korteweg force f_K is much larger than the adhesive force f_{adh} between the drop and the capillary tip. This result can be obtained considering that $f_K \approx \sigma R^2/\lambda$, where $\sigma \approx 10 dyne/cm$ is the liquid-liquid surface tension, $R \approx 10\mu m$ the drop radius and $\lambda \approx 10^{-2}\mu m$ the interface thickness, while $f_{adh} \approx \sigma_{sl} R$, where $\sigma_{sl} \approx 100 dyne/cm$ is the solid-liquid surface tension.

In conclusion, the present section provides experimental evidence that, even in the absence of buoyancy, a single droplet in conditions of non equilibrium can move as a result of a net Korteweg force. This force, resulting from free energy minimization, is proportional to the chemical potential gradient, and therefore it is identically zero in conditions of thermodynamic equilibrium. On the contrary, in conditions of non equilibrium, the Korteweg force induces an instability that, as predicted in numerical simulations by Vladimirova *et al.*, (1999) generates a movement of the drop, even when the initial conditions are isotropic.

3.2 Mixing/demixing of a binary mixture

3.2.1 Introduction

In most of the previous numerical studies on mixing, the mixing of two fluids A and B has been considered as the result of the chaotic advection of one fluid into the other, assuming that the instantaneous velocity of a fluid particle is the solution of the Navier-Stokes equation for a single-phase fluid (Aref, 1984; Ottino, 1990, Wiggins 1991, Fountain et al. 1999). Clearly, this is rigorously true only in the dilute limit and when the fluid mixture is ideal, which means that the enthalpic properties of the fluid mixture are neglected, assuming that the interparticle forces between A and A are equal to those between B and B and those between A and B (Sandler, 1999). This approximation seems to be justified when the flow is turbulent, so that convection dominates any diffusive process resulting from the thermodynamic properties of the system. In general, however, at low Reyonolds numbers this approximation ceases to be valid and the physico-chemical properties of the fluid mixture have to be taken into account. In this section we will present a series of simulations of the mixing process occurring after heating a quiescent and initially phase-separated liquid mixture to a temperature T well above its critical point of miscibility, showing that the process is strongly influenced by the interplay between convection and diffusion. The latter is induced by the velocity fluctuations of the molecules that compose the system at thermal equilibrium and consist of their incoherent, random motion, with no specific preferential direction. On the contrary, convection, when it is not imposed from the outside, can exist only for a system far from equilibrium, as it consists of the collective, coherent motion of its molecules, and is therefore a much faster process than diffusion. As explained by the so-called diffuse interface model, called also model H, in the taxonomy of Hohenberg and Halperin, 1977, convection arises as the system tends to minimize its free energy and, in fact, is induced by a body force that that is proportional to the gradient of the chemical potential. At the late stages of phase separation, after the system has developed well-defined phase interfaces, this body force reduces to the more conventional surface tension, as shown by Jasnow and Vinals (1996), so that the driving force can be thought of as a non-equilibrium attractive force among drops.

3.2.2 Theory

The motion of an incompressible binary fluid mixture composed of two species A and B is described here through a modification of the diffuse interface model. Here, A and B are assumed to have the same viscosities, densities and molecular weight with the composition of the system uniquely determined though the molar fraction ϕ of, say, species A as a function of position $\mathbf{r}$ and time t. If the flow is assumed to be slow enough to neglect

the inertial terms in the Navier-Stokes equation, conservation of mass and momentum lead to the following system of equation,

$$\begin{aligned} \frac{\partial \phi}{\partial t} + \mathbf{v} \cdot \nabla \phi &= -\frac{1}{\rho} \nabla \cdot \mathbf{J}, && (3.1) \\ \eta \nabla^2 \mathbf{v} - \nabla p &= \mathbf{F}_\phi, && (3.2) \\ \nabla \cdot \mathbf{v} &= 0, && (3.3) \\ & && (3.4) \end{aligned}$$

where $\mathbf{v}$ is the average local fluid velocity, $\mathbf{J}$ is the diffusion flux and $\mathbf{F}_\phi$ is a body force. As shown by Mauri et al. (1996), $\mathbf{J}$ is proportional to the gradient of the chemical potential through the relation,

$$\mathbf{J} = -\rho \phi (1 - \phi) D \nabla \tilde{\mu}, \tag{3.5}$$

where D is the molecular diffusivity, and $\tilde{\mu} = \mu_A - \mu_B$ is the generalized (non-dimensional) chemical potential difference between the two species defined as (Landau and Lifshitz, 1953) $\tilde{\mu} = \delta(\Delta g/RT)/(\delta\phi)$. Here Δg denotes the molar free energy of mixing, defined as

$$\Delta g = RT[\phi \log \phi + (1 - \phi) \log(1 - \phi) + \Psi \phi (1 - \phi) + \frac{1}{2} a^2 (\nabla \phi)^2], \tag{3.6}$$

where R is the gas constant, a is a characteristic microscopic length and Ψ is the Margules parameter, which describes the relative weight of enthalpic versus entropic forces. Phase separation occurs whenever the temperature of the system T is lower than the critical point $d^2 g/d\phi^2 = 0$ and $\phi = \frac{1}{2}$, we find that $\Psi_c = 2$ is the critical value of Ψ. Therefore, the single-phase region of the phase diagram corresponds to values $\Psi < 2$, while the two-phase region has $\Psi > 2$. At the end of the phase segregation process, a surface tension σ can be measured at the interface and from that, a can be determined as

$$a \sim \frac{1}{\sqrt{\tau} (\Delta \phi)_{eq}^2} \frac{\sigma M_w}{\rho RT}, \tag{3.7}$$

where $\tau = (\Psi - 2)/2$ while $(\Delta\phi)_{eq}$ is the composition difference between the two phases at equilibrium. This relation can be easily derived considering that $\sigma \sim \rho l (\Delta g)_{eq}$ is the jump in free energy across an interface at equilibrium, which can be estimated from and $l \sim a/\sqrt{\tau}$ is the characteristic interface thickness. In the following, we will assume that $\tau = O(1)$. The body force is given by:

$$\mathbf{F}_\phi = \frac{\rho}{M_w} \frac{\delta g}{\delta \mathbf{r}} = \left(\frac{\rho RT}{M_w} \right) \tilde{\mu} \nabla \phi = \left(\frac{\rho RT}{M_w} \right) [\nabla \tilde{p} - \phi \nabla \mu], \tag{3.8}$$

where $\tilde{p} = \phi \tilde{\mu}$ is a pressure term which does not play any role. In particular, when the system presents well-defined phase interfaces, such as at the late

stages of phase separation, this body force reduces to the more conventional surface tension. Therefore, being proportional to $\tilde{\mu}$, which is identically zero at local equilibrium, $\mathbf{F}_\phi$ can be thought of as a non-equilibrium interfacial force.

Since $\mathbf{F}_\phi$is driven by surface energy, it tends to minimize the energy stored at the interface driving, say, A-rich drops towards A-rich regions. The resulting non-equilibrium attractive force f_A between two isolated drops of radius R separated by a thin film of thickness d can be easily evaluated as $f_A \sim F_\phi R^2 d \sim R^2\sigma/a$. The magnitude of this attractive force is much larger than that of any repulsive interaction among drops due to the presence of surface-active compounds, this explaining why the rate of phase separation in deeply quenched liquid mixtures is almost independent of the presence of surfactants. The ratio between convective and diffusive mass fluxes defines the Peclet number, $N_{Pe} = Va/D$, where V is a characteristic velocity, which can be estimated considering that $V \sim F_\phi a^2/\eta$, with $F_\phi \sim \rho RT/(aM_w)$. Finally we obtain

$$N_{Pe} = \frac{a^2}{D}\frac{\rho}{\eta}\frac{RT}{M_w} \approx \frac{\sigma a}{\eta D}, \tag{3.9}$$

which coincides with the "fluidity" parameter defined by Tanaka and Araki (1998) For systems with very large viscosities, N_{Pe} is small and the model describes a diffusion-driven separation process, as in polymer melts and alloys. For most liquids, however, N_{Pe} is very large, typically $N_{Pe} > 10^3$, showing that diffusion is important only in the vicinity of local equilibrium, when the body force F_ϕ is negligible.

3.2.3 Numerical results

Let's restrict out analysis to two-dimensional systems, so that the velocity $\mathbf{v}$ can be expressed in terms of a stream function ψ, i.e. $v_1 = \partial\psi/\partial r_2$ and $v_2 = -\partial\psi/\partial r_1$. The equations of motion become

$$\frac{\partial\phi}{\partial t} = \nabla\psi \times \nabla\phi - \frac{1}{\rho}\nabla\cdot\mathbf{J}, \tag{3.10}$$

$$\eta\nabla^4\psi = \left(\frac{\rho RT}{M_w}\right)\nabla\tilde{\mu}\times\nabla\phi, \tag{3.11}$$

$$\tag{3.12}$$

where $\mathbf{A}\times\mathbf{B} = A_1B_2 - A_2B_1$.

Since material transport here is diffusion-limited, the length scale of the process is the microscopic length a. Therefore, using the scaling,

$$\tilde{\mathbf{r}} = \frac{1}{a}\mathbf{r}, \tilde{t} = \frac{D}{a^2}t, \tilde{\psi} = \frac{1}{DN_{Pe}}\psi, \tag{3.13}$$

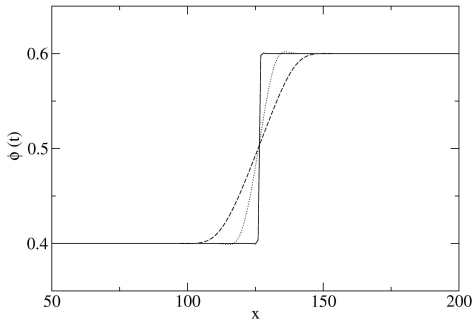

Fig. 3.4: Evolution of the concentration field assuming an initially plane interface for $N_Pe = 0$ and $N_Pe = 10^4$ at time $t = 0.1, 1$, and 5×10^3 for $\Psi = 0$ (left) and $\Psi = 1.9$ (right)

the equations of motion become

$$\frac{\partial \phi}{\partial \tilde{t}} = N_{Pe}\tilde{\nabla}\tilde{\psi} \times \tilde{\nabla}\phi + \tilde{\nabla} \cdot (\tilde{\nabla}\phi - \phi(1-\phi)) \times [2\Psi + \tilde{\nabla}^2]\tilde{\nabla}\phi), \quad (3.14)$$

$$\tilde{\nabla}^4\tilde{\psi} = -\tilde{\nabla}(\tilde{\nabla}^2\phi) \times \tilde{\nabla}\phi. \quad (3.15)$$

$$(3.16)$$

This system of differential equations has been time-integrated on a $L = 1000a$ square domain with periodic boundary conditions using the finite difference scheme described before. First, we simulated the mixing process between two fluids which are initially quiescent and separated by a place interface, $r_1 = L/2$. In this case the body force is identically zero, so that $\mathbf{v} = 0$ and therefore the process does not depend on the Peclet number. In fact the equations seen before are well approximated by the following equation

$$\frac{\partial \phi}{\partial t} = D^* \frac{\partial^2 \phi}{\partial r_1^2}, \quad (3.17)$$

with

$$D^*(\bar{\phi}) = D[1 - 2\Psi\bar{\phi}(1-\bar{\phi})], \quad (3.18)$$

where $\bar{\phi}$ represents the mean value of ϕ, as the neglected terms play a role only at the very beginning of the mixing process, when the interface is still sharp.

As shown in figure 3.4 the results are in perfect agreement with equation, confirming that the mixing process of two fluids separated by an initially phase plane sharp interface remains one-dimensional, does not depend on the Peclet number and is a purely diffusive process, with an effective diffusivity D^* that depends on the thermodynamic properties of the mixture, i.e. the

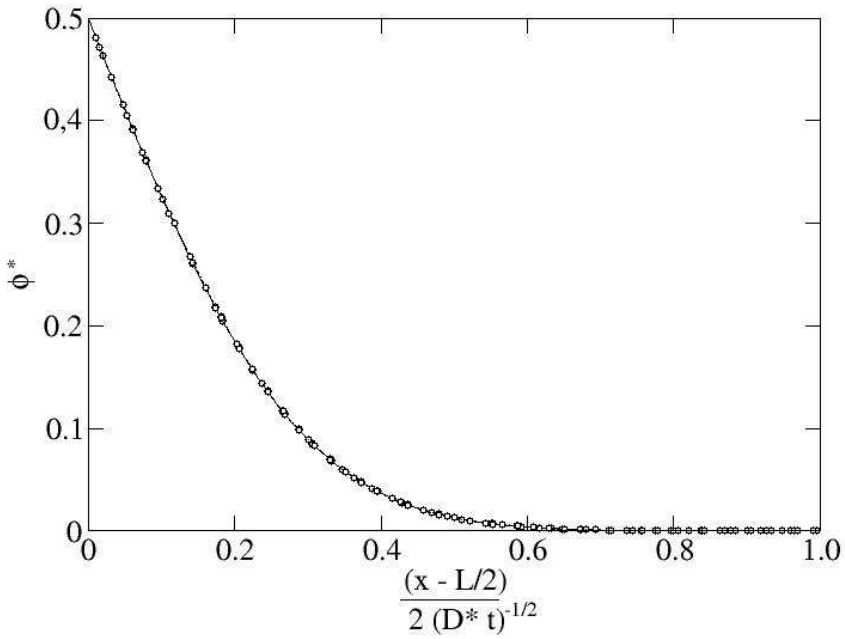

Fig. 3.5: Master curve of the evolution of the concentration field with an initial plane interface for $N_{Pe} = 0$ and $N_{Pe} = 10^4$ for different value of Ψ

value of the Margules parameter ψ. The same result is obtained whenever the initial configuration is one-dimensional, as in the case of an isolated drop. If we simulate the mixing process of more drops, two drops for examples tend to attract each other and even coalesce, provided that the Peclet number is large enough and the drops are initially very close to each other.

This effect is shown in figure 3.6 the evolution of two identical drops with $\Psi = 1.9$ and radius $40a$ that are placed within the quiescent bulk of fluid at a distance of $120a$ from each other. When $N_{Pe} = 0$, the drops do not move and are reabsorbed by diffusion, while when $N_{Pe} = 10^4$, they rapidly coalesce and form a larger isolated single drop. This latter, though, has to be reabsorbed by diffusion too, and, being larger than the original drops, will take approximately twice as long to disappear. Consequently, mixing appears to be faster in the absence of convection.

This effects that we observe in our simulation are in agrement with what Vladimirova et al. (2004).

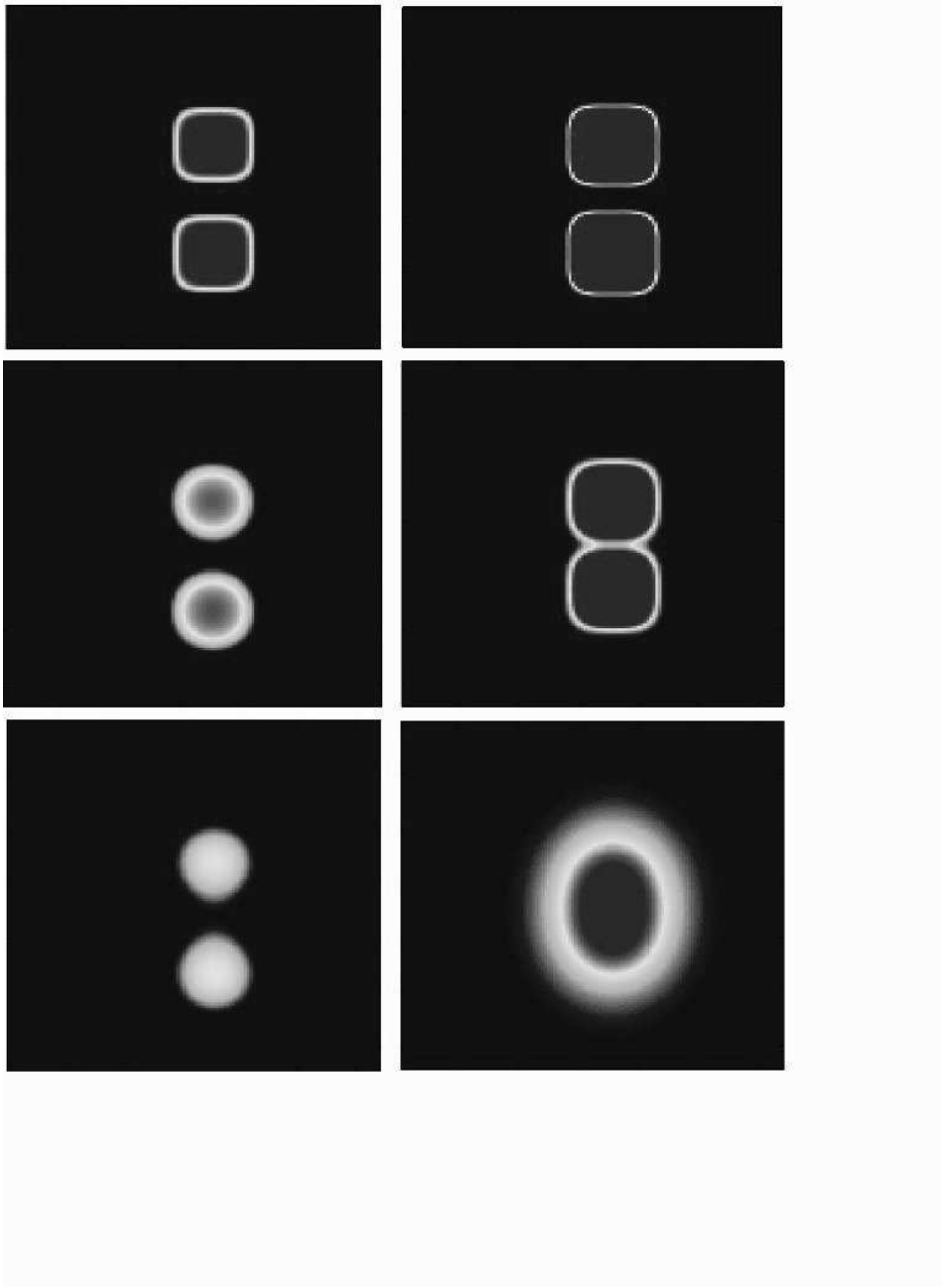

Fig. 3.6: Snapshots of the evolution of two identical drops with $N_{Pe} = 0$ (left) and $N_{Pe} = 10^4$ (right) at time $t = 0, 2, 5 \times 10^3 a^2/D$. The drops have $\Psi = 1.9$, an initial radius of $40a$ and are placed within the bulk fluid at a distance of "120 a" from each other.

3.3 Heat transport during phase separation of liquid mixtures

Reproduced in part from

"Enhanced Heat Transport During Phase Separation of Liquid Binary Mixtures" D. Molin and R. Mauri, *Phys. Fluids*, **19** 074102-1-10 (2007)

3.3.1 Introduction

In general, when a binary mixture is brought from the single phase region of its phase diagram to the two-phase unstable region, it phase separates through a process that is referred to as spinodal decomposition. As shown in many experimental and numerical works, in low viscosity liquid mixtures this process is driven by the convection that is induced by phase transition, which is responsible for the experimentally observed enhanced coalescence among the drops (see Poesio *et al.*, 2006). Accordingly, it comes natural to assume that during phase separation an effective heat diffusivity could be defined, resulting from the fluctuations of the velocity and temperature fields, just like in turbulent flows.

To study this phenomena, we simulated the phase separation of a binary mixture that is confined within a domain whose walls are instantaneously quenched below the critical temperature. Since we are interested in qualitative results, we confine ourselves to 2D simulations which, as shown in previous works, (see Lamorgese and Mauri, 2005 and Lamorgese and Mauri, 2006) produce results that are very similar to their 3D counterparts. As expected, the mixture starts to demix near the walls, where, correspondingly, a strong convection is induced, enhancing the transport of heat.The mixture is modeled through the diffuse interface model (see Anderson *et al.*, 1998 and Lowengrub and Truskinovsky, 1998) (otherwise called model H, in the taxonomy of Hohenberg and Halperin, 1977), which is based on the pioneering work of van der Waals (1979), together with the Ginzburg-Landau theory of phase transition (see Le Bellac, 1991). This model was applied to model the spinodal decomposition of binary mixtures by Cahn and Hilliard (1958) and was later generalized to include hydrodynamics by Kawasaki (1970). In the diffuse interphase model, convection is driven by a non-equilibrium body force, proportional to the gradient of the chemical potential difference. As noted by Jasnow and Viñals (1996), when the system is composed of single-phase domains separated by sharp interfaces, this force, which is generally referred to as the Korteweg force, incorporates capillary effects, and plays the role of a Marangoni force. This was formally proven by Lowengrub and Truskinovsky (1998) and Jacqmin (2000), who performed a careful matched asymptotic expansion and showed that the motion of sharp interfaces between immiscible fluids can be obtained as the outer expansion of the

velocity field, calculated using the diffuse interface approach, and it satisfies the usual Marangoni-type boundary conditions at the interfaces. This model shows that during the early stages of phase separation, initial instabilities grow exponentially, forming, at the end, single-phase micro-domains whose size corresponds to the fastest-growing mode of the linear regime. (Mauri *et al.* (1996)) During the late stages of the process, the system consists of well-defined patches, in which the average concentration is not too far from its equilibrium value (see Vladimirova *et al.*, 1999). At this point, depending on whether mass transfer is dominated by inertial forces, diffusion or viscous forces, the typical domain size grows with time as $R(t) \sim t^{2/3}$, $R(t) \sim t^{1/3}$ or $R(t) \sim t$, respectively (see Furukawa, 1994). The first scaling is observed for large Reynolds number, e.g. when phase transition takes place in pressure-driven fluid flows (see Kendon *et al.*, 2001) or in free convection flows; the second scaling, on the contrary, occurs for very viscous systems, e.g. polymer solutions and alloys, with very weak convection, where phase separation is driven by diffusion (see Siggia, 1979). The third scaling corresponds to low Reynolds - large Peclet fluid flows and it is the most commonly observed in closed systems, with no imposed pressure difference and negligible density variations (see Poesio *et al.*, 2006). In this work, assuming to be in the viscous regime, we show how induced convection enhances heat transfer.

Recently, a dynamic van der Waals theory has been presented by Onuki (2005) and Onuki and Kanatani (2005), to study the motion of a droplet in a single component fluid, subjected to small temperature gradients at zero gravity. When phase change is taken into account, the density difference between the two phases, together with the Korteweg reversible body force, induces a convection that increases the heat flux, so that the temperature gradients within the droplet nearly vanish. As a result, the Marangoni effect arising from surface tension gradients is almost suppressed and the resulting droplet velocity is much reduced. In the present work, since we consider a two-component liquid mixture with constant density, convection is due only to the Korteweg force, so that the effect of that force alone on heat transfer can be studied. In addition, we revisited van der Waals' theory, applying it to binary mixtures, determining on one hand some well known thermodynamic properties of regular mixtures (i.e. mixtures whose components are van der Waals fluids), such as the fact that the excess free energy does not depend on temperature, together with other properties of the non local part of the free energy, that have been overlooked in the past. In particular, we showed that interface thickness, a parameter that appears in the diffuse interface method, is not a constant, as was assumed, for example, in Onuki (2005), but it is proportional to the inverse square root of the temperature. Consider a homogeneous mixture of two species A and B with molar fractions $x_A = \phi$ and $x_B = 1 - \phi$, respectively, which are kept at temperature T and pressure P. For simplicity, we assume that the molecular weights, specific volumes and viscosities of A and B are the same; in particular, that means that we

assume the mixture to be incompressible. The thermodynamic molar Gibbs free energy, g_{th} is a coarse-grained free energy functional given by:

$$g_{th}(\phi) = g_{id}(\phi) + g_{ex}(\phi), \tag{3.19}$$

where g_{id} is the Gibbs free energy of an ideal mixture,

$$g_{id}(\phi) = RT[\phi \ln \phi + (1-\phi)\ln(1-\phi)], \tag{3.20}$$

where R is the gas constant, while g_{ex} is the excess (i.e. non ideal) part of the free energy,

$$g_{ex}(\phi) = RT\Psi\phi(1-\phi), \tag{3.21}$$

where Ψ is a function of T (it cannot depend on P, since the mixture is assumed to be incompressible). This expression, which is generally referred to as the one-parameter Margules correlation (see Prausnitz *et al.*, 1986), can be derived in terms of the difference between the intermolecular potentials among identical and different neighbors. Accordingly, the ideal part of the free energy in Eq. (3.19) represents an entropic contribution, which is proportional to the temperature, while the excess part is an enthalpic term, depending on interparticle potentials and therefore independent of the temperature, so that $\Psi \propto 1/T$. Consequently, considering that at the critical point, when $T = T_C$ and $\phi = \phi_C = 1/2$, the free energy has an inflection point, i.e. $\partial^2 g/\partial\phi^2 = 0$, so that $\Psi_C = 2$, we obtain:

$$\Psi = \frac{2T_C}{T}. \tag{3.22}$$

Mixtures that behave in that way are denoted as regular (see Sandler, 1999). Since $s_{ex} = -(\partial g_{ex}/\partial T)_{P,x}$, we see that for regular mixtures $s_{ex} = 0$, i.e. their entropy equals that of an ideal mixture. In addition, considering that $v_{ex} = (\partial g_{ex}/\partial P)_{T,x}$, since g_{ex} is independent of P, we see that $v_{ex} = 0$, i.e. their specific volume as well equals that of an ideal mixture (in our case, though, this last result is already implicit in the assumption of incompressibility). In order to take into account the effects of spatial inhomogeneities, Cahn and Hilliard (1958) introduced the generalized specific molar free energy g, which is given by the expression

$$g(\phi, \nabla\phi) = g_{th}(\phi) + \Delta g_{nl}(\nabla\phi), \tag{3.23}$$

where

$$\Delta g_{nl}(\nabla\phi) = \frac{1}{2}a^2(\nabla\phi)^2, \tag{3.24}$$

is a non local molar free energy due to changes in composition, where a represents the typical length of spatial inhomogeneities. In Eq. (3.24), a is a characteristic length, roughly equal to the interface thickness at equilibrium which, for a regular mixture, has the same value as i.e. $a = \sqrt{(9\pi T_C/4T)}d$,

where d is the excluded volume length defined previously. Now, consider that, at equilibrium, the mixture is segregated in two phases, separated by a sharp interface. By definition, a surface tension σ can be defined as the extra energy per unit surface associated with this surface. Accordingly, σ is equal to the integral of the Cahn-Hilliard free energy across the interface, so that, as shown by Van der Waals (1979), $\sigma \approx (\rho\lambda/M_w)\,\Delta g_{ex}$, where $\Delta g_{ex} \approx RT\,(\Delta\phi)_{eq}\,a^2/\lambda^2$ is a typical value of the change in the Cahn-Hilliard molar free energy within the interface at equilibrium, while $\lambda \approx a/\sqrt{\tilde{\psi}}$, with $\tilde{\psi} = (\Psi - 2)/2$, is the characteristic interface thickness (Van der Waals (1979)). Therefore we obtain Eq. (3.79) and from there, considering that $(\Delta\phi)_{eq} \approx \tilde{\psi}^{1/2}$, we see that a can be determined from σ as

$$a \approx \tilde{\psi}^{-3/2}\frac{\sigma M_w}{\rho RT}. \tag{3.25}$$

3.3.2 The equations of motion

These equations must be coupled to the equation of energy conservation,

$$\rho c\frac{dT}{dt} + \nabla\cdot\mathbf{j}_q = \dot{q}, \tag{3.26}$$

where c is the molar specific heat (the same for A and B), $\mathbf{j}_q$ is the diffusive heat flux, while $\dot{q}$ is the energy dissipation term. Assuming a simple Fourier constitutive relation, we have:

$$\mathbf{j}_q = -k\nabla T, \tag{3.27}$$

where k is the heat conductivity, that in general, depends on the composition, e.g. $k = k(\phi)$, although here we assume it independent of ϕ. The energy dissipation term is the sum of three contributions: the dissipative work of the external forces, $\mathbf{F}^{(e)}$, viscous dissipation and the enthalpy of mixing:

$$\dot{q} = \mathbf{F}^{(e)}\cdot\mathbf{v} + \eta|\nabla\mathbf{v}|^2 + \dot{h}_{mix}, \tag{3.28}$$

where $\dot{h}_{mix} = \rho h_{ex}\dot{\phi}$ depends on the energy h_{ex} that is either generated or consumed when the two components of the mixture are isothermally mixed together. Note that $\mathbf{F}_\phi$ does not contribute to $\dot{q}$, since it is a reversible force (see Lamorgese and Mauri, 2006). In our case, since viscous dissipation is negligible and there are no external forces, dissipation is due exclusively to the enthalpy of mixing. Now, applying classical thermodynamics, (see Siggia, 1999) we obtain,

$$\frac{h_{ex}}{RT} = -T\left[\frac{\partial(g_{ex}/RT)}{\partial T}\right]_{P,\phi}, \tag{3.29}$$

showing that for regular mixtures, when g_{ex} does not depend on T, $h_{ex} = g_{ex}$, and therefore:

$$\dot{q} = \rho RT\Psi\phi(1-\phi)\dot{\phi}. \tag{3.30}$$

Now we restrict our analysis to two-dimensional systems, so that the velocity $\mathbf{v}$ can be expressed in terms of a stream function ψ, i.e. $v_1 = \partial\psi/\partial r_2$ and $v_2 = -\partial\psi/\partial r_1$. Consequently, we obtain:

$$\frac{\partial\phi}{\partial t} = \nabla\psi \times \nabla\phi - \frac{1}{\rho}\nabla\cdot\mathbf{j}, \tag{3.31}$$

$$\eta\nabla^4\psi = \nabla\mu \times \nabla\phi, \tag{3.32}$$

$$\frac{\partial T}{\partial t} = \nabla\psi \times \nabla T + \alpha\nabla^2 T + \frac{\dot{q}}{\rho c}, \tag{3.33}$$

where $\alpha = k/\rho c$ is the heat diffusivity, while

$$\mathbf{A} \times \mathbf{B} = A_1 B_2 - A_2 B_1. \tag{3.34}$$

Since the main mechanism of mass transport at the beginning of phase segregation in diffusion, the length scale of the process is the microscopic length $\hat{a}$. Therefore, using the scaling:

$$\tilde{r} = \frac{1}{\hat{a}}r; \quad \tilde{t} = \frac{D}{\hat{a}^2}t; \quad \tilde{\psi} = \frac{1}{\alpha D}\psi, \tag{3.35}$$

and substituting Eqs. (3.47) and (3.30) into Eqs. (3.31)-(3.33), we obtain the governing equations in terms of concentration ϕ, stream function ψ and inverse temperature Ψ:

$$\frac{\partial\phi}{\partial\tilde{t}} = N_{Pe}\tilde{\nabla}\tilde{\psi}\times\tilde{\nabla}\phi + \tilde{\nabla}\cdot(\tilde{\nabla}\phi - \phi(1-\phi)[\Psi(2+\tilde{\nabla}^2)\tilde{\nabla}\phi + (2\phi-1)\tilde{\nabla}\Psi]), \tag{3.36}$$

$$\tilde{\nabla}^4\tilde{\psi} = -\tilde{\nabla}(\Psi\tilde{\nabla}^2\phi) \times \tilde{\nabla}\phi, \tag{3.37}$$

$$\frac{\partial\Psi}{\partial\tilde{t}} = -N_{Pe}\tilde{\nabla}\tilde{\psi} \times \tilde{\nabla}\Psi + N_{Le}[\tilde{\nabla}^2\Psi - \frac{2}{\Psi}(\tilde{\nabla}\Psi)^2] - \tilde{c}^{-1}\frac{\partial\phi}{\partial\tilde{t}}, \tag{3.38}$$

where $\tilde{c} = c/R$ is the non-dimensional specific heat, $N_{Le} = \alpha/D$ is the Lewis number, while the non-dimensional term,

$$N_{Pe} = \frac{\hat{a}^2\rho RT}{D\eta}, \tag{3.39}$$

can be interpreted as the Peclet number, that is the ratio between convective and diffusive mass fluxes in the convection-diffusion equation, i.e. $N_{Pe} = V\hat{a}/D$. Here V is a characteristic velocity, which can be estimated

as $V \sim F_\phi \hat{a}^2/\eta = N_{Pe} D/\hat{a}$, where $F_\phi \sim \rho RT/\hat{a}$. The same conclusion can be reached considering that $V \approx \sigma/\eta$ and substituting the expression (3.79) for the surface tension σ. A similar, so called "fluidity" parameter was also defined by Tanaka and Araki (1998). For systems with very large viscosity, N_{Pe} is small, so that the model describes the diffusion-driven separation process of polymer melts and alloys (see DeGennes, 1980 and Vladimirova *et al.*, 1998). For most liquids, however, N_{Pe} is very large, with typical values ranging from 10^3 to 10^5.

3.3.3 Numerical methods

The governing equations (3.36) - (3.38) were solved on a uniform two dimensional square grid with constant width $[(x_i, y_i) = (i\Delta x, j\Delta y), i = 1, N, j = 1, N]$ where $N = 128, 256, 512$, and time discretization $[t = n\Delta t, n = 0, 1, 2, ...]$. The physical dimensions of the grid were chosen such that $\Delta x/\hat{a}$, $\Delta y/\hat{a} = 3/2$; such space discretization was based on a cell-centered, second order accurate approximation. The time step Δt satisfies $\Delta t/(\hat{a}^2/D) \approx 0.01 - 0.001$; such choice was determined semi-empirically in order to maintain the stability of the numerical scheme. Note that the nonlinearity of the equations prevents a rigorous derivation of the stability constraints on Δt, but one can roughly estimate that the size of Δt will scale as $O(\Delta x^4, \Delta y^4)$, which is the order of the highest operator in the discretized system.

The time integration from $t^n = n\Delta t$ to $t^{n+1} = (n+1)\Delta t$ was achieved in three steps. First, we computed the stream function by solving the biharmonic equation (3.32) with the source term evaluated at the time $t^n = n\Delta t$, using a FFT algorithm; second, we computed the inverse temperature distribution, using the concentration field evaluated at the previous step; third, Eq. (3.31) was advanced in time, using the velocity and temperature fields computed from the updated stream function and updated inverse temperature, through a straightforward explicit Eulerian step. This makes the entire scheme $O(\Delta t)$ accurate in time, which is acceptable for our problem, since the size of the time step was kept very small anyway by the stability constraint. The boundary conditions were no flux for the concentration field and no slip for the velocity field at the two walls where the temperature quench is applied, and periodic boundary conditions at the other two walls. The discretization of the derivatives near the boundaries was modified to use only interior points. We introduced some amount of randomness into the system through a background noise in the concentration field, $\delta\phi$, with $\langle\delta\phi\rangle = 0$ and $\langle(\delta\phi)^2\rangle^{1/2} = 0.001$, which was uncorrelated both in space and in time. In two separated sets of simulation the noise was either added in the initial condition only, as in Furukawa (1997), or introduced at each time step and then subtracted at the next time step, only to be replaced with another spatially uncorrelated background noise of the same amplitude, as in Vladimirova *et al.* (1999). This last procedure, which is equivalent to

adding noise to the flux $\mathbf{j}$ on the right hand side of Eq. (1.139), is fully conservative in the sense that the volume integral of the composition ϕ is not altered by addition of the *ad hoc* noise. In fact, since for deep quenches the Ginzburg inequality is satisfied, (see Le Bellac, 1991 and Landau and Lifshitz, 1980) the background noise does not affect the behavior of the system, and only determines the instant of time when the system departs from its initial uniform state: once the linear regime is reached, the presence of the noise becomes irrelevant.

All our simulations were carried out assuming that, initially, the mixture has a uniform critical composition, $\phi_0 = 0.5$ and a temperature $T(t=0) = T_0$ above the critical temperature T_C, so that $\Psi(t=0) = \Psi_0 = 1.9 < \Psi_C = 2$, where $\Psi_C = 2$ is the critical value of the Margules parameter. Then, at time $t = 0$, two of the walls of the box are quenched instantaneously to a temperature T_w well below the critical temperature, so that $\Psi = \Psi_w > 2$ at the walls. Different value of Ψ_w have been considered, ranging from $\Psi_w = 2.1$ to $\Psi_w = 5$. Time was measured as $t = (10^5 \hat{a}^2/D)\tilde{t}_5$ where $\tilde{t}_5 = 10^{-5}\tilde{t}$ is a non-dimensional coarse time. Since typical values of D and $\hat{a}$ are $10^{-5} cm^2/s$ and $10^{-5} cm$, respectively, (Poesio *et al.*, 2006) then $\tilde{t}_5 \sim t/(1s)$.

Various simulations were carried out for different box sizes, Peclet and Lewis numbers, specific heats and quenching depths. In all cases, the mixture starts to phase separate at the walls; then, as heat losses penetrate deeper within the domain, demixing takes place everywhere, until, at steady state, the temperature of the mixture reaches its equilibrium value.

First, we observed that (see Figure 3.7) the process of cooling, as well as that of phase separation, is accelerated by convection. As shown in Figure 3.7a, when $N_{Pe} = 0$, the mixture phase separates through the formation of bicontinuous structures; since the two phases have the same heat conductivity, though, the isothermal lines (not shown here) remain parallel to the walls through the whole process, as they move towards the center of the domain. On the other hand, in the presence of convection, i.e. when $N_{Pe} = 10^2$ (see Figure 3.7b), warm fluid tends to move towards the wall; accordingly, the isothermal lines do not remain parallel to the walls and, most important, they move faster than in the previous case.

The main result of our simulation was to determine how such heat transport enhancement depends on the characteristics of the process, namely the Peclet and Lewis numbers, the specific heat and the quenching depth. The most obvious way to describe the heat transfer enhancement, is through the Nusselt number, which is defined as the ratio between the heat flux J_q at the wall and the heat flux that one would have in the absence of convection, $(J_q)_{N_{Pe}=0}$, i.e.

$$N_{Nu} = J_q / (J_q)_{N_{Pe}=0} . \tag{3.40}$$

Although N_{Nu} would seem to be a function of time, we see that it actually

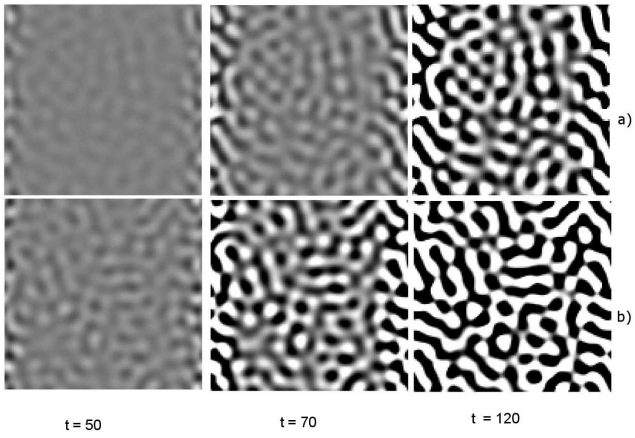

Fig. 3.7: Evolution of the concentration field for $N_{Pe} = 0$ (top) and $N_{Pe} = 10^2$ (bottom) when $N_{Le} = 1$, $\zeta = 0.05$ and with no source term. The snapshots are taken at $t = 50, 70$ and 120, where t is expressed in $\tilde{a}^2/D$ units.

remains almost constant and therefore can be used effectively to characterize the enhancement to heat transport due to phase transition.

Another way to characterize heat transport is through the cooling time. In fact, denoting by $\bar{T}$ the average temperature of the fluid, we know that, in the absence of convection, at long times, $t \gg \tau = L^2/\alpha$, a slab cools down following the equation:

$$T_w - \bar{T} = \Delta T = \Delta T_0 e^{-t/\tau} + O\left(e^{-t/4\tau}\right), \tag{3.41}$$

where τ is a characteristic cooling time and L the width of the domain. We saw that in all cases Eq. (3.41) is satisfied, provided that the heat diffusivity α is replaced with an effective heat diffusivity α^*. Not surprising, we saw that with very good approximation,

$$N_{Nu} = (\tau)_{N_{Pe}=0}/\tau = \alpha^*/\alpha, \tag{3.42}$$

thus confirming that the Nusselt number represents the enhancement to heat transport due to phase transition.

At this point, we show how N_{Nu} depends on the Peclet number, the Lewis number, the specific heat and the quenching depth,

$$\zeta = 1 - \frac{\Psi_c}{\Psi_w} = 1 - \frac{T_w}{T_c}, \tag{3.43}$$

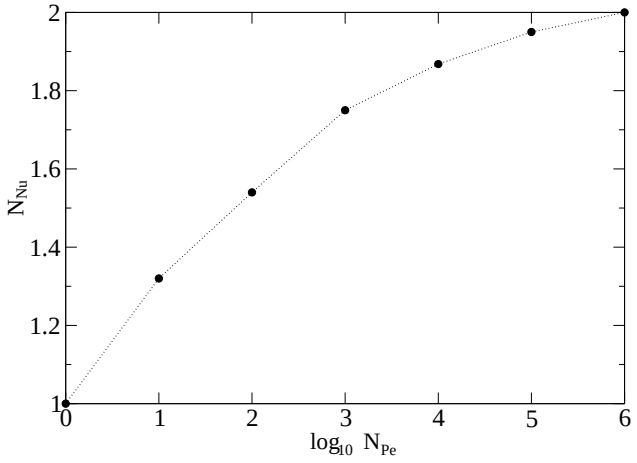

Fig. 3.8: The Nusselt number, N_{Nu}, as a function of the Peclet number, N_{Pe}, when $N_{Le} = 1$, $\zeta = 0.05$, and with no source term.

where $\Psi_c = 2.0$ is the critical value of the Margules coefficient, representing how much below the critical temperature the walls have been cooled down.

First, in Figure 3.8 we see that heat transport increases monotonically with N_{Pe}, until it reaches a plateau at $N_{Nu} \approx 2.0$ when $N_{Pe} \approx 10^6$. This result is in agreement with previous findings (Vladimirova *et al.*, 1999), showing that the induced fluid velocity grows linearly with N_{Pe} for $N_{Pe} < 10^5$, while at larger N_{Pe} it reaches a plateau.

In Figure 3.9 we show the dependence of N_{Nu} on N_{Le}, revealing that the cooling speed increases as the Lewis number increases when $N_{Le} < 1$, it remains constant at $N_{Nu} \approx 1.55$ when $1 < N_{Le} < 10$ and then it decreases when $N_{Le} > 1$. This behavior is due to the fact that, as N_{Le} increases, i.e. α increases and/or D decreases, there are two competing effects. On one hand, as D decreases, N_{Pe} increases, thereby enhancing heat transport, while, on the other hand, as α increases, heat conduction also increases and therefore N_{Nu} tends to decrease. When N_{Le} is small, the first of these effects prevails: in fact, as $N_{Le} \to 0$ (i.e. $D \to \infty$ while α is kept constant), heat transport is only conductive and therefore $N_{Nu} \to 1$. On the other hand, when N_{Le} increases further, the enhancement due to convection reaches a plateau (see Figure 3.8), while conduction continues to increase, so that the Nusselt number starts to decrease and, in fact, $N_{Nu} \to 1$ as $\alpha \to \infty$, i.e. when heat is transported mainly by conduction.

In Figure 3.10 we see the dependence of N_{Nu} on the specific heat $\tilde{c}$. Now, as $\tilde{c}$ measures the heat capacity of the mixture, N_{Nu} decreases as $\tilde{c}$ increases, as expected. However, we see that the influence of the specific heat on the

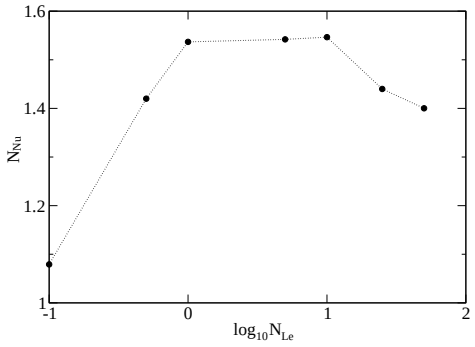

Fig. 3.9: The Nusselt number, $N_N u$, as a function of the nondimensional specific heat, $\tilde{c}$, when $N_{Pe} = 10^2$, $N_{Le} = 1$ and $\zeta = 0.05$

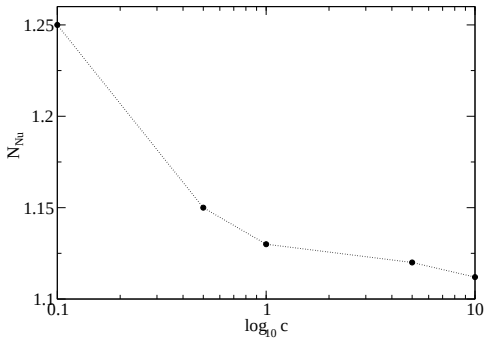

Fig. 3.10: The Nusselt number, N_{Nu} as a function of the Lewis number, N_{Le}, when $N_{Pe} = 10^2$, $\zeta = 0.05$, and with no source term.

cooling speed is really very limited, unless $\tilde{c}$ becomes unreasonably small.

Finally, we determined how the heat transfer enhancement depends on the quenching rate ζ, defined in Eq. (3.43). In Figure 3.11 we show the results of the simulations conducted by keeping $\Psi_0 = 1.9$, $Pe = 0.0$ and 10^2, while $\Psi_w = 2.1$, 2.4, 3.0 and 4.0. Unexpectedly, at first, we see that heat transport is more influenced by convection at low quenching than at high. This is due to the fact that, as ζ increases, conductive heat flux increases proportionally, i.e. $(J_q)_{N_{Pe}=0} \propto \zeta$, while the increase of its convective counterpart is slower, i.e. $\propto \zeta^{1/2}$. In fact, when $\zeta \to \infty$, we see that $N_{Nu} \to 1$, as expected. This result complements Figure 8 of Poesio *et al.* (2007), who found experimentally that, on approaching the critical temperature, i.e. when $\zeta < 0.03$, N_{Nu} tends to 1, as expected. In future works, we intend to simulate this case.

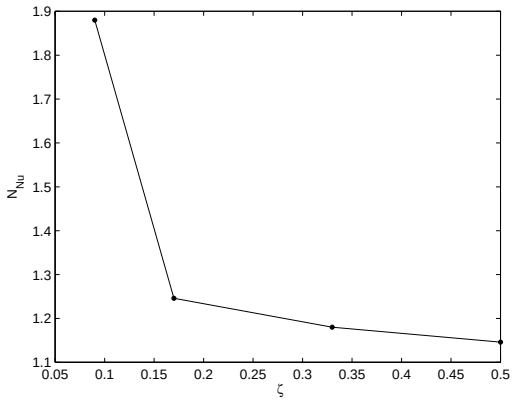

Fig. 3.11: The Nusselt number, N_{Nu} as a function of the quenching depth, ζ, when $N_{Pe} = 10^2, N_{Le} = 1$, and with no source term.

3.4 Composition-dependent heat conductivities's binary mixtures

Reproduced in part from

"Spinodal Decomposition of Binary Mixtures with Composition-Dependent Heat Conductivities" D. Molin and R. Mauri, *Int. J. Engng. Sci*, in press

3.4.1 Introduction

In the present section we would like to show the variation of the morphology of a viscous binary system after an instantaneous quench on two of the four walls that constitute the simulation box. In general, heat is transported with two different modalities, namely conduction and convection. In the first case heat propagates from hot to cold regions via a diffusive process, regulated by heat conductivity, while in the second case heat is transported by a moving fluid. Here, we assume that the fluid is very viscous, so that convection can be neglected. Instead, we intend to show how a difference in the heat conductivities of two components can affect the morphology of the process. In conventional spinodal decomposition, the mixture is quenched instantaneously and, therefore, it phase separates by forming isotropic bicontinuous structures (for a review on spinodal decomposition, see Gunton *et al.*, 1983). A different result is obtained when we simulate spinodal decomposition in a long tube whose walls are quenched instantaneously. In that case, as shown by Vladimirova *et al.* (1998), the morphology of the system during phase separation consists of dendrites aligned along the longitudinal direction, forming typical striped pattern as in the experiments of Sagui and Desai (1994).

In the present simulations, we expect that the anisotropy of the morphology will be further enhanced by the difference in heat conductivity of the two phases. The rationale of this prediction is that the system should tend to maximize heat transfer and therefore the morphology should try to get as close as possible to that corresponding to straight tubular domains spanning the whole width of the channel.

The mixture is described using the diffuse interface model, that is based on the pioneering work by Van der Waals (1979) at the end of the 19th century, then extended by Landau (Landau and Lifshitz, 1980) by developing the mean field theory and finally was applied to binary mixtures by Cahn and Hilliard (1958) at the end of the 1950's. The model shows that during the early stages of the phase separation, initial instabilities grow exponentially, forming single-phase micro-domains whose size corresponds to the fastest-growing mode of the linear regime. During the late stage of the process, the system consists of well-defined patches in which the average concentration is not too far from its equilibrium value. At this point, both analytical

calculations (Lifshitz and Pitaevsky, 1984) and dimensional analysis (Siggia, 1979) predict a growth law of the typical domain size with time, $R(t) \sim t^{1/3}$, due to the Brownian coagulation of droplets. Naturally, while, when the mixture is unbounded, the process of phase separation is isotropic, when the mixture is confined between two walls, the single phase domains will form anisotropic patterns.

3.4.2 The governing equations

Consider a homogeneous mixture of two species A and B with molar fractions $x_A = \phi$ and $x_B = 1 - \phi$, respectively, which are kept at temperature T and pressure P. For simplicity, we assume that the molecular weights, specific volumes and viscosities are constant and that they are the same for the two species, namely, $M_A = M_B = M_w$, $V_A = V_B = V$, $\eta_A = \eta_B = \eta$; in particular, that means that we assume the mixture to be incompressible. The thermodynamic molar Gibbs free energy, g_{th} is a coarse-grained free energy functional given by:

$$g_{th}(\phi) = g_{id}(\phi) + g_{ex}(\phi) \tag{3.44}$$

where g_{id} is the Gibbs free energy of an ideal mixture,

$$g_{id}(\phi) = RT[\phi \ln \phi + (1 - \phi) \ln(1 - \phi)], \tag{3.45}$$

where R is the gas constant, while g_{ex} is the excess part of the free energy,

$$g_{ex}(\phi) = RT\Psi\phi(1 - \phi), \tag{3.46}$$

where Ψ is a function of T (it cannot depend on P, since the mixture is assumed to be incompressible). This expression, generally referred to as the one-parameter Margules correlation, can been derived considering the intermolecular potentials between identical and different neighboring particles (Sandler, 1999; Mauri *et al.*, 1996). The ideal part (3.44) of the free energy is proportional to the temperature and represents an entropic contribution, while the excess part is an enthalpic term and depends on inter-particle potentials. In fact, assuming that our mixture is regular, its entropy equals that of an ideal mixture (Sandler, 1999), i.e. g_{ex} does not depend on T, so that $\Psi \propto 1/T$. Accordingly, considering that the free energy has an inflection point at the critical point, i.e. when $T = T_C$ and $\phi = \phi_C = 1/2$, then we see that $\Psi_C = 2$, and therefore the Margules parameter can be expressed as:

$$\Psi = \frac{2T_C}{T}. \tag{3.47}$$

In order to take into account spatial inhomogeneities, Cahn and Hilliard (1958) introduced the generalized specific molar free energy g, given by the expression:

$$g(\phi, \nabla\phi) = g_{th}(\phi) + \Delta g_{NL}(\nabla\phi), \tag{3.48}$$

where

$$\Delta g_{NL}(\nabla\phi) = \frac{1}{2}a^2(\nabla\phi)^2, \tag{3.49}$$

is a non local molar free energy due to changes in composition, where a represents the typical length of spatial inhomogeneities. As shown in Molin and Mauri (2007), a depends on the temperature as:

$$a = \hat{a}\sqrt{\frac{2T_C}{T}} = \hat{a}\sqrt{\Psi}, \tag{3.50}$$

where $\hat{a}$ is a characteristic length, independent of the temperature. As shown by Van der Waals (1979), as the surface tension σ is the energy stored in the unit area of the interface separating two phases at local equilibrium, we obtain:

$$\sigma = \frac{1}{2}\frac{\rho RT}{M_w}a^2\int(\nabla\phi)^2 dl \sim \frac{\rho RTa}{M_w}, \tag{3.51}$$

where we have considered that, far from the critical point, the molar fraction difference between the two phases at equilibrium, $(\Delta\phi)_{eq}$, and the nondimensional thickness of the interface region at local equilibrium, $\lambda/a \approx \sqrt{\Psi-2}$, are both of $O(1)$. This shows that the characteristic length a can be determined once surface tension is known (see discussion in Vladimirova *et al.*, 2000).

From the molar free energy, we may define a generalized chemical potential difference $\tilde{\mu}$ as,

$$\tilde{\mu} = \frac{\delta(g/RT)}{\delta\phi} = \frac{\partial(g/RT)}{\partial\phi} - \nabla\cdot\frac{\partial(g/RT)}{\partial(\nabla\phi)} = \mu_0 + \ln\frac{\phi}{1-\phi} + \Psi(1-2\phi) - a^2\nabla^2\phi, \tag{3.52}$$

where $\mu_0 = (g_B - g_A)/RT$.

3.4.3 The equations of motion

Imposing that the number of particles of each species is conserved, we obtain the continuity equations for the molar concentrations of species A and B (Vladimirova *et al.*, 2000),

$$\frac{\partial c_A}{\partial t} + \nabla\cdot(c_A\mathbf{v}_A) = 0, \qquad \frac{\partial c_B}{\partial t} + \nabla\cdot(c_B\mathbf{v}_B) = 0, \tag{3.53}$$

where $\mathbf{v}_A$ and $\mathbf{v}_B$ are the mean velocities of the two species. For an incompressible mixture composed of species with identical physical properties, these equations lead to the following continuity equation,

$$\frac{d\phi}{dt} = \frac{\partial\phi}{\partial t} + \mathbf{v}\cdot\nabla\phi = -\nabla\cdot\mathbf{j} \tag{3.54}$$

where $d/dt = \partial/\partial t + \mathbf{v}\cdot\nabla$ is the material derivative, $\mathbf{v} = x_A\mathbf{v}_A + x_B\mathbf{v}_B$ is the average velocity of the mixture, while $\mathbf{j}$ is the diffusive mass flux. The

latter is proportional to the gradient of the generalized chemical potential gradient as:

$$\mathbf{j} = -\phi(1-\phi)D\nabla\tilde{\mu}, \tag{3.55}$$

where D is a composition-independent diffusion coefficient. Finally, substituting (3.72) into (3.55), we obtain

$$\mathbf{j} = -D\nabla\phi + D\phi\,(1-\phi)\left[a^2\nabla\nabla^2\phi + 2\Psi\nabla\phi + (2\phi-1)\,\nabla\Psi\right]. \tag{3.56}$$

Here, the term $D\nabla\phi$ on the RHS represents the regular diffusion flux, while the last term vanishes for small concentrations of either solvents, i.e. when ($\phi \to 0$ or $\phi \to 1$), and for ideal mixtures, i.e. when $a = \Psi = 0$. Note that the a^2 term is always stabilizing, with a being a function of temperature through Eq. (3.50).

Equation (3.54) must be coupled to the traditional heat equation,

$$\rho c\frac{dT}{dt} + \nabla\cdot\mathbf{j}_q = \dot{q}, \tag{3.57}$$

where ρ is the mass density and c the specific heat (which are both assumed to be uniform, here), $\mathbf{j}_q$ is the diffusive heat flux, while $\dot{q}$ is the energy dissipation term. Assuming a simple Fourier constitutive relation for the heat flux, we have:

$$\mathbf{j}_q = -k(\phi)\nabla T, \tag{3.58}$$

where $k(\phi)$ is the composition-dependent heat conductivity. Assuming a linear dependence between heat conductivity and composition, with $k_A = k$ and $k_B = \lambda k$ denoting the heat conductivities of the two species, we obtain:

$$k(\phi) = k\left[\phi + \lambda(1-\phi)\right]. \tag{3.59}$$

Since the problem is invariant upon changing ϕ and λ into $(1-\phi)$ and λ^{-1}, here we will assume, without loss of generality, that $0 < \lambda \leq 1$.

In general, Eqs. (3.54) and (3.57) should be coupled to the equation of momentum conservation. This equation here does not play any role, though, as we assume that heat and molar convection fluxes are negligible compared to diffusion fluxes, that is both molar and thermal Peclet numbers are small, i.e. $N_{PeM} = V\hat{a}/D << 1$ and $N_{PeT} = V\hat{a}/\alpha << 1$, where $\alpha = k/\rho c$ is the heat diffusivity of species A and V is a characteristic velocity. Note that $N_{PeT} = N_{PeM}N_{Le}^{-1}$, where $N_{Le} = \alpha/D$ is the Lewis number, which for most polymer melts ranges from 10^4 to 10^6. Accordingly, $N_{PeM} << 1$ is the leading assumption here, which allows us to state that $\mathbf{v} = \mathbf{0}$, i.e. $d/dt = \partial/\partial t$, in Eqs. (3.54) and (3.57). As shown in previous works (see for example Vladimirova et al., 1999), as $V \approx (\hat{a}\rho RT)\,/\,(M_w\eta)$, this assumption can also be written as $\left(\hat{a}^2\rho RT\right)\,/\,(M_w D\eta) << 1$ and therefore it is satisfied for very viscous mixtures.

The energy dissipation term in Eq. (3.57) is the sum of viscous dissipation and heat of mixing (Molin and Mauri, 2007),

$$\dot{q} = \dot{q}_v + \dot{h}_{mix} = \eta |\nabla \mathbf{v}|^2 + \left(\frac{\rho}{M_w} \right) h_{ex} \dot{\phi}, \tag{3.60}$$

where h_{ex} is the the energy that is generated when one mole of mixture is mixed together isothermally. Now, since from classical thermodynamics (Sandler, 1999) $h_{ex} = -RT^2 \left[\partial (g_{ex}/RT)/\partial T \right]_{P,\phi}$, we see that, for regular mixtures, when g_{ex} does not depend on T, we have:

$$h_{ex} = g_{ex} = RT\Psi\phi(1-\phi). \tag{3.61}$$

From these expressions, we see that $\dot{q}_v \approx \eta V^2/\hat{a}^2$, while $\dot{h}_{mix} \approx \rho RTD/M_w\hat{a}^2$. Therefore, $\dot{q}_v/\dot{h}_{mix} \approx N_{Ec}\, N_{Pr}/N_{Le}\, \hat{c}$, where $N_{Ec} = V^2/c\Delta T$ is the Eckert number, $N_{Pr} = \nu/\alpha$ is the Prandtl number, $N_{Le} = \alpha/D$ is the already defined Lewis number, while $\hat{c} = M_w c/R$ is the non dimensional specific heat. In our case, in agreement with other assumptions, we have: $N_{Ec} << 1$, $N_{Pr} < 1$, $N_{Le} >> 1$ and $\hat{c} >> 1$. Accordingly, $\dot{q}_v << \dot{h}_{mix}$, so that $\dot{q} = \dot{h}_{mix}$. Now, comparing in Eq. (3.57) the diffusive term with the energy dissipation term, we see that $O\left(\nabla \cdot \mathbf{j}_q/\dot{q}\right) = N_{Le}\, \hat{c} >> 1$. Therefore, we may conclude that the dissipation term can be neglected altogether, and the heat equation becomes:

$$\frac{dT}{dt} = \alpha\left(1-\lambda\right)\nabla\phi\cdot\nabla T + \alpha\left[\lambda + \left(1-\lambda\right)\phi\right]\nabla^2 T. \tag{3.62}$$

At this point, scaling (3.54) and (3.62) in terms of

$$\hat{r} = \frac{1}{\hat{a}} r \quad \text{and} \quad \tilde{t} = \frac{D}{\hat{a}^2} t, \tag{3.63}$$

we obtain the following equations governing the concentration field, ϕ, and the Margules parameter Ψ [which is inversely dependent on the temperature T through Eq. (3.47)]:

$$\frac{\partial \phi}{\partial \tilde{t}} = \tilde{\nabla} \cdot \left\{ \tilde{\nabla}\phi - \phi\left(1-\phi\right)\left[\Psi\left(2 + \tilde{\nabla}^2\right)\tilde{\nabla}\phi + \left(2\phi - 1\right)\tilde{\nabla}\Psi \right] \right\}, \tag{3.64}$$

and

$$N_{Le}^{-1}\frac{\partial \Psi}{\partial \tilde{t}} = \left[\lambda + \left(1-\lambda\right)\phi\right]\left[\tilde{\nabla}^2\Psi - \frac{2}{\Psi}\left(\tilde{\nabla}\Psi\right)^2 \right] + \left(1-\lambda\right)\tilde{\nabla}\phi\cdot\tilde{\nabla}\Psi. \tag{3.65}$$

3.4.4 Numerical results

The governing equations (3.64) and (3.65) were solved on a uniform two-dimensional square grid with constant width ($(x^{(i)}, y^{(j)}) = (i\Delta x, j\Delta y), i = 1, \ldots, N_x, j = 1, \ldots, N_y$) and time discretization ($t^{(n)} = n\Delta t, n = 0, 1, 2, \ldots$).

The physical dimensions of the grid and the time step were chosen such that $\Delta x = \Delta y = 2a$, while $\Delta t/(a^2/D) \approx 0.01 - 0.001$. A convergence test with respect to grid refinement was carried out in Lamorgese and Mauri (2005), showing that such grid size is appropriate. The time step was determined semi-empirically, in order to maintain the stability of the numerical scheme. Note that the non-linearity of the equations prevents a rigorous derivation of the stability constraints on Δt, but one can roughly estimate that the size of Δt will scale as $O(\Delta x^4, \Delta y^4)$, which is the order of the highest operator in the discretized system (see discussions in Lamorgese and Mauri, 2005). The space discretization was based on a cell-centered approximation of both the concentration and the inverse temperature variables, ϕ and Ψ. The spatial derivatives on the RHS of Eqs. (3.64) and (3.65) were discretized using a straightforward second-order-accurate approximation. The time integration from $t^{(n)}$ to $t^{(n+1)}$ was achieved in two steps. First, we solved Eq. (3.65) to determine the Margules parameter Ψ at time $t^{(n+1)}$ using $\phi(t^{(n)})$ and $\Psi(t^{(n)})$; then, Eq. (3.64) was solved, determining the concentration field $\phi(t^{(n+1)})$ using $\phi(t^{(n)})$ and $\Psi(t^{(n+1)})$. This makes the entire scheme stable both in time and in space.

Equations (3.64) and (3.65) were solved with periodic boundary conditions along the y-axis, while at the other boundaries, i.e. the walls along the x-axis, we assumed that the material flux is zero, while the temperature is imposed. Initially, at time $t < 0$, the concentration field is uniform, with $\phi = 0.5$, while the Margules parameter is $\Psi = 1.9$, corresponding to a temperature well above its critical value. A random noise is superimposed to the composition field, with $\langle \delta\phi \rangle = 0$ and $\langle (\delta\phi)^2 \rangle^{1/2} = 10^{-2}$, assuming that it is uncorrelated both in space and in time (see Lamorgese and Mauri, 2006). Time is measured using a timescale $10^5 \hat{a}^2/D$, which is typically on the order of 1 second.

The simulations were carried out using different square grids, ranging from 128×128 to 1024×1024, to ensure that the results are independent of the domain size. The results depend on three parameters: a) the Lewis number, $N_{Le} = \alpha/D$, expressing the ratio between thermal and mass diffusivities; b) the heat conductivity ratio, $\lambda = k_A/k_B$; c) the quenching depth.

First, we studied the effects of the first two parameters, i.e. λ and N_{Le}, while the quenching depth was kept constant. Accordingly, we assumed that at time $t = 0$ the two walls are cooled down to two different temperatures, T_{w1} on the left side wall and $T_{w2} < T_{w1}$ on the right side wall, corresponding to $\Psi_{w1} = 2.1$ and $\Psi_{w2} = 3.0$, both well within the two phase region of the phase diagram. This ensures the presence of a temperature gradient within the system, so that a heat flux is always present.

In Figure 3.12, we show some snapshots of our simulations for different values of the conductive ratio and the Lewis number, at different time steps. The cases with small Lewis number, although perhaps not very common in practice, have been included because, as will be shown, they help to

understand the phenomenon. Comparing the results for $\lambda = 0.001$ with those for $\lambda = 0.1$ we see that, as expected, the smaller is λ, the smaller is the average heat conductivity of the mixture, and therefore the shorter it takes to phase separate. In addition we see that, keeping constant the heat conductivity ratio (here $\lambda = 0.001$), when $N_{Le} = 0.01$ the dendritic structures that form during the phase separation tend to align along the y-axis, while when the Lewis number is increased to $N_{Le} = 100$ they tend to align along the x direction. In fact, the main result of our simulations is that the values of the parameters λ and N_{Le} strongly influence the anisotropy of the system morphology.

The isotropy of any given discrete concentration field $\phi_{i,j}$, with $i, j = 1, 2...N$, can be quantified by the isotropy coefficient ξ as follows:

$$\xi = \frac{N_x - N_y}{N_x + N_y}, \tag{3.66}$$

with

$$N_x = \frac{1}{2}\sum_{j=1}^{N}\left[\sum_{i=1}^{N}\left(N - n_{i,j}\, n_{i+1,j}\right)\right] \;\; ; \;\; N_y = \frac{1}{2}\sum_{i=1}^{N}\left[\sum_{j=1}^{N}\left(N - n_{i,j}\, n_{i,j+1}\right)\right], \tag{3.67}$$

where the index $n_{i,j}$ is defined as equal to $+1$ when $\phi_{i,j} > 0.5$ and equal to -1 when $\phi_{i,j} < 0.5$. Clearly, N_x and N_y indicate how many times, moving along the x- and the y-axis, respectively, we cross an interface. Accordingly, $-1 \leq \xi \leq +1$, with $\xi = 0$ when the morphology is isotropic, $\xi = +1$ when it is composed of straight lines along the y-axis, and $\xi = -1$ when it is composed of straight lines along the x-axis. Note that the isotropy coefficient has such a simple definition because we know that the anisotropy can only be along the x or the y axis.

In Table 1 and Figure 3.13 we indicate and represent the value of ξ corresponding to the final, steady state configuration of the mixture for any value of λ and N_{Le}. Without loss of generality, as mentioned above, we have considered only the cases with $\lambda < 1$: the cases with $\lambda > 1$ can be derived from these results with $\lambda' = 1/\lambda$ and $N'_{Le} = N_{Le}/\lambda$.

First of all, we see that, for $\lambda = 1$, the morphology is almost isotropic for any value of the Lewis number, as the two phases have the same heat conductivity. On the other hand, when the difference between the conductivity of the two phases increases, the morphology of the system strongly depends on the value of the Lewis number. Specifically, we see that when the Lewis number is very small, the dendrites tend to align along the y-axis, while, as the Lewis number increases, they turn their orientation towards the x-axis. In fact, when $N_{Le} \ll 1$, heat propagates much slower than mass; accordingly, as soon as the temperature of the slab reaches its critical value, the mixture phase separates immediately. Since the isothermal lines (not

shown here) are in all cases almost parallel to the y-axis, it is therefore not surprising that, in this case, the dendrites will be also aligned along the same direction. On the other hand, when $N_{Le} \gg 1$, heat propagates much faster than mass; our results suggest that in this case the system will tend to maximize the heat flux, forming lines of the more conducting species spanning between the two quenched walls, along the x-axis. Flux maximization is known to occur for linear systems, as a consequence of the minimum entropy production principle. For non linear cases, we are not aware of any similar principle; accordingly, our explanation must be considered only as an attempt to explain our numerical results.

$\lambda \backslash^{N_{Le}}$	0.01	0.1	1	10	100	1000
0.001	0.34	0.20	0.33	0.17	-0.22	-0.43
0.01	0.39	0.12	0.16	0.12	-0.33	-0.42
0.1	0.10	0.14	0.06	0.12	0.16	0.11
1	0.03	0.05	0.01	0.01	0.01	0.01

Table 1 - The isotropy coefficient ξ at steady state for different values of the conductive ratio, λ, and the Lewis number, N_{Le}.

The explanation that was given above is confirmed by the results obtained by varying the quenching depth. First, we studied the phase separation occurring when the the two walls are quenched to the same temperature. In this case, the system corresponds to the specular double of that obtained when the left wall is quenched, while the right wall is insulated. In this case, as shown in Figure 3.14, the mixture tends to phase separate by forming y-oriented dendrites near the insulated wall, in the second case), in agreement with Vladimirova *et al.* (1998). Accordingly, it is only in the presence of a heat flux, i.e. when the two walls are quenched to two different temperatures, that anisotropy might develop perpendicular to the isothermal lines, that is, in our case, along the x-axis. Predictably, this happens when $N_{Le} \gg 1$, so that the tendency of the system to maximize the heat flux can prevail. In fact, when at $\lambda = 0.001$ and $N_{Le} = 100$ we keep $\Psi_{w1} = 2.1$ constant on the left side wall, while Ψ_{w2} on the right side wall is changed from 3.0 to 5.0 (corresponding to a unrealistically large temperature quench), then we see that at steady state the isotropy coefficient ξ changes from -0.22 to -0.53.

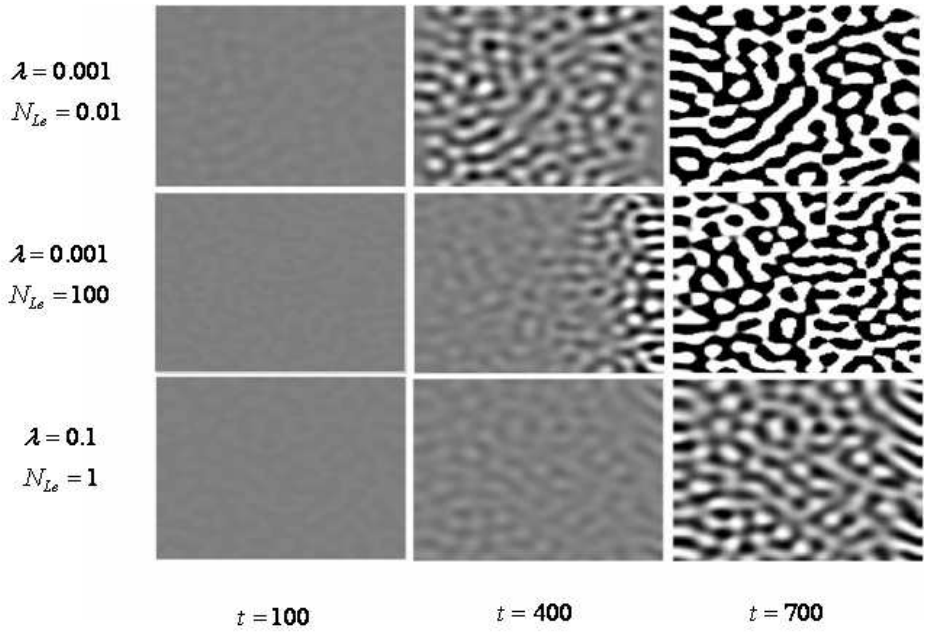

Fig. 3.12: Evolution of the concentration field for different values of the conductive ratio, λ, and the Lewis number, N_{Le}. The snapshots are taken at different times, where t is expressed in $10^5 \hat{a}^2/D$ units.

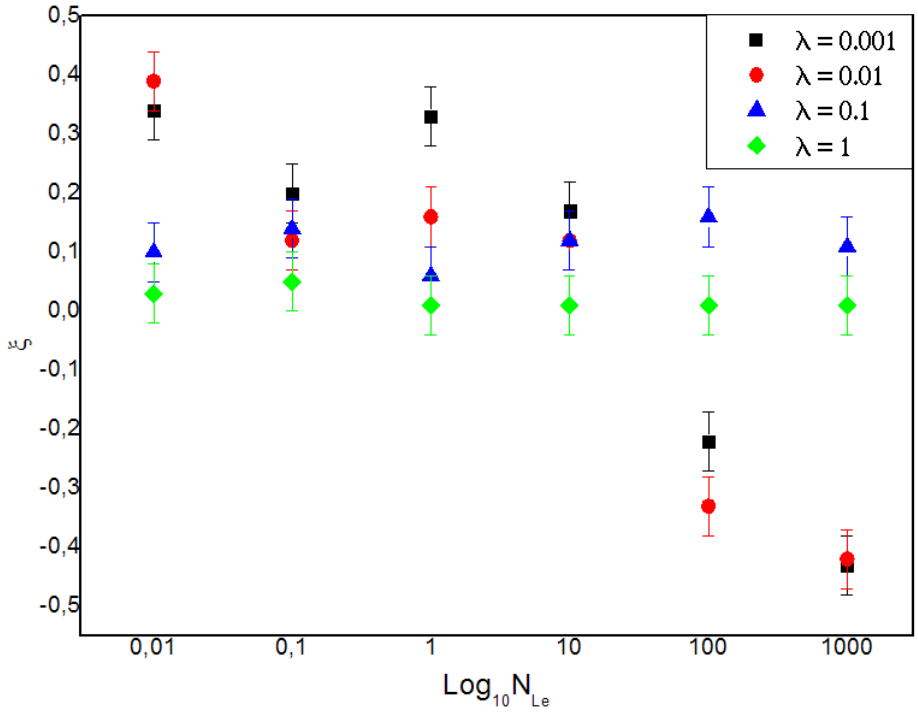

Fig. 3.13: The isotropy coefficient ξ at steady state for different values of the conductive ratio, λ, and the Lewis number, N_{Le}.

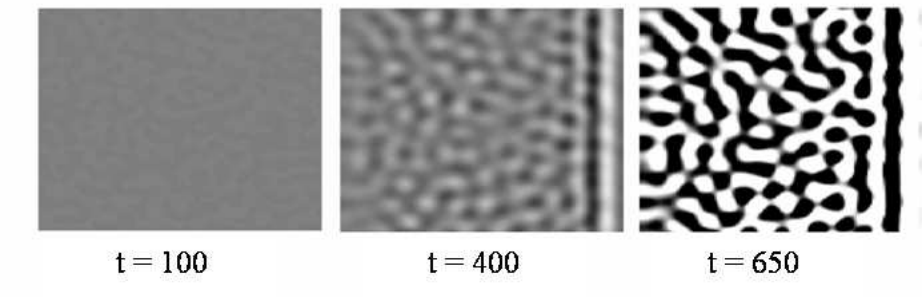

Fig. 3.14: Evolution of the concentration field for $N_{Le} = 0.1$ and $\lambda = 0.001$ when the left wall is quenched, while the right wall is insulated.

3.5 Deformation of drops in shear flow

Reproduced in part from

"Drop Coalescence and Breakup under Shear using the Diffuse Interface Model" D. Molin and R. Mauri, in preparation.

3.5.1 Introduction

In most of the studies of two-phase flow, the equations of conservation of mass, momentum, energy and chemical species are written separately for each phase, assuming that temperature, pressure, density and composition of each phase are equal to their equilibrium values, while at the interface, assumed to be a zero-thickness surface, they are supplemented by appropriate boundary conditions (see for example Davis and Scriven (1982)). Naturally, this results in a free boundary problem, which means that one of the main problems of this approach is to determine the position of the interface. To that extend, many interface tracking methods have been developed, Unverdi and Tryggvason (1992) which have proved very successful in a wide range of situations. However, there are few instances where the interface tracking breaks down. That happens when the interface thickness is comparable to the lengthscale of the phenomenon that is being studied. Typical examples are: a) near-critical fluids, as the interface thickness diverges at the critical point; b) multiphase flows in microdevices; c) motion of the contact line along a solid surface; d) breakup and coalescence of bubbles and droplets.

In front of these difficulties, the diffuse interface (D.I.) method offers an alternative approach (see Hohenberg and Halperin, 1977; Anderson *et al.*, 1998; Lowengrub and Truskinovsky, 1998; Vladimirova *et al.*, 2000 and Nauman and He, 2001). Quantities that in the free boundary approach are localized in the interfacial surface, here are assumed to be distributed within the interfacial volume. For example, surface tension is the result of distributed stresses within the interfacial region, which are often called capillary, or Korteweg, stresses. In general, the interphase boundaries are considered as mesoscopic structures, so that any material property varies smoothly at macroscopic distances along the interface, while the gradients in the normal direction are steep. Accordingly, the main characteristic of the D.I. method is the use of an "order parameter" which undergoes a rapid but continuous variation across the interphase boundary, while it varies smoothly in each bulk phase, where it can even assume constant equilibrium values. For a single-component system, the order parameter is the fluid density, for a liquid binary mixture it is the molar (or mass) fraction, while in other cases it can be any other parameter, not necessarily with any physical meaning, that allows to reformulate free boundary problems. In all these cases, the D.I. model must include a characteristic interface thickness, over which the order

parameter changes. In fact, in the asymptotic limit of vanishing interfacial width, the diffuse interface model reduces to the classical free boundary problem (see Jasnow and Viñals, 1996).

In most of the previous applications, the D.I. method has been applied to study the dynamics of phase separation in near critical fluids. In the present work, we intend to show that this approach can be successfully applied when the two phases are at equilibrium with each other. Accordingly, we chose to study the breakup and coalescence of droplets in shear flows, in the wake of recent works by Keestra *et al.* (2003) and Yue *et al.* (2004), who have studied the morphology of Newtonian and non Newtonian drops under shear using the diffuse interface approach. In particular, here we will focus on the study of a single Newtonian drop, since the original results by Taylor (1932) , this problem has been studied extensively in theoretical (Rallison, 1984) and experimental, (Richardson, 1968; Buckmaster and Flaherty, 1973; Leal, 2004) so that it can be used as an excellent test case. This problem has also been studied using different numerical techniques based on lattice discretization (Halliday *et al.*, 1996 and Wagner and Yeomans, 1997).

All the previous studies of droplet breakup have shown that the straining motion of the external shear promotes drop deformation, while surface tension acts, at first, as a restoring force while, later, when the drop becomes elongated, it may also promote burst. The actual process of break up, though, cannot be modeled by purely fluid mechanical models, unless other hypothesis are introduced, such as Marangoni stresses at the interface, due to the presence of surfactants (Bazhlekov *et al.*, 2006) Without this, or similar, assumption, the model predicts that, when the shear rate exceeds a critical value, the drop continues to elongate, never breaking neither reaching a steady configuration. In particular, since the point of breakup can never be reached, we cannot predict what happens after the burst, such as the formation of satellite drops that has been observed experimentally (Cristini *et al.*, 2003).

Similar problems are encountered in studying flow-induced drop coalescence as well. Using classical fluid mechanics, head-on collision between two drops can be modeled using the thin-film theory of the film drainage process developed by Davis and coworkers (Davis *et al.*, 1989 and Rother *et al.* , 1997), which was recently expanded and completed by Baldessari and Leal (2006), who included the effects of global drop deformation. On the other hand, the behavior of two or more drops in shear flow has not received much attention, with the exception of the work by Keestra *et al.* (2003), who applied the D.I. model this process. In the present work, we intend to extend their work, showing how drop deformation and hydrodynamic interactions play a dominant role in determining whether a pair of colliding drops under shear flow will coalesce, or simply pass around one another. In particular, we intend to study if, for a given drop size and shear flow, there is a minimum distance below which the drops coalesce.

3.5.2 The governing equations

Consider a homogeneous mixture of two species A and B with molar fractions x_A and $x_B = 1 - x_A$, respectively, kept at temperature T and pressure P. For simplicity we assume that the molecular weights, specific volume and viscosities of the two species are equal, so that the molar, volumetric, and mass fractions are all equal to each other, and the mixture viscosity is composition-independent. The equilibrium state of this system is described by the "coarse-grained" free energy functional, that is the molar Gibbs energy of mixing, Δg_{eq},

$$\Delta g_{eq} = g_{eq} - (g_A x_A + g_B x_B), \tag{3.68}$$

where g_{eq} is the energy of the mixture at equilibrium, while g_A and g_B are the molar free energy of pure species A and B, respectively, at temperature T and pressure P. The free energy Δg_{eq} can be expressed as: the sum of an ideal part Δg_{id} and a so-called excess part g_{ex}, with

$$\Delta g_{eq} = RT\left[\phi \log \phi + (1-\phi)\log(1-\phi) + \Psi\phi(1-\phi)\right], \tag{3.69}$$

where $\phi = x_A$, R is the gas constant, while Ψ is a measure of the non-ideality of the mixture and is function of T and P. This equation can also be derived from first principles, (Mauri *et al.*, 1996) showing that Ψ is proportional to the difference between the attractive forces between identical molecules, F_{AA} and F_{BB}, and the attractive forces between different molecules, F_{AB}. In order to account for the effects of spatial inhomogeneities, Cahn and Hilliard (1958) introduced the generalized specific free energy $\tilde{g}$,

$$\tilde{g} = g_{eq} + \frac{1}{2} RT a^2 (\nabla\phi)^2, \tag{3.70}$$

where a represents a typical lengthscale of spatial inhomogeneities. Now, defining the generalized chemical potential difference $\tilde{\mu}$ as

$$\tilde{\mu} = \frac{\partial(\tilde{g}/RT)}{\partial\phi}, \tag{3.71}$$

we obtain,

$$\tilde{\mu} = \mu_0 + log\frac{\phi}{1-\phi} + \Psi(1-2\phi) - a^2\nabla^2\phi, \tag{3.72}$$

where $\mu_0 = (g_B - g_A)/RT$. When $\Psi > 2$, the free energy presents a double well, i.e. an instability region where $\partial^2 g_{eq}/\partial\phi^2 < 0$. Accordingly, if the overall composition lays within that instability region, the mixture phase separates, eventually reaching an equilibrium state, which consists of two coexisting phases, with an interface region separating them. Imposing that in those conditions $\tilde{\mu} = 0$, we can determine the composition profile and find that the interface thickness is $\lambda = a/\sqrt{\Psi - 2}$ (Van der Waals, 1979 and Mauri *et al.*, 1996).

3.5.3 Equations of motion

Imposing that the number of moles of each species is conserved and assuming incompressibility, we obtain the following continuity equations,(Vladimirova *et al.* (2000))

$$\frac{\partial \phi}{\partial t} + \mathbf{v} \cdot \nabla \phi = -\nabla \cdot \mathbf{j}, \qquad \nabla \cdot \mathbf{v} = 0, \tag{3.73}$$

where $\mathbf{v}$ is the average velocity of the mixture, while $\mathbf{j}$ is the diffusive volumetric flux, with the constitutive relation,

$$\mathbf{j} = \phi(1-\phi) D \nabla \tilde{\mu}. \tag{3.74}$$

Finally, substituting Eq. (3.72) into Eq. (3.74), we obtain,

$$\mathbf{j} = -D\nabla\phi + D\phi(1-\phi)\left[a^2 \nabla \nabla^2 \phi + 2\Psi \nabla \phi\right]. \tag{3.75}$$

Here, the term $D\nabla\phi$ represents the regular diffusion flux, while the last term vanishes for small concentrations of either solvents (i.e. $\phi \to 0$ or 1) and for ideal mixtures (i.e. $a = \Psi = 0$).

The above equations of mass conservation must be coupled with the Navier-Stokes equation, where the dynamic terms can be neglected, obtaining,

$$\eta \nabla^2 \mathbf{v} - \nabla \mathbf{p} = -\mathbf{F}_\phi. \tag{3.76}$$

Here η is the mixture viscosity, which, we assume, is composition-independent, while $\mathbf{F}_\phi$ is the Korteweg body force, which equals the generalized gradient of the free energy (Lowengrub and Truskinovsky, 1998 and Lamorgese and Mauri, 2006),

$$\mathbf{F}_\phi = -\left(\frac{\rho RT}{M_w}\right)\phi \nabla \tilde{\mu}. \tag{3.77}$$

In the limit of sharp interfaces located at $\mathbf{r} = \mathbf{r}_s$, this body force reduces to the more conventional surface tension, (Jasnow and Viñals, 1996 and Jacqmin, 2000) i.e.,

$$\mathbf{F}_\phi = \left[\hat{\mathbf{n}}\sigma\kappa + (\mathbf{I} - \hat{\mathbf{n}}\hat{\mathbf{n}}) \cdot \nabla\sigma\right] \delta\left[\hat{\mathbf{n}} \cdot (\mathbf{r} - \mathbf{r_s})\right], \tag{3.78}$$

where σ is the surface tension, while $\hat{\mathbf{n}}$ and κ are the unit vector perpendicular to the interface and the curvature at $\mathbf{r}_s$, respectively. Accordingly, as shown by Van der Waals (1879), since the surface tension is the energy stored in the unit area of the interface, we obtain:

$$\sigma = \frac{1}{2}\left(\frac{\rho RT}{M_w}\right) a^2 \int (\nabla\phi)^2 dl \sim a\left(\frac{\rho RT}{M_w}\right)(\Delta\phi)_{eq}^2 \sqrt{\Psi - 2}, \tag{3.79}$$

where $(\Delta\phi)_{eq}$ is the composition difference between the two phases at equilibrium. Physically, $\mathbf{F}_\phi$ tends to minimize the energy stored at the interface,

and therefore it drives, say, A-rich drops towards A-rich regions, enhancing coalescence.

Now we restrict our analysis to two-dimensional systems, so that the velocity $\mathbf{v}$ can be expressed in terms of a stream function ψ, i.e. $v_1 = \partial\psi/\partial r_2$ and $v_2 = -\partial\psi/\partial r_1$. Consequently, substituting Eq. (3.75) into Eq. (3.73) and Eq. (3.77) into Eq. (3.76), we obtain,

$$\frac{\partial\phi}{\partial t} = \nabla\psi \times \nabla\phi - \nabla \cdot \mathbf{j}, \tag{3.80}$$

$$\eta\nabla^4\psi = \left(\frac{\rho RT}{M_w}\right)\nabla\tilde{\mu} \times \nabla\phi, \tag{3.81}$$

The above equations can be scaled in the following way:

$$\tilde{r} = \frac{1}{a}r, \qquad \tilde{t} = \alpha\frac{D}{a^2}t, \qquad \tilde{\psi} = \frac{1}{\gamma Ra}\psi, \tag{3.82}$$

obtaining,

$$\frac{\partial\phi}{\partial\tilde{t}} = \tilde{\nabla}\tilde{\psi} \times \tilde{\nabla}\phi + \alpha^{-1}\tilde{\nabla} \cdot \left\{\tilde{\nabla}\phi - \phi(1-\phi)[2\Psi + \tilde{\nabla}^2]\tilde{\nabla}\phi\right\}, \tag{3.83}$$

and

$$\tilde{\nabla}^4\tilde{\psi} = -N_{Ca}^{-1}\tilde{\nabla}(\tilde{\nabla^2}\phi) \times \tilde{\nabla}\phi, \tag{3.84}$$

where

$$N_{Ca} = \frac{\eta\gamma R}{\sigma}; \qquad \alpha = \frac{a^2}{D}\frac{\rho}{\eta}\frac{RT}{M_w} \approx \frac{a\sigma}{D\eta}. \tag{3.85}$$

Here N_{Ca} is the capillary number, expressing the ratio between viscous and capillary forces, while α is the ratio between the diffusion time scale, $\tau_D = a^2/D$ and a viscous timescale, $\tau_\sigma = a/V_\sigma$, where $V_\sigma \approx \sigma/\eta$ is a capillary-induced velocity. Accordingly, as in our previous works (Vladimirova *et al.*, 1999; Vladimirova *et al.*, 2000; Lamorgese and Mauri, 2005; Lamorgese and Mauri, 2006) convection resulted from non-equilibrium, capillary effects only, τ_σ was the convection timescale and therefore α was denoted as the Peclet number, as it denoted the ratio between diffusive and convective timescales. Here, however, that would be misleading, since convection is mainly due the imposed shear, so that the characteristic convective timescale $\tau_\gamma = \gamma^{-1}$ can be quite different from τ_σ (in fact, their ratio is the capillary number). Accordingly, we can define a Peclet number $N_{Pe} = \gamma Ra/D$, so that $\alpha \approx N_{Pe}\, N_{Ca}^{-1}$. In the following (and for lack of a better name) we will refer to α as the interfacial number, with reasonable values ranging between 10^3 and 10^6.

3.5.4 Numerical results

The governing equations (3.83) and (3.84) were solved on a uniform two-dimensional square grid with constant width ($(x_i, y_i) = (i\Delta x, j\Delta y), i = 1, N_x, j = 1, N_y$) and time discretization ($t = m\Delta t, n = 0, 1, 2, ...$). The physical dimensions of the grid were chosen such that $\Delta x/a, \Delta y = 2$ while the time step satisfied $\Delta t/(a^2/D) \approx 0.01 - 0.001$, so that the numerical scheme remained robust. Note that the non-linearity of the equations prevents a rigorous derivation of the stability constraints on Δt, but one can roughly estimate that the size of Δt will scale as $O(\Delta x^4, \Delta y^4)$, which is the order of the highest operator in the discretized system. The space discretization was based on a cell-centered approximation of both the concentration variable ϕ and of the stream function ψ. The spatial derivatives in the right-hand side of Eqs. (3.83) and (3.84) were discretized using a straightforward second-order-accurate approximation. The time integration from $t^n = n\Delta t$ to $t^{n+1} = (n + 1)\Delta t$ was achieved in two steps. First, we computed the stream function ψ by solving the biharmonic equation with the source term evaluated at time $t^n = n\Delta t$. Second, Eq.(3.83) was advanced in time, using the velocity field computed from the updated stream function and a straightforward explicit Eulerian step. This makes the entire scheme stable in time and in space.

First, we studied the deformation of an insolated drop under shear when N_{Ca} is not very large. Since the composition field of the drop and that of the ambient fluid are initially at equilibrium with each other, we can assume that such condition will continue to hold during most of the elongation of the drop. Accordingly, the diffusion flux $\mathbf{j}$ in Eq. (3.80) is identically zero and therefore the last term in Eq. (3.83) does not play any role during most of the evolution of the drop. That means that the elongation of the drop depends only on the capillary number and not on the interfacial number. In fact we see that, irrespectively of the value of α, when the capillary number lays below a threshold value, $N^*_{Ca} = 0.1$, the drop deforms and reach a stationary, elongated configuration 3.15, while, on the other hand, when $N_{Ca} > N^*_{Ca}$, the drop continues to stretch indefinitely, until it snaps. The numerical value, $N^*_{Ca} = 0.1$, is in good agreement with classical results based on continuum fluid mechanical models, the slight disagreement probably being due to the fact that here we have used a 2D model.

At this point, we studied the evolution of two identical drops. In that case, the process is far more dynamical, as drops may coalesce during their encounter, if they get sufficiently close to each other. As expected, for small values of N_{Ca}, the drops tend to remain spherical, while for larger values of N_{Ca} drops tend to be deformed by the shear. These deformations, though, occur in conditions of local equilibrium (unless N_{Ca} become very large), so that, as in the case of an isolated drop, the value of α does not play any relevant role as the drops approach one another. As soon as the two

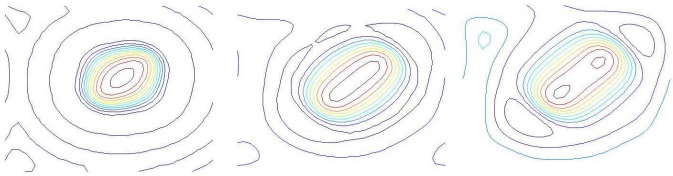

Fig. 3.15: Evolution of deformation of a drop ($N_{Ca} = 0.05$) in shear flow (contour plot).

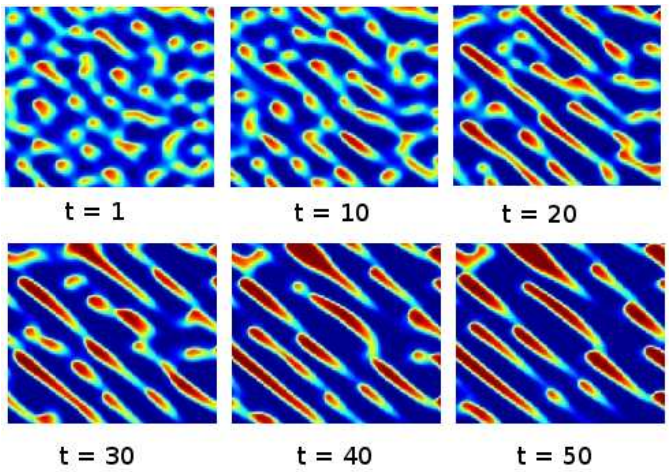

Fig. 3.16: Evolution of deformation of multiple drops ($N_{Ca} = 0.5$) in shear flow (contour plot).

drops get very close, i.e. when their mutual distance become of $O(a)$, then coalescence (or the lack of it) is driven by the diffusive (or antidiffuse) flux and therefore the value of α becomes essential in determining the outcome of the process. For example, in Figure 3.16 we show the encounter between various drops with $N_{Ca} = 0.5$ and with an initial distance around the double of their radius. In almost all cases, the drops stretch and move towards one another, following trajectories that are independent of α. Then, when their mutual distance become of $O(a)$, we see that when $\alpha = 10^3$ the two drops turn around each other and then move on, while when $\alpha = 10^6$ the two drops coalesce.

3.6 Three component system: a different approach

This work has been done under the supervision of Prof. Anderson at the Department of Mechanical Engineering of the Eindhoven University, Eindhoven, The Netherlands

3.6.1 Introduction

Many biomedical, chemical and industrial processes involve mixture of three or more liquids components. In spite of the importance of three-phase flow, most studies of three-phase systems do not consider hydrodynamical interaction (Barrett and Blowey, 1999; Barrett *et al.*, 2001; Bell *et al.*, 1989), due to the difficulties in dealing with hydrodynamics associated with interfaces and triple junctions. Some of the methods used in the past to solve this problem use a projection method (see Smith *et al.*, 2002), or with boundary integral methods that have been used to study the effect of surfactants on drop dynamics and tip-streaming. In Kan *et al.* (1998) the effect of surfactants on the dynamics of rising bubbles is investigated using an immersed boundary/front-tracking algorithm. In Peskin (1977) a hybrid level-set/front-tracking algorithm was used to study the effect of surfactants on capillary waves. Further, in Johnson *et al.* (2000), the effect of surfactants on the evolution of the shape of an initially non spherical drop translating in an otherwise quiescent fluid at low Reynolds number is examined. A combination of the boundary-integral method and a finite-difference scheme is used to solve the coupled fluid dynamics and surfactant transport problem. For this reasons in this section we would like to model and simulate a general three-component system coupled with hydrodynamic. For this purpose we use an extension of the diffuse interface model developed at the university of Eindhoven under the collaboration of Prof. Anderson.

3.6.2 Local balance equations

Consider an arbitrary volume element Ω within V, with boundary Γ and outer normal n. The total mass of component i within Ω is

$$M_i = \int_\Omega \rho_i d^3\mathbf{r}. \tag{3.86}$$

For chemical inter mixtures M_i can only change by a flux across the boundary Γ. Therefore

$$\frac{dM_i}{dt} = \int_\Omega \frac{\partial \rho_i}{\partial t} d^3r + \int_\Gamma \rho_i \mathbf{v}_i \cdot \mathbf{n} d^2r = 0, \tag{3.87}$$

where $\mathbf{v}_i$ is the velocity field of component i. Gauss' theorem can be used to transform the boundary integral into a volume integral. The resulting

volume integral holds for an arbitrary volume element, therefore

$$\frac{\partial \rho_i}{\partial t} + \nabla \cdot (\rho_i \mathbf{v}_i) = 0. \tag{3.88}$$

Conservation of total mass follows from summing equation over all components. This yields

$$\frac{\partial \rho}{\partial t} + \nabla \cdot (\rho \mathbf{v}) = 0, \tag{3.89}$$

where ρ is the density of the mixture

$$\rho = \sum_{i=1}^{N} \rho_i \tag{3.90}$$

and $\mathbf{v}$ is the barycentric velocity

$$v = \sum_{i=1}^{N} c_i \mathbf{v}_i, \text{ with mass fraction } c_i = \rho_i / \rho. \tag{3.91}$$

We can also define the velocities $\mathbf{w}_i$ relative to the barycentric velocity

$$\mathbf{w}_i = \mathbf{v}_i - \mathbf{v}. \tag{3.92}$$

These velocities are called diffusion velocities. Combining eq 3.92 and eq. 3.89 yields

$$\frac{\partial \rho_i}{\partial t} + \nabla \cdot (\rho_i \mathbf{v}) = -\nabla \cdot (\mathbf{j}_i), \tag{3.93}$$

where $\mathbf{j}_i = \rho_i \mathbf{w}_i$ is the diffusion mass flow per unit area per unit time. Summing this equation over all components we should again obtain equation therefore:

$$\sum_{i=1}^{N} \rho_i \mathbf{w}_i = 0. \tag{3.94}$$

This shows that only $N-1$ of the diffusion velocities are independent. Instead of using the N independent velocities $\mathbf{v}_i$ we can also use the barycentric velocity and the $N-1$ independent diffusion velocities as set of independent variables. The momentum P of a volume element can change due to contact and body forces. The equation of motion for Ω reads

$$\frac{dP}{dt} = \frac{d}{dt} \int_\Omega \rho \mathbf{v} d^3 r = \int_\Gamma \tau \cdot \mathbf{n} d^2 r + \int_\Omega \rho \mathbf{f}^{ex} d^3 \mathbf{r}, \tag{3.95}$$

where τ is the extra stress tensor and $\rho \mathbf{f}^{ex}$ is the total external force density, defined by

$$\rho \mathbf{f}^{ex} = \sum_{i=1}^{N} \rho_i \mathbf{f}_i^{ex}. \tag{3.96}$$

The same arguments as used for mass balance result in the following local momentum balance equation

$$\frac{\partial \rho \mathbf{v}}{\partial t} + \nabla \cdot (\rho \mathbf{v}\mathbf{v}) = \nabla \cdot \tau + \rho \mathbf{f}^{ex}. \tag{3.97}$$

Using local mass balance this can be rewritten as

$$\rho \frac{d\mathbf{v}}{dt} = \nabla \cdot \tau + \rho \mathbf{f}^{ex}, \tag{3.98}$$

where $d/dt = \partial/\partial t + v \cdot \nabla$. In the absence of heat sources the first law of thermodynamics for an open system states that the change in the sum of kinetic and internal energy (dE) equals the work done by contact and body forces (dW) plus the total energy flux (dQ). That is

$$\frac{dE}{dt} = \frac{dW}{dt} + \frac{dQ}{dt} \tag{3.99}$$

where E, being the sum of the internal energy U and the kinetic energy K, can be written as

$$E = U + K = \sum_{i=1}^{N} \int_{\Omega} \rho_i (u_i + \frac{1}{2} v_i \cdot v_i) d^3\mathbf{r}, \tag{3.100}$$

with u_i the specific internal energy of component i and v_i the velocity field of component i. Using equations and, E can be rewritten as

$$E = \int_{\Omega} \rho (u + \frac{1}{2} \mathbf{v}\mathbf{v}) d^3\mathbf{r}, \tag{3.101}$$

where

$$u = \sum_{i=1}^{N} (c_i u_i + \frac{1}{2} c_i w_i \cdot w_i) = \tilde{u} + \frac{1}{2} \sum_{i=1}^{N} c_i w_i \cdot w_i. \tag{3.102}$$

The second term on the right hand side is the kinetic energy of diffusion and $\tilde{u}$ is the 'true' internal energy, in the equilibrium sense. However, in most cases, the kinetic energy of diffusion can be neglected. In the sequel we will use the approximation $u = \tilde{u}$. The performed work and the energy flux can be written as

$$\frac{dW}{dt} = \int_{\Gamma} \tau \cdot v \cdot n d^2 r + \sum_{i=1}^{N} \int_{\Omega} \rho_i f_i^{ex} \cdot v d^3 r, \tag{3.103}$$

$$\frac{dQ}{dt} = -\int_{\Gamma} q \cdot n d^2 r. \tag{3.104}$$

The resulting local energy balance equation is

$$\rho \frac{d}{dt} (u + \frac{1}{2} \mathbf{v}\mathbf{v}) = \nabla \cdot (\tau \cdot v) - \nabla \cdot q + \rho f^{ex} \cdot v + \sum_{i=1}^{N} f_i^{ex} \cdot \rho_i w_i. \tag{3.105}$$

Mass and momentum conservation can be used to single out the kinetic contribution to equation. This results in

$$\rho \frac{du}{dt} = \tau : \nabla v + \nabla \cdot q + \sum_{i=1}^{N} f_i^{ex} \cdot \rho_i w_i. \tag{3.106}$$

In the following problems we are going to use only gravity as an external force, which is the same for each component. In this case the last term on the right hand side equals zero. In summary the local balance equations for mass, momentum and energy in a gravity field are:

$$\frac{d\rho}{dt} = -\rho \nabla \cdot \mathbf{v}, \tag{3.107}$$

$$\rho \frac{dc_i}{dt} = -\nabla \cdot j_i, \tag{3.108}$$

$$\rho \frac{dv}{dt} = \nabla \cdot \tau + \rho f_g, \tag{3.109}$$

$$\rho \frac{du}{dt} = \tau : \nabla \mathbf{v} - \nabla q. \tag{3.110}$$

To complete this set of equations we need additional equations for the mass, momentum and energy flux, j_i, τ and q respectively. To this end we follow the phenomenological approach of classical irreversible thermodynamic forces appearing in the entropy production σ. The entropy production appears in the local balance equation for the entropy s, which can be written as

$$\rho \frac{ds}{dt} = -\nabla \cdot j_s + \sigma. \tag{3.111}$$

This equation states that the entropy of a volume element can change because of entropy in-and outflow, represented by the entropy flux j_s, and because of irreversible processes taking place within the element, represented by the entropy production σ. According to the second law of thermodynamics σ has to be non-negative

$$\sigma \geq 0. \tag{3.112}$$

For reversible transitions or systems in equilibrium $\sigma = 0$. To find a more explicit expression for σ we need to relate changes in the entropy to changes in the other properties appearing in the other local balance equations. This can be done by considering the Gibbs relation.

3.6.3 Gibbs relation

From classical thermodynamics it is known that, for a homogeneous system in equilibrium, the internal energy is a function of the entropy s and the densities ρ_i. Here we consider inhomogeneous fluids. In the spirit of the

equilibrium diffuse-interface theory, the internal energy u is also a function of density gradients

$$u = u(s, \rho_i, \nabla\rho_i). \tag{3.113}$$

The total differential of this equations is

$$du = \frac{\partial u}{\partial s}ds + \sum_{i=1}^{N}\frac{\partial u}{\partial \rho_i}d\rho_i + \sum_{i=1}^{N}\frac{\partial u}{\partial \nabla\rho_i}d\nabla\rho_i, \tag{3.114}$$

where the partial differentiations are such that all other independent variables are kept constant. Using the thermodynamic relation $\partial\tilde{u}/\partial t = T$, equation can be rewritten as a non-classical Gibbs relation

$$Tds = du - \sum_{i=1}^{N}\frac{\partial u}{\partial \rho_i}d\rho_i - \sum_{i=1}^{N}\frac{\partial u}{\partial \nabla\rho_i}d\nabla\rho_i \tag{3.115}$$

To be able to couple the Gibbs relation to the local balance equations of the previous section we have to write it in a local form. To write it in a local form we now assume that, even though the total system is necessarily in equilibrium, the Gibbs relation remains valid for a volume element travelling with the barycentric velocity $\mathbf{v}$. This approximation is also called the local equilibrium approximation (de Groot and Mazur, 1984).

$$T\frac{ds}{dt} = \frac{du}{dt} - \sum_{i=1} N\frac{\partial u}{\partial \rho_i}\frac{d\rho_i}{dt} \tag{3.116}$$

Using the local mass balance equations and this equation can be rewritten as

$$T\frac{ds}{dt} = \frac{du}{dt} - \frac{p_0}{\rho^2}\frac{d\rho}{dt} - \sum_{i=1}^{N}\mu_{0i}\frac{dc_i}{dt} - \sum_{i=1}^{N}\frac{\partial u}{\partial \nabla\rho_i}\frac{d\nabla\rho_i}{dt}, \tag{3.117}$$

where the homogeneous part of the chemical potential and the pressure are given by

$$\begin{aligned} \mu_{0i} &= \frac{\partial \rho u}{\partial \rho_i} - Ts, \\ p_0 &= \sum_{i=1} N\rho_i\mu_{0i} - \rho u + \rho Ts, \end{aligned}$$

respectively.

The gradient term in equation still needs to be evaluated. An expression for $d\nabla\rho_i/dt$ can be found by taking the gradient of the local mass balance equation for component i. After some manipulations we find

$$\frac{d\nabla\rho_i}{dt} = -\nabla\mathbf{v}\cdot\nabla\rho_i - \nabla(\rho_i\nabla\cdot\mathbf{v}) - \nabla\nabla\cdot\mathbf{j}_i. \tag{3.118}$$

We can now combine equations and . Using local mass balance together with the identities $\nabla \cdot \mathbf{v} = \mathbf{I} : \nabla \mathbf{v}$ and

$$\frac{\partial u}{\partial \nabla \rho_i} \cdot \nabla \mathbf{v} \cdot \nabla \rho_i = \frac{\partial u}{\partial \nabla \rho_i} \nabla \rho_i : \nabla \mathbf{v} \tag{3.119}$$

we obtain

$$\rho T \frac{ds}{dt} = (\tau - \tau_r) : \nabla \mathbf{v} - \nabla \cdot (\mathbf{q} - \mathbf{q}_r - \mathbf{q}_d) + \sum_{i=1}^{N} \mu_i \nabla \cdot \mathbf{j}_i, \tag{3.120}$$

with

$$\begin{aligned}
\tau_r &= -p\mathbf{I} - \sum_{i=1}^{N} \frac{\partial \rho u}{\partial \nabla \rho_i} \nabla \rho_i, && (3.121)\\
\mathbf{q}_r &= \sum_{i=1}^{N} \frac{\partial \rho u}{\partial \nabla \rho_i} \rho_i \nabla \cdot \mathbf{v}, && (3.122)\\
\mathbf{q}_d &= \sum_{\partial \rho u}^{\partial \nabla \rho_i} \nabla \cdot \mathbf{j}_i, && (3.123)\\
\mu_i &= \frac{\partial \rho u}{\partial \rho_i} - \nabla \cdot \frac{\partial \rho u}{\partial \nabla \rho_i} - Ts, && (3.124)\\
p &= \sum_{i=1}^{N} \rho_i \mu_i - \rho u + \rho T s. && (3.125)\\
& && (3.126)
\end{aligned}$$

Note that μ_i has the same mathematical form as the chemical potential in sections which was obtained by variational differentiation of the free energy functional. It's necessary now to find a correct expression for the entropy production. Dividing eq. 3.106 by T and rearranging the terms we obtain:

$$\rho \frac{ds}{dt} = -\nabla \cdot \mathbf{j}_s + \sigma \tag{3.127}$$

with

$$\begin{aligned}
\mathbf{j}_s &= \frac{1}{T}(\mathbf{q} - \mathbf{q}_r - \mathbf{q}_d - \sum_{i=1}^{N} \mu_i \mathbf{j}_i), && (3.128)\\
\sigma &= \frac{1}{T}(\tau - \tau_r) : \nabla \mathbf{v} + (\mathbf{q} - \mathbf{q}_r - \mathbf{q}_d) \cdot \nabla \frac{1}{T} - \sum_{i=1}^{N} \mathbf{j}_i \cdot \nabla \frac{\mu_i}{T}. && (3.129)\\
& && (3.130)
\end{aligned}$$

The entropy production has a simple structure: it is the sum of the products of the thermodynamics fluxes and forces. In equilibrium both fluxes and forces vanish. The equilibrium relations are therefore given by

$$\mathbf{j}_i = 0, \tau = \tau_r \text{ and } \mathbf{q} = \mathbf{q}_r. \tag{3.131}$$

Here we have identified τ_r and $\mathbf{q}_r$ as the reversible parts of the stress tensor and the energy flux, respectively. Besides the isotropic pressure contribution, there is also an anisotropic contribution, there is also an anisotropic contribution, there is also an anisotropic contribution to τ_r, which depends on the density gradients. This means that, at an interface between two fluids, the tangential stress is not equal to the normal stress. We shall see later on that this difference is closely related to the interfacial tension. To find phenomenological relations for the thermodynamic fluxes we have to consider the dissipative part of the entropy production.

3.6.4 Phenomenological equations

Let's derive the phenomenological equations for the thermodynamic fluxes, using the principle of classical irreversible thermodynamics: the fluxes are assumed to be linea functions of the independent forces appearing in the entropy production. To write the entropy production as a linear combination of independent fluxes and forces we have to split up the first term on the right hand side of equation in a deviatoric and a diagonal part.

$$\sigma = \frac{1}{T}\tau_v^d : \nabla_d \mathbf{v} + \frac{1}{3T} Tr(\tau_v)\nabla\cdot\mathbf{v} + \mathbf{q}_h \nabla\frac{1}{T} + \mathbf{q}_h \nabla\frac{1}{T} - \sum_{i=1}^{N} \mathbf{j}_i \cdot \nabla\frac{\mu_i}{T} > 0, \quad (3.132)$$

where $\tau_v = \tau - \tau_r$ is the viscous stress tensor and $\mathbf{q}_h = \mathbf{q} - \mathbf{q}_r - \mathbf{q}_d$ is the heat flux, T_r is the trace operator and τ_v^d and $\nabla_d \mathbf{v}$ are the deviatoric and a diagonal part we separate the contribution of shear viscosity and bulk viscosity. We now assume that the fluxes are linear functions of the independent forces appearing in 3.132. Keeping in mind that fluxes and forces of different tensorial character can not couple, we obtain the following phenomenological relations

$$\begin{aligned}
\tau_v^d &= \frac{\Lambda_s}{2T}[\nabla\mathbf{v} + \nabla\mathbf{v}^T - \frac{2}{3}\nabla\cdot\mathbf{v}\mathbf{I}], && (3.133)\\
\frac{1}{3}Tr(\tau_v) &= \frac{\Gamma_b}{T}\nabla\cdot\mathbf{v}, && (3.134)\\
\mathbf{q}_h &= \Gamma_{qq}\nabla\frac{1}{T} + \sum_{k=1}^{N-1}\Gamma_{qk}\nabla(\frac{\mu_k - \mu_N}{T}), && (3.135)\\
\mathbf{j}_i &= \Gamma_{iq}\nabla\frac{1}{T} + \sum_{k=1}^{N-1}\Gamma_{ik}\nabla(\frac{\mu_k - \mu_N}{T}). && (3.136)\\
& && (3.137)
\end{aligned}$$

We have assumed that the viscous stress tensor is symmetric and we used the fact that only $N-1$ of the diffusion fluxes are independent. The total viscous stress tensor $\tau_v = \tau_v^d + Tr(\tau_v)\mathbf{I}/3$ is the extra stress tensor and the

coefficients $\Gamma_s/(2T)$ and Γ_b/T can be identified as the shear and bulk viscosity, respectively. The relations for $\mathbf{q}_h$ and $\mathbf{j}_i$ include so-called cross effects: the diffusion flux depends not only on the chemical potential gradients but also on the temperature gradient and the energy flux also depends on the chemical potential gradients. All these equations constitute a complete set of equations, which can be solved with the appropriate initial and boundary conditions.

3.6.5 Quasi-incompressible systems

So far we have considered non-isothermal, compressible systems. In this thesis, however, we are mainly concerned with incompressible, (nearly) isothermal systems. For an incompressible, isothermal fluid the density depends only on the mass fractions c_i. If there is no volume change upon mixing, the reciprocal density is a linear function of the mass fractions

$$\frac{1}{\rho} = \sum_{i=1}^{N-1} \frac{c_i}{\varrho_i - \varrho_N} + \frac{1}{\varrho_N}, \tag{3.138}$$

where ϱ_i is the density of component i as a pure substance. Mixtures which obey equation are called simple mixtures. For incompressible systems, the internal energy is a function of c_i rather than the densities ρ_i. That is

$$u = u(s, c_i, \nabla c_i) \qquad i = 1, ..., N-1$$

This has some important consequences. The first one is that the pressure can not be defined as in previous section. Ont he other hand, as pointed out by Joseph and Renardy (1993), for a mixture of individually incompressible fluids with different densities the density changes if the composition changes. More specifically we obtain:

$$\nabla \cdot \mathbf{v} = \sum_{i=1}^{N-1} \kappa_i \nabla \cdot \mathbf{j}_i \text{ with } \kappa_i = \frac{1}{\rho^2}\frac{\partial \rho}{\partial c_i} = \frac{1}{\varrho_N} - \frac{1}{\varrho_i}. \tag{3.139}$$

A second important consequence of equation is that the structure of the entropy production changes. Not only because the time derivatives of c_i and ∇c_i instead of ρ_i and $\nabla \rho_i$ appear in the Gibbs relation now, but also because the divergence of the velocity field is no longer an independent thermodynamic force. This effect was also reported by Lowengrub and Truskinovsky (1977), The Gibbs relation for a quasi-incompressible system is:

$$T\frac{ds}{dt} = \frac{du}{dt} - \sum_{i=1}^{N-1} \frac{\partial u}{\partial c_i}\frac{dc_i}{dt} - \sum_{i=1}^{N-1} \frac{\partial u}{\partial \nabla c_i}\frac{d\nabla c_i}{dt}, \tag{3.140}$$

where dc_i/dt is given by equation and

$$\frac{d\nabla c_i}{dt} = -\nabla \mathbf{v} \cdot \nabla c_i - \nabla(\frac{1}{\rho}\nabla \cdot \mathbf{j}_i). \tag{3.141}$$

Combining the local energy balance equation and the Gibbs relation now yields

$$\rho T \frac{ds}{dt} = (\tau - \tau_r) : \nabla \mathbf{v} - \nabla \cdot (\mathbf{q} - \mathbf{q}_d) + \sum_{i=1}^{N-1} (\mu_i - \mu_N) \nabla \cdot \mathbf{j}_i, \tag{3.142}$$

with

$$\begin{aligned} \tau_r &= -\rho \sum_{i=1}^{N-1} \frac{\partial u}{\partial \nabla c_i} \nabla c_i, & (3.143)\\ \mathbf{q}_d &= \rho \sum_{i=1}^{N-1} \frac{\partial u}{\partial \nabla c_i} \nabla \cdot \mathbf{j}_i, & (3.144)\\ \mu_i - \mu_N &= \frac{\partial u}{\partial c_i} - \frac{1}{\rho}\nabla \cdot (\rho \frac{\partial u}{\partial \nabla c_i}). & (3.145)\\ & & (3.146) \end{aligned}$$

As stated above, to find a correct expression for the entropy production in terms of independent forces and fluxes we have to include the fact that $\nabla \cdot \mathbf{v}$ and $\nabla \cdot \mathbf{j}_i$ are not independent. Using equation and slitting up $\nabla \mathbf{v}$ into a deviatoric part and a diagonal part we obtain

$$\rho T \frac{ds}{dt} = (\tau - \tau_r) : \nabla_d \mathbf{v} - \nabla \cdot (\mathbf{q} - \mathbf{q}_d) + \sum_{i=1}^{N-1} (\mu_i^\bullet - \mu_N^\bullet) \nabla \cdot \mathbf{j}_i, \tag{3.147}$$

where

$$\mu_i^\bullet - \mu_N^\bullet = \mu_i - \mu_N - \frac{1}{3}\kappa_i Tr(\tau - \tau_r). \tag{3.148}$$

The entropy production for an isothermal system is now given by

$$\sigma = \frac{1}{T}(\tau - \tau_r) : \nabla_d \mathbf{v} - \frac{1}{T} \sum_{i=1}^{N-1} \mathbf{j}_i \cdot \nabla(\mu_i^\bullet - \mu_N^\bullet). \tag{3.149}$$

The equilibrium relations are now

$$\mathbf{j}_i = 0 \text{ and } \tau - \tau_r = -p\mathbf{I}, \tag{3.150}$$

with p is an arbitrary pressure field. The chemical potential difference $\mu_i^\bullet - \mu_N^\bullet$ can also be written as

$$\mu_i^\bullet - \mu_N^\bullet = \mu_i - \mu_N + \kappa_i p. \tag{3.151}$$

Using the same technique as in the previous section, neglecting bulk viscosity, we obtain the following phenomenological equations for the viscous stress tensor and the diffusion flux

$$\tau_v = \nu[\nabla \mathbf{v} + \nabla \mathbf{v} - \frac{2}{3}\nabla \cdot \mathbf{v}\mathbf{I}], \tag{3.152}$$

$$\mathbf{j}_i = \frac{1}{T}\sum_{i=1}^{N-1} \Gamma_{ik}\nabla(\mu_k^\bullet - \mu_i^\bullet), \tag{3.153}$$

where μ is he shear viscosity. The local momentum balance equation can now be written as

$$\rho\frac{d\mathbf{v}}{dt} = -\nabla p - \nabla \sum_{i=1}^{N-1} \rho\frac{\partial u}{\partial \nabla c_i}\nabla c_i + \nabla \tau_v + \rho \mathbf{f}_g. \tag{3.154}$$

We can make one further simplification concerning the gradient term in the momentum equation. The second term on the right hand side can be rewritten as

$$-\frac{1}{\rho}\nabla p + \nabla f + \sum_{i=1}^{N-1} \mu_i \nabla c_i = -\nabla(f + \frac{p}{\rho}) + \sum_{i=1}^{N-1}(\mu_i^\bullet - \mu_N^\bullet)\nabla c_i. \tag{3.155}$$

Defining the specific Gibbs free energy as $g = f + p/\rho$, the momentum equation can now be written as

$$\frac{d\mathbf{v}}{dt} = -\nabla g + \sum_{i=1}^{N-1}(\mu_i^\bullet - \mu_N^\bullet)\nabla c_i + \frac{1}{\rho}\nabla \cdot \tau_v + \mathbf{f}_g. \tag{3.156}$$

In summary, the local mass, mass fraction and momentum balance equations for an in-homogeneous, quasi-incompressible, isothermal fluid mixture are

$$\frac{d\rho}{dt} = -\rho\nabla \cdot \mathbf{v}, \tag{3.157}$$

$$\rho\frac{dc_i}{dt} = \frac{1}{T}\nabla \cdot \sum_{i=1}^{N-1} \Gamma_{ik}\nabla(\mu_k^\bullet - \mu_N^\bullet) \tag{3.158}$$

$$\mu_k^\bullet - \mu_N^\bullet = \frac{\partial f}{\partial c_i} - \frac{1}{\rho}\nabla(\rho\frac{\partial f}{\partial c_i}) + \kappa_i p, \tag{3.159}$$

$$\frac{d\mathbf{v}}{dt} = -\nabla g + \sum_{i=1}^{N-1}(\mu_i^\bullet - \mu_N^\bullet)\nabla c_i + \frac{1}{\rho}\nabla \cdot \eta[\nabla \mathbf{v} \tag{3.160}$$

$$+ \nabla \mathbf{v}^T - \frac{2}{3}\nabla \cdot \mathbf{v}\mathbf{I}] + \mathbf{f}_g \tag{3.161}$$

$$\tag{3.162}$$

3.6.6 Free energy

Different expressions of $F(\mathbf{c})$ are needed in order to model miscible, partially miscible and fully immiscible system The $F(\mathbf{c})$ has to been chosen in an appropriate way to reproduce the system we want to study. It is possible to elaborate different kind of free energy to describe different kind of systems. It is possible to model different kind of systems, where the three phases are all miscible, partially miscible or fully immiscible with each other.

In order to compare our results with the one reported in Kim *et al.* (2004) the following expression for the free energy was used:

$$f(c_1, c_2) = \frac{1}{4}[c_1^2 c_2^2 + (c_1^2 + c_2^2)(1 - c_1 - c_2)^2 - c_1 c_2 (1 - c_1 - c_2)]. \quad (3.163)$$

This function can be represent on a Gibbs triangle, with a minima in the center of the triangle .

3.6.7 Numerical methods

Instead of solving the entire set of equations in a coupled way, we decouple the set into a flow problem equations and a concentration problem equations. The flow problem is solved using a primitive variable i.e. the velocity-pressure formulation and discretized by a standard Galerkin finite element method (GFEM).

Let's analyze the application of the Galerkin method to the diffuse interface model.

3.6.8 Weak form of the diffuse-interface model

We consider the diffuse-interface model in a region Ω, with the flow equations according to Stokes flow:

$$\begin{aligned} -\nabla \cdot (2\eta \mathbf{D}) + \nabla p &= \mathbf{f} + \rho\mu\nabla c, \text{ in } \Omega & (3.164)\\ \nabla \cdot \mathbf{u} &= 0, \text{ in } \Omega & (3.165)\\ & & (3.166) \end{aligned}$$

where $\mathbf{D} = (\nabla \mathbf{u} + \nabla \mathbf{u}^T)/2$, and the equations for the concentration c and chemical potential μ are given by:

$$\begin{aligned} \frac{\partial c}{\partial t} + \mathbf{u} \cdot \nabla c &= 0 \text{ in } \Omega & (3.167)\\ \alpha c - \beta c^3 + \kappa \nabla^2 c + \mu &= 0 \text{ in } \Omega & (3.168)\\ & & (3.169) \end{aligned}$$

In Eq. 3.164 the coefficient ρ in the right-hand side forcing term is the density of the fluid. However, the inertia terms in the momentum balance,

which also contain ρ, are assumed to be negligible. The weak form of the flow equations is similar to the example for the Poisson equation: find u and p such that

$$\begin{aligned}(\mathbf{D}_v, 2\eta\mathbf{D}) - (\nabla\cdot\mathbf{D}) - (\nabla\cdot\mathbf{v}, p) &= (\mathbf{v}, \tau_N)_{\Gamma_N} + (\mathbf{v}, \mathbf{f}) + (\mathbf{v}, \rho\mu\nabla c) \text{ for all } \mathbf{v} \\ (q, \nabla\cdot\mathbf{u}) &= 0, \text{ for all } q\end{aligned}$$

using appropriate spaces for $\mathbf{u}, p, \mathbf{v}$ and q. In this equation $\mathbf{D}_v$ is defined by

$$\mathbf{D}_v = (\nabla\mathbf{v} + \nabla\mathbf{v}^T)/2 \tag{3.170}$$

The weak form of the c and μ equations can easily be derived and reads: find c and μ such that

$$\begin{aligned}(r, \frac{\partial c}{\partial t} + \mathbf{u}\cdot\nabla c) + M(\nabla r, \nabla\mu) &= 0 \text{ for all } r \\ (s, \alpha c - \beta c^3) - \kappa(\nabla s, \nabla c) + (s, \mu) &= 0 \text{ for all } s\end{aligned}$$

using appropriate spaces for c, μ, r and s. The weak form can be used to obtain an approximate solution using the Galerkin FEM technique. For this we divide the region into elements:

$$\Omega = \bigcup_e \Omega_e, \Omega_e \bigcap \Omega_f = \emptyset \text{ for } e \neq f \tag{3.171}$$

and interpolate $\mathbf{u}, p, c$ and μ by polynomials on each element:

$$\begin{aligned}\mathbf{u}_h = \sum_k \phi_k(x)\mathbf{u}_k &= \tilde{\phi}^T(x)\tilde{\mathbf{u}} \\ p_h = \sum_k \psi_k(x)p_k &= \tilde{\psi}^T(x)\tilde{p} \\ c_h = \sum_k \phi_k(x)c_k &= \tilde{\phi}^T(x)\tilde{c} \\ \mu_h = \sum_k \phi_k(x)\mu_k &= \tilde{\phi}^T(x)\tilde{\mu}\end{aligned}$$

where $\tilde{\phi(x)}$ and $\tilde{\psi(x)}$ are global shape functions. Note, that c and μ are interpolated using the same shape function as the velocity vector.

3.6.9 Time discretization of the diffuse-interface model

At the initial time t_0 we solve the flow equations without the right-hand side term $\rho\mu\nabla c$ to obtain an initial flow solution. Also the initial field $c^0 = c(t_0)$

should be specified. Then we do a time stepping where we first solve the equations for c^{n+1} and μ^{n+1} using the values of $\mathbf{u}^n$ and c^n at the current time t^n. For this we use an implicit Euler scheme:

$$\begin{aligned}(r, \frac{c^{n+1-c^n}}{\Delta t}) + \mathbf{u}^n \cdot \nabla c^{n+1}) + M(\nabla r, \nabla \mu^{n+1}) &= 0 \text{ for all } r \\ (s, \alpha c^{n+1} - \beta[c^{n+1}]^3) - \kappa(\nabla s, \nabla c^{n+1}) + (s, \mu^{n+1}) &= 0 \text{ for all } s\end{aligned}$$

where Δt is the time step. This is a non-linear equation, which we solve by Picard iteration:

$$\begin{aligned}(r, \frac{c_{i+1} - c^n}{\Delta t} + \mathbf{u}^n \cdot \nabla c_{i+1}) + M(\nabla r, \nabla \mu_{i+1}) &= 0 \text{ for all } r \\ (s, (\alpha c_i - \beta c_i^2) c_{i+1}) - \kappa(\nabla s, \nabla c_{i+1}) + (s, \mu_{i+1}) &= 0 \text{ for all } s\end{aligned}$$

for $i = 0, 1...$ with $c_0 = c^n$, until convergence. Then we solve the flow equations to obtain u^{n+1} and p^{n+1} using c^{n+1} and μ^{n+1}.

These discretized equations written in matrix for read:

$$\begin{pmatrix} \mathbf{S_v} & \mathbf{L^T} \\ \mathbf{L} & \mathbf{0} \end{pmatrix} \begin{pmatrix} \mathbf{v} \\ p \end{pmatrix} = \begin{pmatrix} \mathbf{Mf_v} \\ \mathbf{0} \end{pmatrix} \tag{3.172}$$

where $\mathbf{v}$ is the discretized velocity, p is the discretized pressure, $\mathbf{S_v}$ is the stiffness matrix containing the viscous terms, $\mathbf{L}$ is the matrix due to divergence operation, $\mathbf{L^T}$ is the matrix for the gradient operator, $\mathbf{M}$ is the mass matrix, and $\mathbf{f_v}$ is the right hand side containing the $\frac{1}{CaC_h}(\mu \nabla c - \nabla f)$ term. The discretized set of linear algebraic equations is solved using an integrated metho with an iterative solver with incomplete Cholesky decomposition as preconditioner. In the integrated method both velocity and pressure are used as unknowns i.e. degrees of freedom. Due to the absence of pressure in the continuity equation, a zero block appears in the main diagonal of the matrix. It is therefore possible that the first pivot during the elimination process for the ILU preconditioner is zero. In order to ensure that this does not happen, unknowns are renumbered per level, and also globally, so that first velocities and then the pressure unknowns are used during the matrix assembling. Taylor-Hood quadrilateral elements, with continuous pressure, that employ a biquadratic approximation for velocity and a bilinear approximation for pressure are used. Two second-order differential equations that constitute a concentration problem are solved in a coupled way. For the temporal discretization of equation a first-order Euler implicit scheme is employed so that the discretized time derivative reads: $\frac{c^n - c^{n-1}}{\Delta t}$ where Δt is the item step size, and the superscript n represents the current time label. The non-linear c^3 term in equation is linearized bu a standard

Picard iteration which yields $(c_{i-1}^n)^2 c_i^n$ where subscript i represents the i^{th} Picard iteration at time level n. A spectral element method (Patera, 1984; Timmermans et al., 1994) is used for spatial discretization of the set of equations. In this method, similar to finite element method, the computational domain is divided into N_{el} non-overlapping sub-domains Ω_e and a spectral approximation is applied on each element. The basis functions, ϕ, that are used for spatial discretization, are high-order Lagrange interpolation polynomials through Gauss-Lobatto integration points defined per element. The full discretized set of linearized equations, written in matrix form, reads:

$$\begin{bmatrix} \mathbf{M} + \Delta t \mathbf{N}^{n-1} & \frac{\Delta t}{Pe}\mathbf{S} \\ (1-(c_{i-1}^n)^2)\mathbf{M} - C_h^2 \mathbf{S} & \mathbf{M} \end{bmatrix} \begin{bmatrix} c_i^n \\ \mu_i^n \end{bmatrix} = \begin{bmatrix} \mathbf{M} c_0^{n-1} \\ \mathbf{0} \end{bmatrix} \tag{3.173}$$

where c_i^n is the discretized concentration at the i^{th} Picard iteration at time step n, μ_i^n is the discretized chemical potential at the i^{th} Picard iteration at time step n, c_0^{n-1} is the discretized concentration at time step $n-1$, $\mathbf{M}$ is the mass matrix, $\mathbf{N}$ is the convection matrix, $\mathbf{S}$ is the diffusion matrix. This set is solved using the above mentioned iterative solver. The scheme to advance in time is as follows:

1. Initialize c_0^0 to be the locally equilibrated concentration profile.
2. Compute μ^0, f and η.
3. Solve the system for velocity with terms containing concentration treated explicitly.
4. Solve the system iteratively for concentration and chemical potential for the two components. Iterations are required due to the non-linear term. Iteration is started with $c_{i-1}^n = c^{n-1}$ and stopped when max $|c_i^n - c_{i-1}^n| \leq \delta_c$.
5. Update the time and repeat steps 2-4

Implementation of the numerical method descrived above is in TFEM, a finite element package, developed in the Eindhoven University, by Prof. Martien Hulsen.

3.6.10 Numerical results

The numerical analysis of the behavior of a phase transition of a binary mixture in presence of a compatibilizer have been carried on a grid with dimensions of $(0,0)$ in the left bottom corner to $(1,1)$ in the top right corner. In each simulation a grid with 60 x 60 mesh and a time step of $\Delta t = 10^{-3}$ has been used. A thermal fluctuation of $O(10^{-5})$ was imposed introducing a random noise at the concentration level. A biperiodic boundary condition

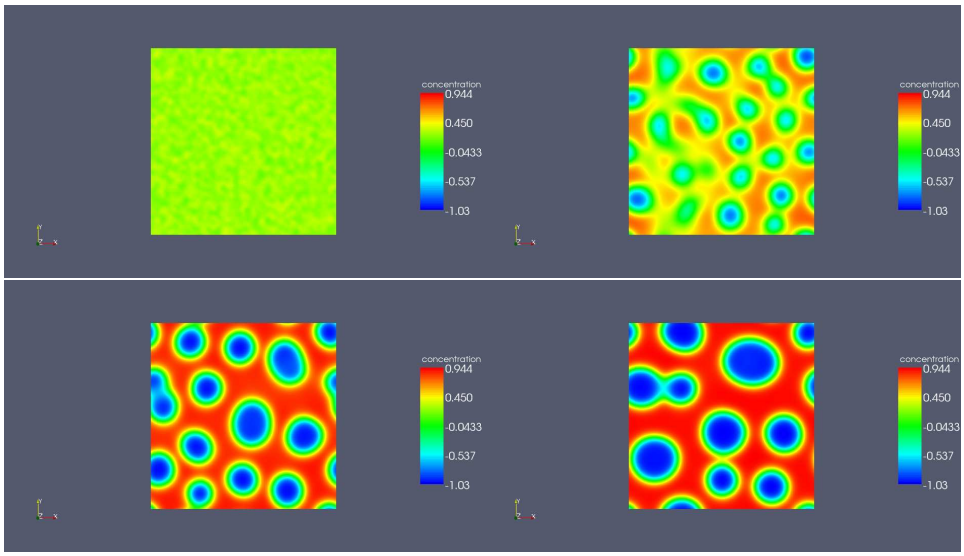

Fig. 3.17: Spinodal decomposition of a binary mixture. The snapshots are taken at different times steps: 0.001, 1.0, 1.5, 2.0

for c, μ, and v has been used. To describe the formation and disappearing of the binary structure a correlation function has been defined as:

$$G(\mathbf{r},t) = \frac{1}{N^d}\sum((c(x+\mathbf{r},t) - c_{av}) \cdot (c(x,t) - c_{av}), \tag{3.174}$$

where $\mathbf{r}$ and x are the lattice vectors, N is the number of grid points, c_{av} the average concentration and d the dimensionality, $d = 2$. Radial averaging s carried out using a Brillouin zone function to eliminate any directional effects:

$$g(r,t) = \frac{1}{N_r}\sum_{r-\Delta(r/2)|x|<r+\Delta(r/2)} g(r,t). \tag{3.175}$$

The initial composition is given by:

$$\begin{aligned} c_1 &= 0.25 + 0.3(0.5 - rand(x,y)) \\ c_2 &= 1 - c_1(x,y) \\ c_3 &= 0.0 \end{aligned}$$

where the $rand(x,y)$ is a random number ranging between 0 and 1, and the value 0.25 lies in the spinodal region. In this case there is no third phase.

As shown in figure (3.17), during the time evolution, spinodal decomposition occurs first then the phases separate. Then a third component is

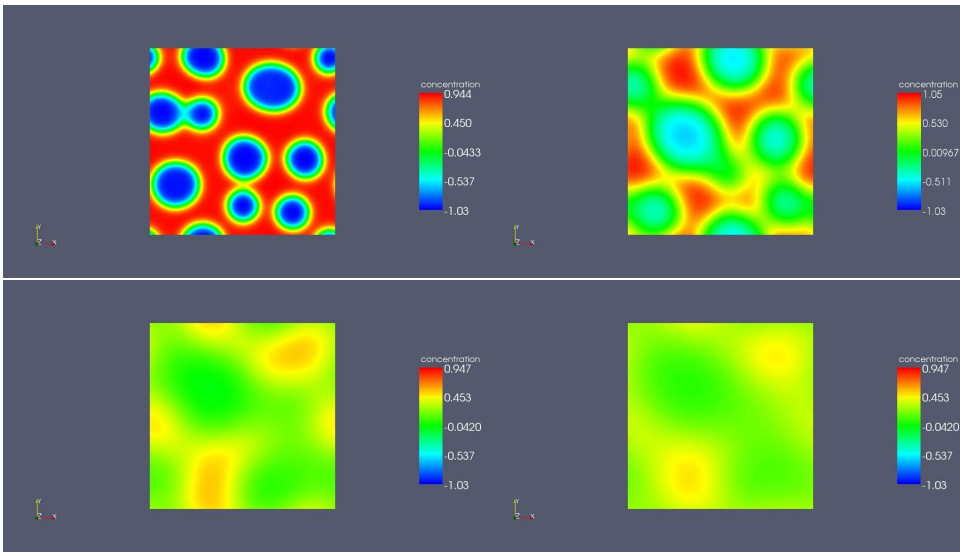

Fig. 3.18: Mixing of the binary mixture in presence of the third component at different time steps: t=0.001, 0.5, 1.0, 2.0

added to the phase separated system, and in agreement with what Kim and Lowengrub (2005) shown the structure tends to disappear 3.18, and the mixtures return to a single-phase system.

This can be quantify using the concentration correlation function (see eq. (3.175). As shown in Figure (3.19) when the spinodal decomposition takes place, the correlation function tends to evolve in a structured function. Instead, after the addition of the third component, the structure disappear, and the mixtures become homogeneous as before the spinodal decomposition (Figure 3.20) .

3.6.11 Coalescence of two drops

In the first set of numerical experiments we tried to reproduce the variation of the interfacial thickness and of the interfacial tension in two different cases: a) very diffusive polymer, b) non-diffusive polymer. To do it we used the three phase model with the partially miscible energy formulation. The drop is initially made by the first phase that is immiscible with the matrix, and by a second high diffusive phase, that is instead miscible with the matrix. During the simulation, the second phase spreads from the drop to the matrix causing a variation in the interfacial thickness of the drop itself. Following the experimental results from Tufano et al. we tried to observe the attraction and repulsion between two drops varying the mobility parameter in the diffusion interface equations to model different kind of polymers. When the Peclet number is around approximately $10 - 100$ and the interfaces are

close the drops tend to attract each other and to coalesce as shown in figure (3.21). As the Peclet number decrees, and the diffusion increase, the two drops tend to coalesce faster. When the Peclet number is approximately $10^4 - 10^5$ the drops do not move and no coalescence occurs (3.23). This phenomena is observed both numerically and experimentally. A possible explanation to the coalescence that occurs between the drops is that the closer the interfaces are, the faster the liquid between them is squeezed out. In the diffuse interface model, the interfacial tension is inversely proportional to the thickness of the diffuse layer. Hence, the prescribed inhomogeneous thickness is equivalent to prescribing an interfacial tension gradient. These gradients lead to Marangoni stresses that are responsible for the attraction between the interfaces. When the two drops were initially placed at distance in which there is no overlap of the diffusive layer no attraction occurs. In figure (3.21) the coalescence of two different drops is shown. In figure (3.22) we shown the variation of the distance between the two interfaces versus time for two different couple of drops with $Pe = 100$ and $Pe = 10$ with different initial diameter and distance, and different capillary numbers.

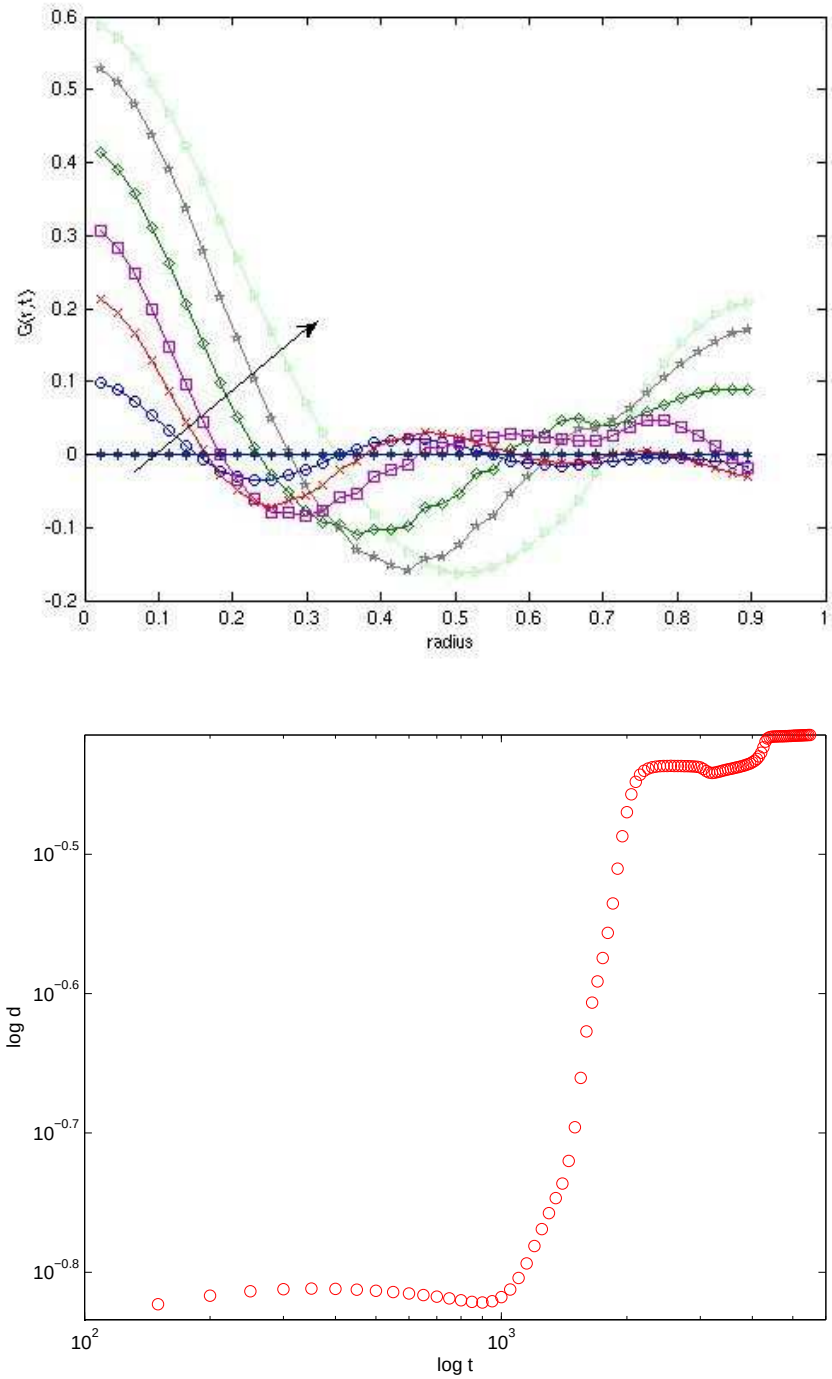

Fig. 3.19: Results of the simulation: (a)Concentration correlation function at various time step for the separation of the binary mixture (the arrow indicate the increasing of the time step), (b) structure size as a function of time.

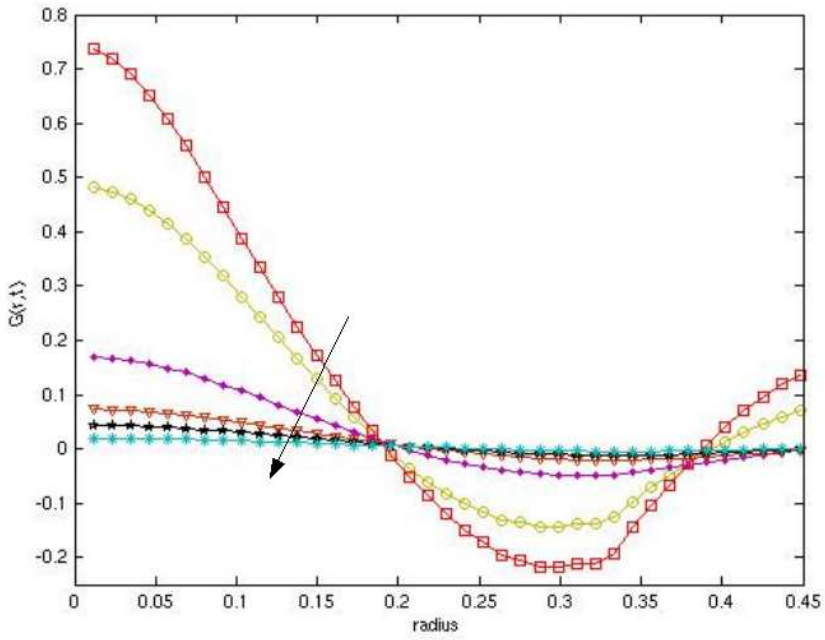

Fig. 3.20: Concentration correlation function at various time step for the mixing of the two phase system after the addition of the third component

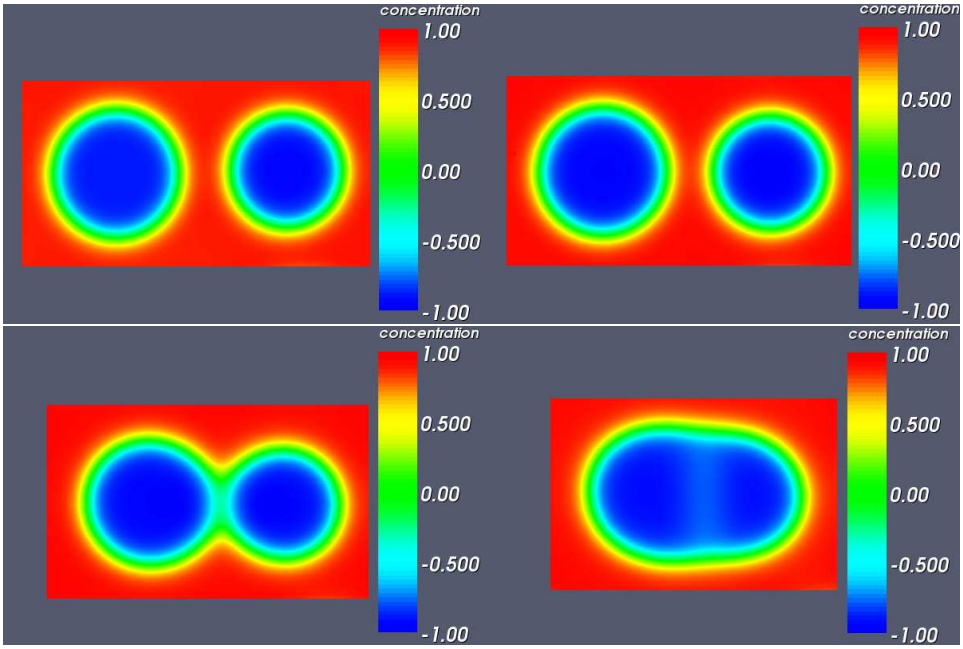

Fig. 3.21: Coalescence of two drops of the diffusive material with different radius at different time steps: t=0.001, 1.2, 2.5, 2.75.

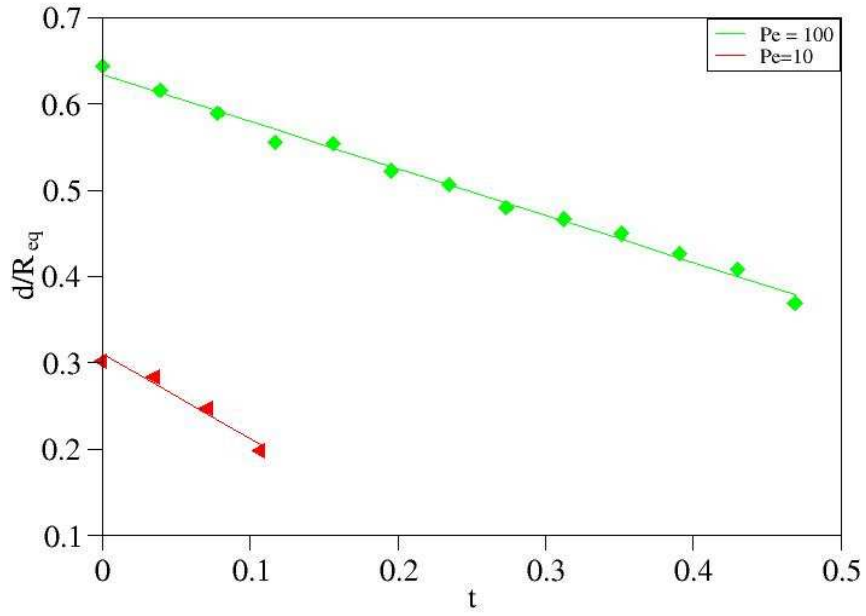

Fig. 3.22: Ratio between the distance and the equivalent radius of the two drops versus time at Pe = O(10) and Pe = O(100), with same value of the diffuse thickness and capillary number.

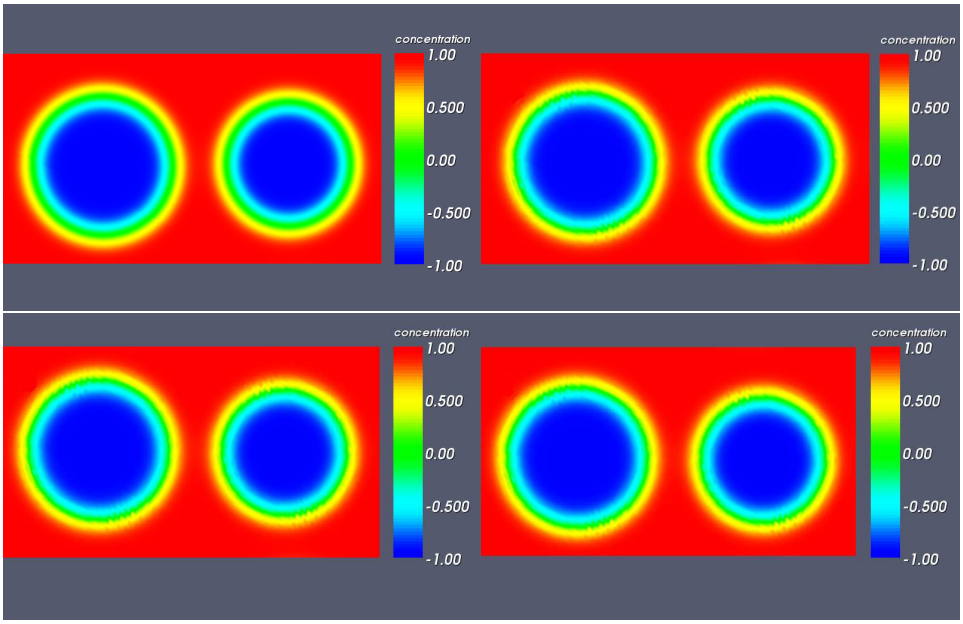

Fig. 3.23: Absence of coalescence between two drops with a Peclet number of 10^5 at different time steps: t = 0.1, 1.2, 2.5, 2.75.

Chapter 4

Conclusions

During the three years of the project we extended the diffuse interface (DI) method and apply it to engineering related problems, particularly related to mixing and demixing of two fluids. To do that, first the DI model itself was validated, showing that, in agreement with its predictions, a single drop immersed in a continuum phase moves whenever its composition and that of the continuum phase are not at mutual equilibrium [D. Molin, R. Mauri, and V. Tricoli, "Experimental Evidence of the Motion of a Single Out-of-Equilibrium Drop," Langmuir 23, 7459-7461 (2007)]. Then, we developed a computer code and validated it, comparing its results on phase separation and mixing with those obtained previously. At this point, the DI model was extended to include heat transport effects in regular mixtures. In fact, in the DI approach, convection and diffusion are coupled via a nonequilibrium, reversible body force that is associated with the Kortweg stresses. This, in turn, induces a material flux, which enhances both heat and mass transfer. Accordingly, the equation of energy conservation was developed in detail, showing that the influence of temperature is two-folded: on one hand, it determine phase transition directly, as the system is brought from the single-phase to the two-phase region of its phase diagram. On the other hand, temperature can also change surface tension, that is the excess free energy stored within the interface at equilibrium. These effects were described using the temperature dependence of the Margules parameter. In addition, the heat of mixing was also taken into account, being equal to the excess free energy. [D. Molin and R. Mauri, "Diffuse Interface Model of Multiphase Fluids," Int. J. Heat Mass Tranf., submitted]. The new model was applied to study the phase separation of a binary mixture due to the temperature quench of its two confining walls. The results of our simulations showed that, as heat is drawn from the bulk to the walls, the mixture tends to phase separate first in vicinity of the walls, and then, deeper and deeper within the bulk. During this process, convection may arise, due to the above mentioned non equilibrium reversible body force, thus enhancing

heat transport and, in particular increasing the heat flux at the walls [D. Molin, and R. Mauri, "Enhanced Heat Transport during Phase Separation of Liquid Binary Mixtures," Phys. Fluids 19, 074102-1-10 (2007)]. The model has been extended then and applied to the case where the two phases have different heat conductivities. We saw that heat transport depends on two parameters, the Lewis number and the heat conductivity ratio. In particular, varying these parameters can affect the orientation of the domains that form during phase separation. Domain orientation has been parameterized using an isotropy coefficient ξ, varying from -1 to 1, with $\xi = 0$ when the morphology is isotropic, $\xi = +1$ when it is composed of straight lines along the transversal (i.e. perpendicular to the walls) direction, and $\xi = -1$ when it is composed of straight lines along the longitudinal (i.e. parallel to the walls) direction [D. Molin, and R. Mauri, "Spinodal Decomposition of Binary Mixtures with Composition-Dependent Heat Conductivities," Chem. Eng. Sci. (2008)]. In order to further extend the model, we removed the constraint of a constant viscosity, and simulated a well known problem of drops in shear flows. There we found that, predictably, below a certain threshold value of the capillary number, the drop will first stretch and then snap back. At lager capillary numbers, though, we predict that the drop will stretch and then, eventually, break in two or more satellite drops. On the other hand, applying traditional fluid mechanics (i.e. with infinitesimal interface thickness) such stretching would continue indefinitely [D. Molin and R. Mauri, " Drop Coalescence and Breakup under Shear using the Diffuse Interface Model," in preparation]. Finally, during a period of three months at the Eindhoven University, we extended the DI model to a three component fluid mixture, using a different form of the free energy, as derived by Lowengrub and Coworkers.. With this extension, we simulated two simple problems: first, the coalescence/repulsion of two-component drops immersed in a third component continuum phase; second, the effect of adding a third component to a separated two phase system. Both simulations seem to capture physical behaviors that were observed experimentally [D. Molin, R. Mauri and P. Anderson, " Phase Separation and Mixing of Three Component Mixtures," in preparation].

Bibliography

[1] Anderson, D.M., McFadden, G.B., and Wheeler, A.A. (1998). Diffuse-interface methods in fluid mechanics, *Annu. Rev. Fluid Mech.*. **30**, 139.

[2] Antanovskii, L. K. (1995). A phase field model of capillarity, *Physics of Fluids*. **7**, 747.

[3] Antanovskii, L.K. (1996). Microscale theory of surface tension, *Physical Review E*. **54**, 6285.

[4] Argyris, J. H. (1963). *Recent advances in matrix method of structural analysis*, Pergamon, Elmsford, N.Y.

[5] Aubin, J. P. (1972). *Approximation of elliptic boundary value problems*. Wiley-Interscience, New York.

[6] Babuska, I. and Aziz, A. K. (1972). Lectures on the Mathematical Foundations of the finite element method with applications to partial differential equations, Academic, New York, 1.

[7] Baker, A. J. (1971). A Finite element computational theory for the mechanics and thermodynamics of a viscous compressible multi-species fluid. Bell Aerospace Research Rept. 95000-920200.

[8] Baker, A. J. (1973). Finite element solution algorithm for viscous incompressible fluid dynamics, *Int. J. Num. Meth. Eng.*. **6**, 89.

[9] Baker, A. J. (1974). A finite element algorithm for the Navier-Stokes equations. NASA CR-2391.

[10] Baldessari, F. and Leal, L.G. (2006). Effect of overall drop deformation on flow-induced coalescence at low capilalry numbers, *Phys. of Fluids*. **18**, 013602 .

[11] Barrett J.W. and Blowey J.F. (1999). An improved error bound for a finite element approximation of a model for phase separation of a multi-component alloy, *IMA J. Numer. Anal.*. **19**, 147.

[12] Barrett J.W. and Blowey J.F., and Garcke H. (2001). On fully practical finite element approximations of degenerate Cahn-Hilliard systems, *M2AN Math. Model. Numer. Anal.*. **35**, 713.

[13] Batchelor, G.K. (1967). *An Introduction to Fluid Dynamics*, Cambridge University Press.

[14] Bell J., Collela P., and Glaz H. (1989). A second-order projection method for the incompressible Navier-Stokes equations, *J. Comp. Phys.*. **85**, 257.

[15] Bird, R.B. Stewart, W.E. and Lightfoot, E.N. (1960). *Transport Phenomena*, Wiley, New York.

[16] Bazhlekov, I.B. Anderson, P.D. and Meijer, H.E.H. (2006). Numerical investigation of the effect of insoluble surfactants on drop deformation and breakup in simple shear flow, *J. Colloid. Interface Sci.*. **298**, 369.

[17] Buckmaster, J.D. and Flaherty, J.E. (1973). The bursting of two-dimensional drops in slow viscous flow *J. Fluid Mech.*. **60**, 625 .

[18] Burkhart, B.E. Gopalkrishnan, P.V.Hudson, S.N. Jamieson, A.M. Rother, M.A. and Davis, R.H.(2001). Droplet growth by coalescence in binary fluid mixtures, *Phys. Rev. Lett.*. **87**, 098304 .

[19] Cahn, J.W. and Hilliard, J.E. (1958). Free energy of a nonuniform system. I. Interfacial free energy, *The Journal of Chemical Physics*. **28**, 258.

[20] Cahn, J.W. and Hilliard, J.E. (1959). Free energy of a nonuniform system. III. Nucleation in a two-component incompressible fluid, *The Journal of Chemical Physics*. **31**, 688.

[21] Cahn, J.W. (1961). On spinodal decomposition, *Acta Metallica*. **9**, 795.

[22] Califano, F. and Mauri, R. (2004). Drop size evolution during the phase separation of liquid mixtures, *Industrial & Engineering Chemistry Research*. **43**, 349.

[23] Chou, Y. C. and Goldburg, W. I. (1979). Phase separation and coalescence in critically quenched isobutyric-acid$\mathring{\text{U}}$water and 2,6-lutidine$\mathring{\text{U}}$water mixtures, *Phys. Rev. A*. **20**, 2105, and references therein.

[24] Ciarlet, P. G. and Raviart, P. A. (1972). General Lagrange and Hermite interpolation in R^n with applications to the finite element method *Arch. Rat. Mech. Anal.*. **46**, 177.

[25] Chung, T. J. and Chiou, J. N. (1976). Analysis of unsteady compressible boundary layer flow via finite elements, *Computers Fluids*. **4**, 1

[26] Clough, R. W. (1960). The finite element method in plane stress analysis, *Proc. 2d Conf. Electronic Computation*, American Society of Civil Engineers, Pittsburg, Pennsylvania, 345.

[27] Cristini, V. Guido, S. Alfani, A.Q. Blawzdziewicz, J. and Lowenberg, M. (2003). Drop breakup and fragment size distribution in sehar flow, *J. Rheol.*. **47**, 1283.

[28] Cussler, E.L. Diffusion, Cambridge Univ. Press. - Davis, H.T. and Scriven, L.E. (1982). Stress and structure in fluid interfaces, *Advances in Chemical Physics*. **49**, 357.

[29] Davis, H.T. and Scriven L.E. (1982) Stress and structure in fluid interfaces, *Adv. Chem. Phys.*. **49**, 357.

[30] Davis, R.H. Schonberg, J.A. and Rallison, J.M. (1989). The lubrication force between two viscous drops, *Phys. Fluids A*, **1**, 77.

[31] DeGennes, P.G. (1980). Dynamics of fluctuations and spinodal decomposition in polymer blends, *J. Chem. Phys.*. **72**, 4756.

de Groot, S.R. and Mazur, P. (1984). *Non-equilibrium termodynamics*. Dover Publications, Inc., New York.

[32] Evans, M. E. and Harlow, F. H. (1957). The particle-in-cell method for hydrodynamic calculation. Los Alamos Scientific Lab., Rept. No. LA-2139, Los Alamos, New Mexico.

[33] Finlayson, B. A. *The method of weighted residuals and variational principles*, Academic, New York.

[34] Furukawa, H. (1994). Role of inertia in the late stage of a phase separation of a fluid, *Physica A*. **204**, 237 (1994).

[35] Furukawa, H. (1997). Dynamics of phase separation of a simple fluid mixture: Comparison between molecular dynamics and numerical integration of the phenomenological equation, *Phys. Rev. E*. **55**, 1150.

[36] Galerkin, B. G. (1915). Series occuring in some problems of elastic stability of rods and plates, *Eng. Bull.*. **19**, 897.

[37] Gibbs, J.W. (1876). On the equilibrium of heterogeneous substances, reprinted in Scientific Papers by J. Willard Gibbs, Vol. 1, Dover, New York (1961).

[38] Guenoun, P.; Gastaud, R.; Perrot, F.; Beysens, D. (1987). Spinodal decomposition patterns in an isodensity critical binary fluid: Direct-visualization and light-scattering analyses, *Phys. Rev. A*. **36**, 4876.

[39] Gunton, J.D., San Miguel, M., Sahni, P.S., (1983). In Domb, C. & Lebowitz, J.L. (Eds.). *Phase Transition and Critical Phenomena*, Vol. 8. London: Academic Press.

[40] Gupta, R. Mauri, R. and Shinnar, R. (1999). Phase separation of liquid mixtures in the presence of surfactants, *Industrial & Engineering Chemistry Research*. **38**, 2418.

[41] Gupta, R.; Mauri, R.; Shinnar, R. (1996). Liquid-Liquid Extraction Using the Composition Induced Phase Separation Process, *Ind. Eng. Chem. Res.. 35*, 2360.

[42] Halliday, I. Care, C.M. Thompson, S. and White, D. (1996). Induced burst of fluid drops ina two-component lattice Bhatbager-Gross-Krook fluid, *Phys. Rev. E*. **54**, 2573.

[43] Hohenberg, P.C. and Halperin, B.I. (1977). Theory of dynamic critical phenomena, *Review of Modern Physics*. **49**, 435.

[44] Israelachvili, J.H. (1992). Intermolecular and Surface Forces, Academic Press.

[45] Jacqmin, D. (2000). Contact-line dynamics of a diffuse fluid interface, *Journal of Fluid Mechanics* **402**, 57.

[46] Jasnow, D. and Viñals, J. (1996). Coarse-grained description of thermo-capillary flow, *Physics of Fluids*. **8**, 660.

[47] Johnson, R.A. and Borhan, A. (2000). Stability of the shape of a surfactant-laden drop translating at low Reynolds number, *Phys. Fluids*. **12** 773.

[48] Josef, D. D. and Renardy Y. Y. (1993). *Fundamentals of two-fluid dynamics*. Springer-Verslag, New York.

[49] Kan, H.C. Udaykumar, H.S. Shyy, W. and Tran-Son-Tay, R. (1998). Hydrodynamics of a compound drop with application to leukocyte modeling, *Phys. Fluids*. **10** 760.

[50] Karpov, V.G. (1995). Negative Diffusion and Clustering of Growing Particles, *Phys. Rev. Lett.*. **75**, 2702.

[51] Karpov, V.G.; Oxtoby, D.W. (1997) Self-organization of growing and decaying particles, *Phys. Rev. E*. **55**, 7253.

[52] Kawasaki, K. (1970). Kinetic equations and time correlation functions of critical fluctuations, *Annals of Physics*. **61**, 1.

[53] Kogi, O. Yuya, K. Kim, H. Kitamura, N. (2001). Auto-Oscillated Vibration of Single Micrometer-Sized Oil Droplets in Aqueous Surfactant Solution . *Langmuir*, **17**, 7456.

[54] Keestra, B.J. Van Puyvelde, P.C.J. Anderson, P.D. and Meijer, H.E.H. (2003). Diffuse interface modeling of the morphology and theology of immiscible polymer blends, *Phys. Fluids*. **15**, 2567.

[55] Kendon, V.M. Cates, M.E. Pagonabarraga, I. Desplat, J.C. and Bladon, P. (2001). Inertial effects in tree dimensional spinodal decomposition of a symmetric binary fluid mixture, textitJ. Fluid Mech.. **440**, 147.

[56] Korteweg, D.J. (1901). Sur la forme que prennent les équations du mouvement des fluides si l'ont tient compte des forces capillaires causées par des variations de densité considérables mais continues et sur la theorie de la capillarité dans l'hypothèse d'une variation continue de la densité, *Archive Néerlandèse des Sciences Exactes de la Nature. Serie II* **6**, 1.

[57] Lamorgese, A.G. and Mauri, R. (2002). Phase separation of liquid mixtures, *in Nonlinear Dynamics and Control in Process Engineering Recent Advances*, G. Continillo, S. Crescitelli, M. Giona, eds., Springer, pp. 139-152.

[58] Lamorgese, A.G. and Mauri, R. (2005). Nucleation and spinodal decomposition of liquid mixtures, *Physics of Fluids*. **17**, 034107.

[59] Lamorgese, A.G. and Mauri,R. (2006). Mixing of macroscopically quiescent liquid mixtures, *Phys. Fluids*. **18**, 044107 .

[60] Landau, L.D. and Lifshitz, E.M. (1980). *Statistical Phyysics, Part I*, Pergamoin Press.

[61] Lavrenteva, O.M.; Nir, A. (2001). Spontaneous thermocapillary interaction of drops: Unsteady convective effects at high Peclet numbers *Phys. Fluids*. **13**, 368.

[62] Leal, G. (2004). Flow induced coalescence of drops in a viscous fluid, *Phys. Fluids*. **16**, 1833 .

[63] Le Bellac, M. (1991). *Quantum and Statistical Field Theory*, Clarendon Press.

[64] Lifshitz, E.M., Pitaevsky, L.P., (1984). *Kinetic Physics*. Pergamon Press, New York. Ch. 100.

[65] Lions, J. L. and Magenes, E. (1972). Non-homogeneous boundary-value problems and applications, Vol I, Springer-Verlag.

[66] Lynn, P. O. (1974). Least squares finite element analysis of laminar boundary layers. *Int. J. Num. meth. Eng.*. **8**, 865.

[67] Von Leibnitz, G.W.F. (1765). *Nouveaux Essais sur l'Entendement Humain*, book II, Ch. IV. Here Leibnitz applied to the natural world the statement "Natura non facit saltus" that in 1751 Lineus (i.e. C. von Linné) in Philosophia Botanica, Ch. 77, had referred to species evolution.

[68] Lowengrub, J. and Truskinovsky, L. (1997). Quasi-incompressible Cahn-Hilliard fluids and topological transitions, *Proceedings of the Royal Society*, London, Series A **454**, 2617.

[69] Lucretius, Titus Carus (50 B.C.E.). *De Rerum Natura*, Book I "Corpus inani distinctum, quoniam nec plenum naviter extat nec porro vacuum."

[70] Macedo, E.A. Rasmussen, P. (1987). *Liquid-Liquid Equilibrium Data Collection. Supplement 1*, Chemistry Data Series, Vol. V, Part 4. DECHEMA, Frankfurt, Germany, p. 52.

[71] Magome, N. Yoshikawa, K. (1996). Nonlinear Oscillation and Amebalike Motion in an Oil/Water System *J. Phys. Chem.*. **100**, 19102.

[72] Martiouchev, L.M. Seleznev, V.D. (2000). Maximum-entropy production principle as a criterion for the morphological-phase selection in the crystallization process. Doklady Physics 45, 129-131.

[73] Mauri, R. Shinnar, R. and Triantafyllou, G. (1996). Spinodal decomposition in binary mixtures, *Physical Review E.* **53**, 2613.

[74] Mauri, R. Califano F. Calvi, E. Gupta, R. and Shinnar, R. (2003). Convection-driven phase segregation of deeply quenched liquid mixtures, *Journal of Chemical Physics.* **118**, 8841.

[75] Maxwell, J.C. (1876). *Capillary action*, reprinted in Scientific Paper of James Clerk Maxwell, Vol. 2, Dover, New York (1952), pp. 541-591.

[76] Nauman, E.B. and He, D.Q. (2001). Nonlinear diffusion and phase separation *Chem. Engng. Sci.*. **56**, 1999 .

[77] Oden, J. T. (1972). Finite elements of nonlinear continua, McGraw-Hill, New York.

[78] Oden, J. T. and Reddy J. N. (1976). *Introdution to Mathematical Theory of Finite Elements*, Wiley, new York.

[79] Olson, M. E. (1972). Formulation of a variational principle-finite element method for viscous flows. *Proc Variational Meth. Eng.* Southampton University, 5.27

[80] Onsager, L., (1931). Reciprocal relations in irreversible processes. II. Physical Review 38, 2265-2279. Note that Eq. (5.9) already expresses the principle of maximum entropy production.

[81] Onuki, A. (2005). Dynamic Van der Waals theory of two-phase fluids in heat flow, *Phys. Rev. Lett.* **94**, 054501.

[82] Onuki, A. and Kanatani, K. (2005). Droplet motion with phase change in a temperature gradient, *Phys. Rev. E.* **72**, 066304.

[83] Patankar, S. V. (1980). *Numerical heat transfer and fluid flow*, Hemisphere, Washington, D.C.

[84] Peskin C.S. (1977). Numerical analysis of blood flow in the heart, *J. Comput. Phys.*, **25** 220.

[85] Pismen, L.M. and Pomeau, Y. (2000). Disjoining potential and spreading of thin liquid layers in the diffuse-interface model coupled to hydrodynamics, *Physical Review E.* **62**, 2480.

[86] Pismen, L.M. (2001). Nonlocal diffuse interface theory of thin films and moving contact line, *Physical Review E.* **64**, 021603.

[87] Poesio, P. Lezzi, A.M. and Beretta, G.P. First evidences of convective heat transfer enhancement induced by spinodal decomposition, *Phys. Rev. E* (in press).

[88] Poesio, P. Cominardi, G. Lezzi, A.M. Mauri, R. and Beretta, G.P. (2006). The effects of quenching rate and viscosity on spinodal decomposition, *Phys. Rev. E.* **74**, 011507 .

[89] Poisson, S.D. (1831). *Nouvelle Theorie de l'Action Capillaire*, Paris, Bachelier.

[90] Popinsku, Z. and Baker, A. J. (1976). An implicit finite element algorithm for the boundary layer equations, *J. Comp. Phys.*. **21**, 55.

[91] Prausnitz, J. M. Lichtenthaler, R.N. and Gomes de Azevedo E. (1986) *Molecular Thermodynamics of Fluid-Phase Equilibria, 2nd ed.* Prentice-Hall, New York.

[92] Rallison, J.M. (1984). The deformation of small viscous drops and bubbles in shear flows, *Annu. Rev. Fluid. Mech.* **16**, 45.

[93] Lord Rayleigh (1892). On the theory of surface forces - Compressible fluids. *Philosophical Magazine* **33**, 209.

[94] Lord Rayleigh (1877). Theory of sound, 1st Ed., Revised, Dover, New York, 1945.

[95] Richardson, S. (1968). Two-dimensional bubbles in slow viscous flows, *J. Fluid Mech.* **33**, 476 .

[96] Ritz, W. (1909). Uber Eine Neue Methode zur Losung Gewisser Variations-Probleme der Mathematischen Physik, *J. Reine Angew. Math.*, **135**, 1.

[97] Rother, M.A. Zinchenko, A.Z. and Davis, R.H. (1997). Buoyancy-driven coalescence of slightly deformable drops, *J. Fluid Mech.*. **346**, 117 , and references therein.

[98] Rowlinson, J.S. and Widom, B. (1982). *Molecular Theory of Capillarity*, Oxford University Press.

[99] Sagui, C., Desai, R.C., (1994). Kinetics of phase separation in two-dimensional systems with competing interactions, *Physical Review E.* 49, 2225.

[100] Sandler, I.S. (1999). *Chemical and Engineering Thermodynamics*, 3rd ed., Ch. 7, Wiley, New York.

[101] Santonicola, G. , Mauri, R. and Shinnar, R. (2001). Phase separation of initially non-homogeneous liquid mixtures, *Industial & Engineering Chemistry Research* **40**, 2004.

[102] Siggia, E.D. (1979). Late stages of spinodal decomposition in binary mixtures, *Physical Review A* **20**, 595.

[103] Smith K.A., Solis F.J., and Chopp D.L. (2002). A projection method for motion of triple junctions by levels sets, *Interfaces Free Bound.*, 4, 263.

[104] Strang, G. and Fix, G. J. (1973). *An analysis of the finite element method*, Prentice Hall, Englewood Cliffs, New Jersey.

[105] Stone, H.A. (1994). Dynamics of drop deformation and breakup in viscous fluids *Annu. Rev. Fluid. Mech.* **26**, 65.

[106] Tanaka, H. (1996). Coarsening mechanisms of droplet spinodal decomposition in binary fluid mixtures. *Journal of Chemical Physics* **105**, 10099.

[107] Tanaka, H. (1995). Hydrodynamic interface quench effects on spinodal decomposition for symmetric binary fluid mixtures. *Phys. Rev. E*, **51**, 1313.

[108] Tanaka, H. and Araki, T. (1998). Spontaneous double phase separation induced by rapid hydrodynamic coarsening in two-dimensional fluid mixtures, *Physical Review Letters* **81**, 389.

[109] Taylor, G.I. (1932). The viscosity of a fluid containing small drops of another fluid, *Proc. Roy. Soc.* **138**, 41 .

[110] Tsemakh, D. Lavrenteva, O.M. Nir, A. (2004). *Int. J. Multiphase Flow. 30*, 1337.

[111] Turner, M. Clough, R. Martin, H. and Topp, L. (1956). Stiffness and deflection analysis of complex structures. *J. Aero. Sci.*, **23**, 805.

[112] Ullmann, A. Ludmer, Z. Shinnar, R. (1995). Phase transition extraction using solvent mixtures with critical point of miscibility. *AIChE J.*, **41**, 489.

[113] Unverdi, S.O. and Tryggvason, G. (1992). A front-tracking method for viscous, incompressible, multi-fluid flows, *J. Comput. Phys.* **100**, 25 .

[114] Valls, O.T. and Farrell, J.E. (1993). Spinodal decomposition in a three-dimensional fluid model. *Physical Review E* **47**, R36, and references therein.

[115] Vladimirova, N. Malagoli, A. and Mauri, R. (1998). Diffusion-driven phase separation of deeply quenched mixtures, *Physical Review E* **58**, 7691.

[116] Vladimirova, N., Malagoli A., and Mauri, R. (1999a). Diffusio-phoresis of two-dimensional liquid droplets in a phase-separating system, *Physical Review E.* **60**, 2037.

[117] Vladimirova, N., Malagoli A., and Mauri, R. (1999b). Two-dimensional model of phase segregation in liquid binary mixtures, *Physical Review E* **60**, 6968.

[118] Vladimirova, N., Malagoli A., and Mauri, R. (2000). Two-dimensional model of phase segregation in liquid binary mixtures with an initial concentration gradient, *Chemical Engineering Science* **55**, 6109.

[119] Vladimirova, N. and Mauri, R.. (2004). Mixing of viscous liquid mixtures, *Chemical Engineering Science* **59**, 2065.

[120] Van der Waals (1893). The thermodynamic theory of capillarity under the hypothesis of a continuous variation of density [J.S. Rowlinson, *Journal of Statistical Physics* **20**, 200 (1979), English transl.].

[121] Wagner, J. and Yeomans, J.M. (1997). Effect of shear on droplets in abinary mixture, *Int. J. Mod. Phys. C* **4**, 773 .

[122] Wong, N. C. Knobler, C. (1981) Light-scattering studies of phase separation in isobutyric acid + water mixtures: Hydrodynamic effects. *Phys. Rev. A*, **24**, 3205, and references therein.

[123] Yue, P. Feng, J.J. Liu, C. and Shen, J. (2004). A diffuse-interface method for simulating two-phase flows of complex fluids, *J. Fluid Mech.* **515**, 293.

[124] Zienkewicz, O. C. and Cheung, Y. K. (1965). Finite elements in the solution of field problems, *The Engineer*, 507

Ringraziamenti

Desidero ringraziare il Prof. Roberto Mauri per avermi introdotto nell'affascinante mondo del modello ad interfacce diffuse e per il continuo supporto e aiuto durante i tre anni di dottorato.

Il prof. Anderson, per avermi permesso di lavorare per tre mesi al dipartimento di Ingegneria meccanica dell'Università di Eindhoven e per le interessanti e istruttive discussioni.